AD-A086 491 NORTHWESTERN UNIV EVANSTON IL DEPT OF CIVIL ENGINEERING F/G 20/11
THE SURFACE SINGULARITY OF CRACKS.(U)
OCT 79 Z P BAZANT, L F ESTENSSORO AFOSR-75-2859
UNCLASSIFIED 79-10/2515 AFOSR-TR-80-0457 NL

NORTHWESTERN UNIVERSITY
The Technological Institute
Department of Civil Engineering
Evanston, Illinois 60201

LEVEL II

THE SURFACE SINGULARITY OF CRACKS

By Zdeněk P. Bažant and Luis F. Estenssoro

Structural Engineering Report

No. 79-10/251s

October 1979

The Technological Institute
Northwestern University
Evanston, Illinois 60201

UNCLASSIFIED
SECURITY CLASSIFICATION OF THIS PAGE (When Data Entered)

REPORT DOCUMENTATION PAGE	READ INSTRUCTIONS BEFORE COMPLETING FORM
1. REPORT NUMBER: AFOSR-TR-80-0457	2. GOVT ACCESSION NO.: AD-A086 491	3. RECIPIENT'S CATALOG NUMBER
4. TITLE (and Subtitle): THE SURFACE SINGULARITY OF CRACKS.	5. TYPE OF REPORT & PERIOD COVERED: INTERIM report
	6. PERFORMING ORG. REPORT NUMBER
7. AUTHOR(s): ZDENEK P. BAZANT, LUIS F. ESTENSSORO	8. CONTRACT OR GRANT NUMBER(s): AFOSR-75-2859
9. PERFORMING ORGANIZATION NAME AND ADDRESS: NORTHWESTERN UNIVERSITY, DEPARTMENT OF CIVIL ENGINEERING, EVANSTON, ILLINOIS 60201 — 401292	10. PROGRAM ELEMENT, PROJECT, TASK AREA & WORK UNIT NUMBERS: 2307 B1, 61102F
11. CONTROLLING OFFICE NAME AND ADDRESS: AIR FORCE OFFICE OF SCIENTIFIC RESEARCH/NA, BLDG 410, BOLLING AIR FORCE BASE, D C 20332	12. REPORT DATE: Oct 79
	13. NUMBER OF PAGES: 159
14. MONITORING AGENCY NAME & ADDRESS (if different from Controlling Office): 12 161	15. SECURITY CLASS. (of this report): UNCLASSIFIED
	15a. DECLASSIFICATION/DOWNGRADING SCHEDULE

16. DISTRIBUTION STATEMENT (of this Report)

Approved for public release; distribution unlimited.

14 79 10 25 15

17. DISTRIBUTION STATEMENT (of the abstract entered in Block 20, if different from Report)

18. SUPPLEMENTARY NOTES

19. KEY WORDS (Continue on reverse side if necessary and identify by block number)

SOLID MECHANICS
FRACTURE
STRESS FIELD
CRACK
FINITE ELEMENT METHOD

20. ABSTRACT (Continue on reverse side if necessary and identify by block number)

The three-dimensional singular stress field near the terminal point O of the crack front edge at the surface of an elastic body is investigated. Displacements are assumed to be of the form $r^{\lambda} p^{p} F(\theta,\phi)$ where spherical coordinates r, θ, ϕ are used, and where p is the distance from the singularity line (crack front edge or notch edge) and p is a given constant. The variational principle governing the displacement distribution on a unit sphere about point O is derived from the differential equations of equilibrium, and more directly, from the potential energy. A finite element method developed on the unit sphere is used to reduce

DD FORM 1 JAN 73 1473

401292

UNCLASSIFIED
SECURITY CLASSIFICATION OF THIS PAGE (When Data Entered)

the problem to the form $\underset{\sim}{k}(\lambda)\underset{\sim}{x} = 0$ where $\underset{\sim}{x}$ is the column matrix of the nodal values of the displacements on the unit sphere and $\underset{\sim}{k}(\lambda)$ is a square matrix, all coefficients of which are quadratic polynomials in λ. It is proved that the variational principle as well as the matrix $\underset{\sim}{k}$ must be nonsymmetric, which implies that complex eigenvalues λ are possible. Several numerical and analytical solutions are compared and agree closely with the present work. By energy flux arguments it is found that the front edge of propagating crack must terminate at the surface obliquely at a certain angle, whose dependence upon the inclination of a crack plane is also solved. The angle is the same for Model II and III, but different for Mode I. For Mode I, the surface point trails behind the interior of the propagating crack, while for Modes II and III it moves ahead. Consequently, a combination of Mode I with Modes II and III is impossible at the surface terminal point of a propagating crack whose plane is orthogonal. When the plane is inclined, the three intensify factors can combine only in certain fixed ratios. The crack edge angle is a function of the angle of the crack plane. Some results are also presented for notches and for cracks that intersect a two-material interface.

Research Project on "Three-Dimensional Singularities in Cracked Elastic Solids"

Sponsored by Air Force Office of Scientific Research
Project Directors and Principal Investigators: Z.P. Bažant and L.M. Keer

THE SURFACE SINGULARITY OF CRACKS*

By Zdenek P. Bažant and Luis F. Estenssoro

Structural Engineering Report
No. 79-10/251s

October 1979

~~The Technological Institute~~
Northwestern University
Evanston, Illinois 60201
Dept. of Civil Eng.

* Abbreviated version of this report appeared in International Journal of Solids and Structures, Vol. 15, 1979, pp. 405-426, with Addendum in Vol. 16, 1980 (in press).

ABSTRACT

The three-dimensional singular stress field near the terminal point O of the crack front edge at the surface of an elastic body is investigated. Displacements are assumed to be of the form $r^{\lambda}\rho^{p}F(\theta,\phi)$ where spherical coordinates r, θ, ϕ are used, and where ρ is the distance from the singularity line (crack front edge or notch edge) and p is a given constant. The variational principle governing the displacement distribution on a unit sphere about point O is derived from the differential equations of equilibrium, and more directly, from the potential energy. A finite element method developed on the unit sphere is used to reduce the problem to the form $\underset{\sim}{k}(\lambda)\underset{\sim}{x} = 0$ where $\underset{\sim}{x}$ is the column matrix of the nodal values of the displacements on the unit sphere and $\underset{\sim}{k}(\lambda)$ is a square matrix, all coefficients of which are quadratic polynomials in λ. It is proved that the variational principle as well as the matrix $\underset{\sim}{k}$ must be nonsymmetric, which implies that complex eigenvalues λ are possible. Several numerical and analytical solutions are compared and agree closely with the present work. By energy flux arguments it is found that the front edge of a propagating crack must terminate at the surface obliquely at a certain angle, whose dependence upon the inclination of a crack plane is also solved. The angle is the same for Modes II and III, but different for Mode I. For Mode I, the surface point trails behind the interior of the propagating crack, while for Modes II and III it moves ahead. Consequently, a combination of Mode I with Modes II and III is impossible at the surface terminal point of a propagating crack whose plane is orthogonal.

When the plane is inclined, the three intensify factors can combine only in certain fixed ratios. The crack edge angle is a function of the angle of the crack plane. Some results are also presented for notches and for cracks that intersect a two-material interface.

ACKNOWLEDGMENT

Financial support from the U.S. Air Force Office of Scientific Research under Grant No. 75-2859 to Northwestern University is gratefully acknowledged. Professor L. M. Keer, co-director and co-principal investigator of this grant, is thanked for his valuable comments and discussions, and especially for providing the results of certain analytical solutions of certain cases which could be used to check the computer program.

TABLE OF CONTENTS

LIST OF FIGURES

INTRODUCTION

Crack propagation in thin sheets is undoubtedly influenced by the surface termination of the crack front edge, where the planar elasticity solution for the crack-tip singularity does not apply and the singular stress field is of three-dimensional nature. A similar situation arises when the crack front edge intersects a two-material interface. Knowledge of the three-dimensional singularity is needed to determine the curved shape of the crack front edge across a thin sheet or plate, and the energy release rate for the advance of the crack front edge as a whole.

The three-dimensional displacement field near the terminal point of the crack front edge at the surface of an elastic body is investigated in Chapter I using spherical corrdinates r, θ, ϕ. The basic idea of the present method of solution consists of an extension of the Knein-William's method [1,2] by assuming that all three displacements are of the form $r^{\lambda}\rho^{p}F(\theta,\phi)$ [3], where ρ is the distance from the singularity line, such as the crack front edge or notch edge; p is a given constant; $F(\theta,\phi)$ is an arbitrary function of the coordinates θ and ϕ; r is the distance from the terminal point O; and λ is the strength singularity exponent. Similar techniques for solving two-dimensional axisymmetric problems have also been employed in Refs. [4,5,6]. A partly similar approach has been used by Swedlow and Karabin [7].

The variational equation governing the displacement distribution on a unit sphere about the singularity point O is derived from the

differential equations of equilibrium and boundary conditions, and an alternate derivation is obtained more directly from the potential energy. It is proved that the variational principle must be non-symmetric and therefore complex eigenvalues λ are possible. Thus, the variational principle is of general applicability since it can handle crack and notches of any orientation and size as well as problems of two dissimilar materials.

The variational equation derived in Chapter I is suitable for solution by numerical techniques. In Chapter II, the finite element method is applied and the problem is reduced to the form $\underset{\sim}{k}(\lambda)\underset{\sim}{x} = 0$, where $\underset{\sim}{x}$ is the column matrix of the nodal values of the displacements on the unit sphere and $\underset{\sim}{k}(\lambda)$ is a banded square matrix, all coefficients of which are quadratic polynomials in λ. The method of search for the eigenvalue involves a conversion to a non-homogeneous system of equations and an iteration scheme. This method has been used in connection with other problems which lead to equations of this type [3]. Convergence patterns of the eigenvalues calculated with increasing number of finite elements is studied carefully and an extrapolation technique, based on Richardson's h^m deferred approach to the limit [8] is proposed.

Recently, various numerical and analytical solutions related to this work have been published. Benthem [9] and Kawai, Fagitaui, and Kamagai [10] obtained different analytical solutions to the problem of a Mode I crack whose front edge and plane are perpendicular to the surface. However, there is some question on the convergence of the method presented by the latter authors, whose solutions disagree

with the results of Benthem as well as the present work. Also, significant progress has been made in potential theory problems by Morrison and Lewis [11] and by Keer and Parihar [12], [13]. The former authors succeeded in obtaining a differential equation with the use of conical coordinates suited for their problems. Keer and Parihar obtained a singular intergral equation which is solved numerically. They extended their solution to some three-dimensional singularities in the interior of an elastic space which is irreducible to potential theory [14a]. Keer and Parihar also solved the problem of rigid corner stamp of small angle on a semi-infinite body for which the solution is complex [14b].

These solutions provide a valuable check on the present method of solution and are compared separately in Chapter III, where further numerical results are presented. These are; a crack whose front edge and plane are perpendicular to the surface, where it is shown that Modes II and III are coupled and inseparable at the surface point; a crack whose front edge is inclined but whose plane remains perpendicular to the surface in all modes; and a crack whose front edge and plane are inclined in all modes. From energy flux considerations, these results show that upon propagation the surface point of a crack in symmetric opening will trail behind its interior, while in antisymmetric openings the surface point will move ahead of the crack interior. It is also shown that for an orthogonal crack in combined openings, the surface point will propagate in either symmetric mode or antisymmetric modes, but not in a combination. The numerical

results are compared with some recently reported fractographic measurements provided by Bell and Feeney [15].

Recently, John P. Benthem of Delft, Netherlands privately communicated (April, 1978) results based on a finite difference method directly applied to the differential equations of equilibrium and boundary conditions. His results, which have not yet been published, are also compared in Chapter III. They agree quite closely with the present solutions.

CHAPTER I

VARIATIONAL EQUATION FOR THE EIGENSTATES

1.1 Introduction

The most powerful method used to determine near-singularity fields is that of asymptotic analysis (separation of variables). The method was first used by Knein [1] (who thanked T. von Kármán for suggesting the basic approach) in a problem of plane elasticity, later solved independently by Williams [2] and Karp and Karal [16]. Recently, various authors have extended this procedure to three dimensions to investigate the near-singularity behavior for different problems [3,11-14].

The present work makes use of the same method in order to formulate a general variational equation for cracked or notched linear elastic bodies. The formulation consists of the classical differential equations of equilibrium of linear elasticity and the boundary conditions associated with the problem. A variational statement is proposed and then reduced to a variational equation applicable to numerical methods.

The variational equation determines the behavior of the material near the point of singularity. The basic assumption is that near such a point the leading terms of displacement components are of the form $r^{\lambda}F(\theta,\phi)$, where λ is an unknown constant and $F(\theta,\phi)$ an arbitrary function of the angles θ and ϕ.

1.2 Governing Equations of Elasticity

The problems considered in this work deal with singularities in a linear elastic material. As a first step, the equations governing such material are introduced. For reasons which will become clear in later sections, these equations are written in the spherical coordinate system (r,θ,ϕ) and in terms of their respective displacement components (u,v,w). No dynamic terms or body forces are present since the solution is confined to small neighborhoods of the singularity.

A.) Equations of equilibrium.

The well known classical differential equations of equilibrium expressed in terms of dilatation and rotation and transformed to spherical coordinates, take the form [Ref. 17, pages 141 and 56]:

$$(\bar{\lambda} + 2\mu)r \sin\theta \frac{\partial\Delta}{\partial r} - 2\mu\{\frac{\partial}{\partial\theta}(\tilde{\omega}_\phi \sin\theta) - \frac{\partial\tilde{\omega}_\theta}{\partial\phi}\} = 0 \qquad (1.1a)$$

$$(\bar{\lambda} + 2\mu)\sin\theta \frac{\partial\Delta}{\partial\theta} - 2\mu\{\frac{\partial\tilde{\omega}_r}{\partial\phi} - \frac{\partial}{\partial r}(r\tilde{\omega}_\phi \sin\theta)\} = 0 \qquad (1.1b)$$

$$(\bar{\lambda} + 2\mu)\frac{1}{\sin\theta}\frac{\partial\Delta}{\partial\phi} - 2\mu\{\frac{\partial}{\partial r}(r\tilde{\omega}_\theta) - \frac{\partial\tilde{\omega}_r}{\partial\theta}\} = 0 \qquad (1.1c)$$

where $\bar{\lambda}$ and μ are the Lamé's constants, Δ is the cubical dilatation and $\tilde{\omega}_r$, $\tilde{\omega}_\theta$, and $\tilde{\omega}_\phi$ are the components of rotation:

$$\Delta = \frac{1}{r^2\sin\theta}\{\frac{\partial}{\partial r}(r^2 u \sin\theta) + \frac{\partial}{\partial\theta}(rv \sin\theta) + \frac{\partial}{\partial\phi}(rw)\} \qquad (1.2a)$$

$$2\tilde{\omega}_r = \frac{1}{r^2 \sin\theta}\left\{\frac{\partial}{\partial\theta}(rw\sin\theta) - \frac{\partial}{\partial\phi}(rv)\right\} \tag{1.2b}$$

$$2\tilde{\omega}_\theta = \frac{1}{r^2 \sin\theta}\left\{\frac{\partial u}{\partial\phi} - \frac{\partial}{\partial r}(rw\sin\theta)\right\} \tag{1.2c}$$

$$2\tilde{\omega}_\phi = \frac{1}{r}\left\{\frac{\partial}{\partial r}(rv) - \frac{\partial u}{\partial\theta}\right\} \tag{1.2c}$$

B.) Strain-displacement relations.

When a body is slightly deformed the strain-displacement relationships written in spherical coordinates take the form [Ref. 17, page 56]:

$$e_{rr} = u_{,r} \tag{1.3a}$$

$$e_{\theta\theta} = \frac{1}{r} v_\theta + \frac{1}{r} u \tag{1.3b}$$

$$e_{\phi\phi} = \frac{1}{r \sin\theta} W_\phi + \frac{1}{r} v \cot\theta + \frac{1}{r} u \tag{1.3c}$$

$$e_{\theta\phi} = \frac{1}{r} w_\theta - \frac{1}{r} w \cot\theta + \frac{1}{r \sin\theta} v_\phi \tag{1.3d}$$

$$e_{\phi r} = \frac{1}{r \sin\theta} u_\phi + w_r - \frac{1}{r} w \tag{1.3e}$$

$$e_{r\theta} = v_r - \frac{1}{r} v + \frac{1}{r} u_\theta \tag{1.3f}$$

where, single subscripts on u, v, and w indicate partial derivatives, and double subscripts on e indicate strains.

C.) Stress-strain relations

When a linear-elastic isotropic homogeneous material is slightly strained the stress components are linear functions of the strain components. With the strain components defined by Eqs. (1.3 a-f) the stress components are [Ref. 17, page 126]:

$$\sigma_{rr} = \bar{\lambda}\, e + \mu u\, e_{rr} \tag{1.4a}$$

$$\sigma_{\theta\theta} = \bar{\lambda}\, e + \mu u\, e_{\theta\theta} \tag{1.4b}$$

$$\sigma_{\phi\phi} = \bar{\lambda}\, e + \mu u\, e_{\phi\phi} \tag{1.4c}$$

$$\sigma_{\theta\phi} = \mu\, e_{\theta\phi} \tag{1.4d}$$

$$\sigma_{\phi r} = \mu\, e_{\phi r} \tag{1.4e}$$

$$\sigma_{r\theta} = \mu\, e_{r\theta} \tag{1.4f}$$

where,

$$e = e_{rr} + e_{\theta\theta} + e_{\phi\phi} \tag{1.4g}$$

Then, the surface tractions, T_i, on a surface of unit normal, $\underset{\sim}{n}_i$, written in index notation, are [Ref. 18, page 64]:

$$T_i = \sigma_{ij}\underset{\sim}{n}_j \ , \quad i,j = r,\theta,\phi \tag{1.5}$$

D.) Comment

It is well known that the material behavior near a crack tip or a notch apex will be nonlinear. As is also typical of all cases possessing singularity regions. The stress values will, in fact, become unbounded at the singularity, although actually the maximum stress cannot exceed that at which plastic flow takes place. Nevertheless, the theory of linear elasticity can adequately describe the not too close stress field if the plastic region is small. The present work is limited to such cases.

1.3 The Williams' Method

Consider the mathematical representation of a crack plane intersecting a semi-infinite elastic body. Fig. 1.1 shows, as an example, a crack plane as well as its crack front edge to be normal to the surface. For illustration purposes, an imaginary body is cut out by a spherical surface of small radius and centered at the point where the crack front edge and the surface meet, i.e., point 0, Fig. 1.1. This normal presentation is used to indicate spherical coordinates, although the equations of elasticity apply to the entire body.

A.) Separation of variables.

Consider the point O, located at the smooth line OO' terminating at point O, e.g., Fig. 1.1. Let r,θ,ϕ be a spherical coordinate system centered at point O, such that ray $\theta = 0$ coincides with the crack front edge, line OO'. It will be assumed that in the vicinity of point O the displacement components in the r,θ,ϕ directions are functions whose dependence on r can be separated from their dependence on θ and ϕ, i.e., the separation of variables technique will be applied:

$$u(r,\theta,\phi) = r^{\lambda}F(\theta,\phi) \tag{1.6a}$$

$$v(r,\theta,\phi) = r^{\lambda}G(\theta,\phi) \tag{1.6b}$$

$$w(r,\theta,\phi) = r^{\lambda}H(\theta,\phi) \tag{1.6c}$$

with the restriction that the exponent λ have a limiting value $Re(\lambda) > -\frac{1}{2}$, in order for the strain energy to remain finite near point O, $r \to 0$. Hence, the objective of this work is to find the smallest possible value for the exponent λ, $Re(\lambda) > -\frac{1}{2}$, giving the gravest state of stress for the vicinity of point O.

In this sense, point O is considered a singular point, line OO' a singular line, and λ the eigenvalue.

The proof for the well-established theorems of uniqueness and existence for the problems considered here is beyond the scope of

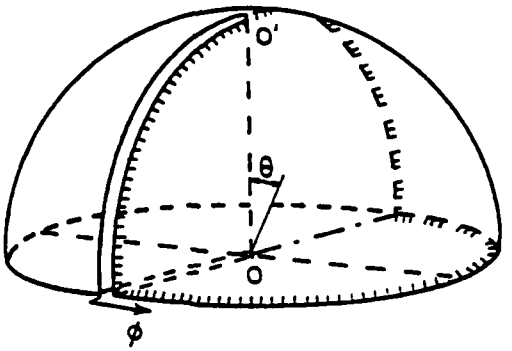

Fig. 1.1: Geometry of the crack intersecting a surface, in spherical coordinates.

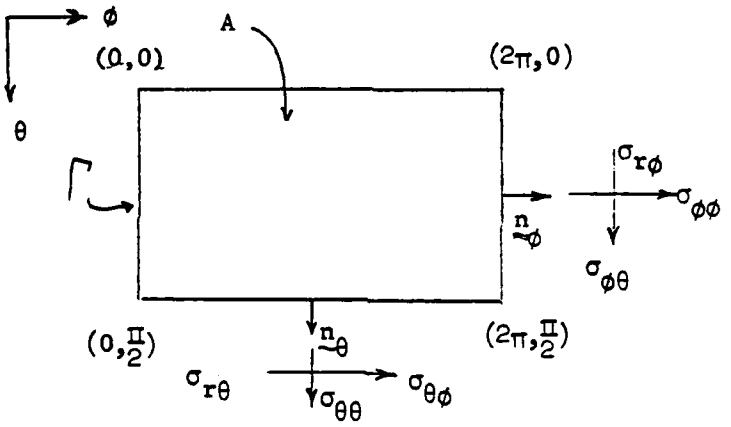

Fig. 1.2: Domain to be solved in fictitious (θ-φ)-plane.

this work. Even for regular finite regions, these theorems are already "not distinguished by simplicity" [19, page 89]. Benthem [9] who solved analytically one of the problems presented in Chapter III, writes: "The following theorems, though without proof, will be considered to be valid for elastic regions in the form of infinite cones (semi-infinite bodies).

i.) If an infinite conical region is loaded by stresses which behave along the generators like $r^{\lambda-1}$ and the displacements are prescribed which are zero or behave like r^{λ}, then there is generally a solution for the interior stresses of the form $\sigma_{xx} = r^{\lambda-1} f_{xy}(\theta\phi)$, etc. with the exception of an infinite enumerable set of values for λ.

ii.) For every value of λ of the infinite enumerable set meant under (i.), there exists a state of stress given by the above expressions, whereof the prescribed stresses and displacements are zero. Such states of stress are called the eigenfunctions of the cone in question.

iii.) The infinite enumerable states of stress (with $\mathrm{Re}(\lambda) > -\frac{1}{2}$) meant in (ii.), are able, in principle, to meet every set of three boundary conditions at r = constant (a finite cone) provided the boundary conditions do not require a concentrated force or moment at the vertex.

These three theorems are, if not proved, generally accepted in the corresponding two-dimensional analysis of wedges [2,20,21]."

B.) Modified equations of equilibrium.

Substituting the expressions (1.6a-c) into the differential equations of equilibrium (1.1a-c) it was found that the radial co-

ordinate, mainly, $r^{\lambda-1}$ factors out of the equations. The following equations of equilibrium in the r,θ, and φ directions in terms of the functions F,G, and H and the exponent λ result:

$$X_r = (Q+2)(\lambda-1)(\lambda F + F + G_\theta + G\cot\theta + \frac{1}{\sin\theta} H_\phi) - [(\lambda+1)G_\theta - F_{\theta\theta}]$$

$$- \cot\theta[(\lambda+1)G - F_\theta] + \frac{1}{\sin\theta}(\frac{1}{\sin\theta} F_{\phi\phi} - H_\phi - \lambda H_\phi) = 0 \qquad (1.7a)$$

$$X_\theta = (Q+2)(\lambda F_\theta + 2F_\theta + G_{\theta\theta} + G_\theta \cot\theta - \frac{1}{\sin^2\theta} G + \frac{1}{\sin\theta} H_{\theta\phi}$$

$$- \frac{\cos\theta}{\sin^2\theta} H_\phi) - \frac{1}{\sin\theta}(H_{\theta\phi} + H_\phi \cot\theta - \frac{1}{\sin\theta} G_{\phi\phi})$$

$$+ \lambda[(\lambda+1)G - F_\theta] = 0 \qquad (1.7b)$$

$$X_\phi = \frac{1}{\sin\theta}(Q+2)(\lambda F_\phi + 2F_\phi + G_\phi \cot\theta + \frac{1}{\sin\theta} H_{\phi\phi})$$

$$- \lambda(\frac{1}{\sin\theta} F_\phi - H - \lambda H) + (H_{\theta\theta} + H_\theta \cot\theta - \frac{1}{\sin^2\theta} H$$

$$+ \frac{\cos\theta}{\sin^2\theta} G_\phi - \frac{1}{\sin\theta} G_{\theta\phi}) = 0 \qquad (1.7c)$$

where, subscripts of F,G, and H denote partial derivatives, e.g., $F_{\theta\theta} = \partial^2 F/\partial\theta^2$, ν = Poisson ratio,

$$Q = 2\nu/(1-2\nu) \tag{1.8}$$

and X_r, X_θ , X_ϕ symbolically represent the new modified equations of equilibrium in the r, θ, and ϕ directions, respectively.

C.) Modified stress-strain relations.

Substituting Eqs. (1.6a-c) into the expressions for the spherical stress components, Eqs. (1.4a-f), the following modified stress expresssions result:

$$s_{rr} = \frac{1}{\mu r^{\lambda-1}} \sigma_{rr} = Q(\lambda F + 2F + G_\theta + G \cot\theta + \frac{1}{\sin\theta} H_\phi) + 2\lambda F \tag{1.9a}$$

$$s_{r\theta} = \frac{1}{\mu r^{\lambda-1}} \sigma_{r\theta} = \lambda G - G + F_\theta \tag{1.9b}$$

$$s_{\theta\theta} = \frac{1}{\mu r^{\lambda-1}} \sigma_{\theta\theta} = Q(\lambda F + 2F + G_\theta + G \cot\theta + \frac{1}{\sin\theta} H_\phi) + 2(G_\theta + F) \tag{1.9c}$$

$$s_{\theta\phi} = \frac{1}{\mu r^{\lambda-1}} \sigma_{\theta\phi} = H_\theta - H \cot\theta + \frac{1}{\sin\theta} G_\phi \tag{1.9d}$$

$$s_{r\phi} = \frac{1}{\mu r^{\lambda-1}} \sigma_{r\phi} = \frac{1}{\sin\theta} F_\phi + \lambda H - H \tag{1.9e}$$

$$s_{\phi\phi} = \frac{1}{\mu r^{\lambda-1}}\ \sigma_{\phi\phi} = Q(\lambda F + 2F + G_{\theta} + G \cot\theta + \frac{1}{\sin\theta}\ H_{\phi})$$

$$+ 2(\frac{1}{\sin\theta}\ H_{\phi} + G \cot\theta + F) \qquad (1.9f)$$

in which μ is the elastic shear modulus, and $s_{rr},\ldots,s_{\phi\phi}$ symbolically represent the stresses.

D.) Comment.

It is interesting to note that one may expect an infinite enumerable number of real and complex eigenvalues λ, i.e., not a continuous spectrum, for the problem of a semi-infinite homogeneous body. Furthermore, the real part of each of the complex roots with positive real part is always greater than the smallest positive real root, which is also the case for plane problems and is rigorously proved in Ref. [16]. Therefore, the dominant term that governs the behavior near point O, Fig. 1.1, is given by the smallest real root.

Of course, this last observation will not apply to problems of a crack intersecting two-material interfaces. In such cases all eigenvalues λ are expected to be complex in nature, such as those found in plane strain elasticity [22,23]. The term of interest will then be given by the smallest $Re(\lambda)$.

It may be desired to write a generalized Fourier analysis to include the displacement fields for different eigenvalues which must result from the solution of an infinite set of equations. However, the orthogonality properties in three-dimensions might be insufficient to

determine their participation. This is also the case in plane problems, as Williams [24] noted: "... let it suffice to point out that the solutions $f(\lambda,\alpha,\nu) = 0$ yield an infinite number of eigenvalues which may be complex. After ordering these values according to their absolute magnitudes, one may construct from them an infinite set of eigenfunctions whose elements are non-orthogonal. Furthermore, the completeness of the set, although intuitively probable, has not been mathematically established." The present literature seems to lack the proof for the completeness of the set, even for two dimensional problems.

In any event, let such set intuitively exist for the three dimensional problem. Then, in the vicinity of point O, the behavior of the displacement and stress fields will be determined by the eigenfunction characterized by the smallest eigenvalue; provided the loading near such point is not critical, see theorem (iii.) page 12.

1.4 Construction of a Variational Equation

A.) Cartesian $(\theta\text{-}\phi)$-plane.

Finite element studies are simplified when flat planes, rather than curved surfaces are used. Expecting that the solution to these problems will make use of numerical techniques, the domain O'ACO of a unit sphere from Fig. (1.1) is visualized in a fictitious $(\theta\text{-}\phi)$-plane shown in Fig. (1.2). This approach has been successfully developed in Ref. [3,page 226].

The singularity ray OO', Fig. (1.1) placed on the pole of its spherical coordinate system appears in the $(\theta\text{-}\phi)$-plane as a straight line segment at $\theta = 0$. The surface of the semi-infinite body $\theta = \pi/2$,

$0 \leq \phi \leq 2\pi$ appears in the $(\theta\text{-}\phi)$-plane as a straight line segment $\theta = \pi/2$, $0 \leq \phi \leq 2\pi$, etc.

Let then $\underset{\sim}{n} = (n_\theta, n_\phi)$ be the unit normal to the surface of the body when plotted in the $(\theta\text{-}\phi)$-plane, with θ and ϕ being regarded as the cartesian coordinates in such a fictitious plane. Thus, $\underset{\sim}{n} = (-d\theta/ds, d\phi/ds)$ where s is the length of a boundary curve, or $n_\theta/n_\phi = -d\theta/d\phi$ where $d\theta$ and $d\phi$ are increments along such boundary in the θ and ϕ directions, respectively.

B.) Free surface conditions.

It will be assumed that in a sufficiently small neighborhood of point 0, Fig. (1.1), there are no loads applied at the body surfaces (surfaces formed by radial rays emanating from point 0), or at the cracked surfaces.

Indeed, the purpose of this work is to determine all possible states, called eigenstates which are strictly characterized by the eigenvalues λ. Hence, surface loads may be prescribed at body surfaces sufficiently remote from point 0, for which the differential equations of equilibrium but not the boundary conditions will be satisfied. According to the principle of superposition the actual state of stress for given boundary conditions can be expressed as a linear combination of its eigenstates. But, as far as the eigenvalues λ are concerned these boundary conditions are irrelevant, as it is also true in planar problems, where $\lambda = \frac{1}{2}$ for any loading combination.

Therefore, without loss of generality, it will be assumed that all body surfaces are formed by radial rays, and that the boundary conditions

at the free surfaces in close vicinity of point 0, Fig. (1.1), are:

$$\text{body surface: } \sigma_{\theta\theta} = \sigma_{\theta r} = \sigma_{\theta\phi} = 0 \quad \text{at } \theta = \pi/2 \tag{1.10a}$$

$$\text{crack plane: } \sigma_{\phi\phi} = \sigma_{\phi r} = \sigma_{\phi\theta} = 0 \quad \text{at } \phi = 0, 2\pi \tag{1.10b}$$

These boundary conditions written as surface tractions p_r, p_θ, and p_ϕ in the $(\theta\text{-}\phi)$-plane take the form:

$$p_r = s_{r\theta} n_\theta \sin\theta + s_{r\phi} n_\phi = 0 \tag{1.11a}$$

$$p_\theta = s_{\theta\theta} n_\theta \sin\theta + s_{\theta\phi} n_\phi = 0 \tag{1.11b}$$

$$p_\phi = s_{\theta\phi} n_\theta \sin\theta + s_{\phi\phi} n_\phi = 0 \tag{1.11c}$$

No boundary conditions are specified at infinity, $r \to \infty$; only the local problem of stress singularity at point 0, $r \to 0$, is considered, and hence, a small domain about point 0 is required.

C.) Variational statement.

The differential equations (1.7a-c) together with the boundary conditions (1.11a-c) may be combined to form the following variational statement in the $(\theta\text{-}\phi)$-plane:

$$\iint_A (X_r \delta F + X_\theta \delta G + X_\phi \delta H) \sin\theta \, d\theta \, d\phi - \int_s (p_r \delta F + p_\theta \delta G + p_\phi \delta H) ds = 0 \tag{1.12}$$

in which s is the length of the boundary of the region of the (θ,ϕ)-plane; A is the area of such region; and $\delta F, \delta G$, and δH are arbitrary continuous functions of θ and ϕ which have piece-wise continuous derivatives and satisfy all displacement boundary conditions, if any. Conversely, from the fact that Eq. (1.2) must hold for any kinematically admissible functions $\delta F, \delta G$, and δH it follows that Eqs. (1.7a-c) and (1.11a-c) must be satisfied. Thus, the variational statement (1.12) must be equivalent to Eqs. (1.7a-c) and (1.11a-c).

The variational statement presented in Eq. (1.12), is analogous to the three-dimensional statement one forms in order to obtain the strain energy [18], except that integration with respect to r has already been carried out in the unit sphere, since the r dependence can be factored out, see Eqs. (1.7a-c) and (1.11a-c).

D.) Variational equation.

The variational statement, Eq. (1.12) involves second derivates of F,G, and H, which are contained in the expressions for X_r, X_θ, and X_ϕ, Eqs. (1.7a-c). Since numerical techniques give rise to larger error for higher order derivatives, it is necessary to transform Eq. (1.12) to a form which involves no higher than first order derivatives of F,G,H and of $\delta F, \delta G, \delta H$. Also, to be able to apply the finite element method it is necessary that during this transformation the boundary integral in Eq. (1.12) be included in the variational equation; otherwise the natural boundary conditions would not be satisfied when the finite element method is used.

Indeed, a transformation by Green's integral theorem [18, page 279] applied in the Cartesian $(\theta\text{-}\phi)$-plane has been found, such that both objectives are reached simultaneously. The formulation is given in detail in Appendix A. The resulting variational equation is:

$$\iint_A (\Phi_F \delta F + \Phi_{F_\theta} \delta F_\theta + \Phi_{F_\phi} \delta F_\phi + \Phi_G \delta G + \Phi_{G_\theta} \delta G_\theta + \Phi_{G_\phi} \delta G_\phi + \Phi_H \delta H + \Phi_{H_\theta} \delta H_\theta + \Phi_{H_\phi} \delta H_\phi) \sin\theta \, d\theta d\phi = 0 \tag{1.13}$$

in which $\delta F_\theta = \partial \delta F / \partial \delta, \ldots, \delta H_\phi = \partial \delta H / \partial \phi$ and the following notations are made

$$\Phi_F = [Q(1-\lambda) + 2][(\lambda+2)F + G_\theta + G \cot\theta + \frac{1}{\sin\theta} H_\phi] - 2\lambda(\lambda+2);$$

$$\Phi_{F_\theta} = (\lambda - 1)G + F_\theta; \quad \Phi_{F_\phi} = \frac{1}{\sin\theta} [\frac{1}{\sin\theta} F_\phi + (\lambda - 1)H];$$

$$\Phi_G = \{(Q+2)[(\lambda+2)F + G_\theta + G \cot\theta + \frac{1}{\sin\theta} H_\phi] - 2(G_\theta + F) - 2\lambda F\}\cot\theta - 2(F_\theta - G) - \lambda(\lambda+1)G - \lambda F_\theta;$$

$$\Phi_{G_\theta} = Q[(\lambda+2)F + G_\theta + G \cot\theta + \frac{1}{\sin\theta} H_\phi] + 2(G_\theta + F);$$

$$\Phi_{G_\phi} = \frac{1}{\sin\theta}\left(H_\theta - H\cot\theta + \frac{1}{\sin\theta}G_\phi\right);$$

$$\Phi_H = -\left[\left(H_\theta - H\cot\theta + \frac{1}{\sin\theta}G_\phi\right)\cot\theta + 2\left(\frac{1}{\sin\theta}F_\phi - H\right)\right.$$

$$\left. + \lambda(\lambda+1)H + \frac{\lambda}{\sin\theta}F_\phi\right];$$

$$\Phi_{H_\theta} = H_\theta - H\cot\theta + \frac{1}{\sin\theta}G_\phi;$$

$$\Phi_{H_\phi} = \frac{1}{\sin\theta}\left\{Q\left[(\lambda+2)F + G_\theta + G\cot\theta + \frac{1}{\sin\theta}H_\phi\right]\right.$$

$$\left. + 2\left(\frac{1}{\sin\theta}H_\phi + G\cot\theta + F\right)\right\} \qquad (1.14)$$

where $\Phi_F,\ldots,\Phi_{H_\phi}$ are not partial derivatives of some function Φ, and are used only for notation.

Thus, the variational statement of the problem is: Functions F, G, and H are the solution of the problem if and only if they satisfy Eq. (1.13) for any kinematically admissible variation $\delta F, \delta G$, and δH.

Existance of the variational equation which contains no boundary integral, Eq. (1.13), indicates that natural boundary conditions, Eqs. (1.11a-c), will be automatically fulfilled when the finite element method is used.

E.) Comment.

Alternatively, it is possible to derive Eq. (1.13) from Eq. (1.12) by means of Stokes theorem applied to a unit sphere. It has been checked that this gives the same result. It has been also checked that Eq. (1.13) can be transformed back to Eq. (1.12) by means of Gauss or Stokes theorems. For the sake of brevity these derivations are not given. Instead, an alternate and independent derivation of the one just given is derived in the next section.

1.5 Alternative Derivation of the Variational Equation

The basic variational equation, Eq. (1.13) can also be derived from the principle of strain energy. The derivation is more direct but involves certain steps which were difficult to foresee at the early stages of this project without recourse to the derivation just presented.

A.) Principle of minimum potential energy.

The total potential energy stored within a linear elastic body of volume V and surface S, when no body forces or dynamic terms are present, is:

$$U = \int_V \psi \, r^2 \sin\theta \, dr d\theta d\phi - \int_S (T_r u + T_\theta v + T_\phi w) ds \qquad (1.15)$$

where T_r, T_θ, T_ϕ are the surface tractions defined in Eq. (1.5), and ψ is the strain energy density:

$$\psi = \frac{\mu}{2}\{Q(u_r + \frac{1}{r}v_\theta + \frac{2}{r}u + \frac{1}{r\sin\theta}w_\phi + \frac{1}{r}v\cot\theta)^2 + 2[u_r^2$$

$$+ (\frac{1}{r}v_\theta + \frac{1}{r}u)^2 + (\frac{1}{r\sin\theta}w_\phi + \frac{1}{r}v\cot\theta + \frac{1}{r}u)^2]$$

$$+ (v_2 - \frac{1}{r}v + \frac{1}{r}u_\theta)^2 + (\frac{1}{r}w_\theta - \frac{1}{r}w\cot\theta + \frac{1}{r\sin\theta}v_\phi)^2$$

$$+ (\frac{1}{r\sin\theta}u_\phi + w_r - \frac{1}{r}w)^2\} \qquad (1.16)$$

in which,

$$Q = 2\nu/(1 - 2\nu) \qquad (1.17a)$$

$$\mu = E/2(1 + \nu) \qquad (1.17b)$$

E is the Young's modulus and ν the Poisson's ratio characterizing the linear elastic material.

According to the principle of minimum potential energy, the state of equilibrium is a state for which the first variation of the total potential energy vanishes. Thus, consider the displacement variations

$$\delta u = \epsilon\,\bar{u} \qquad (1.18a)$$

$$\delta v = \epsilon\,\bar{v} \qquad (1.18b)$$

$$\delta w = \varepsilon \bar{w} \tag{1.18c}$$

where E is a variable parameter and $\bar{u},\bar{v},\bar{w}$ are any chosen displacement distribution which are sufficiently smooth and satisfy all kinematic boundary conditions. Then, the state of equilibrium is determined by the first variation of U, Eq. (1.15):

$$\delta U = \varepsilon\left[\frac{\partial U}{\partial \varepsilon}\right]_{\varepsilon=0} = \int_V (\psi_u \delta u + \psi_{u_r} \delta u_r + \ldots + \psi_{w_\phi} \delta w_\phi) r^2 \sin\theta \, dr d\theta d\phi$$

$$- \int_S (T_r \delta u + T_\theta \delta v + T_\phi \delta w) ds = 0 \tag{1.19}$$

B.) An unorthodox step.

If Eqs. (1.6a-c) were substituted directly into Eq. (1.19) $r^{2\lambda}$ would factor out. However, the remaining expression would not be able to satisfy the equations of equilibrium when Gauss theorem is applied to Eq. (1.19). To circumvent this critical problem, consider the terms $\psi_{u_r} \delta u_r$, $\psi_{v_r} \delta v_r$, and $\psi_{w_r} \delta w_r$ separately from Eq. (1.19). These terms can be simplified by Gauss theorem as:

$$\int_V (\psi_{u_r} \delta u_r + \psi_{v_r} \delta v_r + \psi_{w_r} \delta w_r) dv =$$

$$\int_V \{\frac{d}{dr}(\psi_{u_r} \delta u) - \delta u \frac{d}{dr} \psi_{u_r} + \frac{d}{dr}(\psi_{v_r} \delta v) - \delta v \frac{d}{dr} \psi_{v_r}$$

$$+ \frac{d}{dr}(\psi_{w_r} \delta w) - \delta w \frac{d}{dr} \psi_{w_r}\} dV \tag{1.20}$$

where d/dr is the total derivative with respect to r.

Applying the Gauss theorem to the sum of the first, third and fifth terms of Eq. (1.20) and placing them back into Eq. (1.19) gives

$$\delta U = \int_V \{(\psi_u - \frac{d}{dr}\psi_{u_r})\delta u + \psi_{u_\theta}\delta u_\theta + \psi_{u_\phi}\delta u_\phi$$

$$+ (\psi_v - \frac{d}{dr}\psi_{v_r})\delta v + \psi_{v_\theta}\delta v_\theta + \psi_{v_\phi}\delta v_\phi$$

$$+ (\psi_w - \frac{d}{dr}\psi_{w_r})\delta w + \psi_{w_\theta}\delta w_\theta + \psi_{w_\phi}\delta w_\phi\}dV$$

$$+ \int_S \{(\psi_{u_r}\delta u + \psi_{v_r}\delta v + \psi_{w_r}\delta w)n_r$$

$$- T_r\delta u + T_\theta\delta v + T_\phi\delta w\}ds = 0 \qquad (1.21)$$

For the particular problems studied here, the surface integral of Eq. (1.21) vanishes because of the boundary conditions conveyed by these problems, i.e.:

If the surface tractions, Eq. (1.5), are expanded, one obtains that on the free surfaces near point O [see Fig. (1.1) and Eqs. (1.10a-b)]:

i) $\sigma_{rr} = \psi_{u_r}$, which is not present on any surface formed by rays emanating from point O.

ii) $\sigma_{r\theta} = \psi_{v_r} = 0$ on the body surface, $\theta = \pi/2.$, $\sigma_{r\theta}$ is not presend on the crack plane $\phi = 0$.

iii) $\sigma_{r\phi} = \psi_{w_r} = 0$ on the crack plane $\phi = 0$, but not present on the body surface $\theta = \pi/2$.

iv) because of the free surface conditions the remaining terms are also zero and because of (i-iii):

$$T_r = \sigma_{r\theta} n_\theta + \sigma_{r\phi} n_\phi = 0 \tag{1.22a}$$

$$T_\theta = \sigma_{\theta\theta} n_\theta + \sigma_{\theta\phi} n_\phi = 0 \tag{1.22b}$$

$$T_\phi = \sigma_{\theta\phi} n_\theta + \sigma_{\phi\phi} n_\phi = 0 \tag{1.22c}$$

which are analogous to the boundary conditions given by Eq. (1.11a-c).

If the expressions (1.6a-c) are <u>now</u> substituted into Eq. (1.21) one would obtain the same basic variational equation, Eq. (1.13), after integration with respect to r is performed on the unit sphere and transformed to the $(\theta$-$\phi)$-plane.

C.) Lack of symmetry and non-existence of a minimum principle.

It is particularly noteworthy that the integrand of Eq. (1.13) or Eq. (1.21) is non-symmetric, and so is the system of linear equations, Eq. (1.12), which is Eq. (1.13) applied to finite elements, $(k_{ij} \neq k_{ji})$. This means that the variational equation cannot be written in the form of a classical stationary principle [18], $\delta W = 0$ (or minimum principle, W = min.), which would yield Eq. (1.13). For an elastic material this might seem surprising. However, a deeper analysis indicates that it must be so.

Assume that the integrand of Eq. (1.13) is symmetric with F,G, and H. Then the discrete eigenvalue problem for λ resulting from Eq. (1.13) would have to be a symmetric matrix $k_{ij} = k_{ji}$, Eq. (2.12). This implies that all roots λ would have to be real. But this cannot be possible because the same variational equation, Eq. (1.13), must hold also for plane strain problems with two material interfaces, whose solution are known to exhibit oscillating singularities [22,23] for which λ is complex. Hence, Eq. (1.13) cannot be symmetric. This contrasts with the analogous potential theory problem for which a minimum variational principle in the $(\theta$-$\phi)$-plane does exist [3], with the consequence that in potential theory the eigenvalue λ is always real.

To prove that the variational equation Eq. (1.13) must be non-symmetric, it is sufficient to show that it must be so in the special case of plane elasticity. This can be done by dropping out the integration over θ and substituting $\theta = \pi/2$ and then setting $G = v = 0$ in Eq. (1.13). In that case, the most general quadratic functional involving $F(\phi), H(\phi), F'(\phi) = \partial F/\partial\phi$, and $H'(\phi) = \partial H/\partial\phi$ is:

$$W = \int_0^{\phi_1} [\tfrac{1}{2}(A_1F^2 + A_2F'^2 + A_3H^2 + A_4H'^2) + A_5FF' + A_6FH$$

$$+ A_7FH' + A_8F'H + A_9F'H' + A_{10}HH']d\phi \qquad (1.23)$$

The associated Euler equations [18] are:

$$A_1F - A_2F'' + A_6H + (A_7-A_8)H' - A_9H'' = 0 \tag{1.23a}$$

$$A_3H - A_4H'' + F - (A_7-A_8)F' - A_9F'' = 0 \tag{1.23b}$$

and the corresponding natural boundary conditions at $\phi = 0$ or $\phi = \phi$, are

$$A_2F' + A_5F + A_8H + A_9H' = 0 \tag{1.24a}$$

$$A_4H' + A_7F + A_9F' + A_{10}H = 0 \tag{1.24b}$$

The actual differential equations for F and H, as obtained by substituting $u = r^{\lambda}F(\phi)$ and $w = r^{\lambda}H(\phi)$ into the planar differential equations of equilibrium in the polar coordinate system (r,ϕ), given by Karp and Karal [16], have the form

$$C_1(a_oF + a_2F'' + a_1H') = 0 \tag{1.25a}$$

$$C_2(b_oH + b_2H'' + b_1F') = 0 \tag{1.25b}$$

and the actual boundary conditions

$$C_3(c_1F' + c_2H) = 0 \tag{1.26a}$$

$$C_4(c_3H' + c_4F) = 0 \tag{1.26b}$$

where C_1, C_2, C_3, and C_4 are aribtrary non-zero constants; and a_o, a_1, a_2; b_o, b_1, b_2; c_1, c_2, c_3, c_4 are certain given constants.

Equating the coefficients of all corresponding terms of Eqs. (1.23a-b) and (1.24a-b) with Eqs. (1.25a-b) and (1.26a-b) one obtains a system of 14 linear algebraic equations for $A_1, \ldots, A_{10}$, $C_1, \ldots, C_4$. Unknowns $A_1, \ldots, A_{10}$ can easily be found, which leaves a system of four linear equations for $C_1, \ldots, C_4$ which are homogeneous. The determinant of this equation system was found to equal λ. Because λ cannot be restricted to equal zero, it follows that $C_1, \ldots, C_4$ cannot be non-zero. Thus, there is no way to make Eqs. (1.23a-b) and (1.24a-b) equivalent to Eqs. (1.25a-b) and (1.26a-b), which means that a variational functional W does not exist for plane problems. So, it cannot exist for the three-dimensional problem as well.

D.) Comment.

Indeed, the two derivations take somewhat different procedures from those found from classical variational methods in linear elasticity. But, it is noteworthy that both derivations complement each other in the following manner:

a.) The boundary conditions in the $(\theta\text{-}\phi)$-plane, Eqs. (1.11a-c) have to be included in the first derivation (see Appendix A), while in the second they vanish because of the free stress surfaces, Eqs. (1.22a-c).

b.) In the first derivation the boundary conditions (mainly, σ_{rr} not being present on any surface when surface tractions are considered;

$\sigma_{r\theta} = 0$ on $\theta = \pi/2$, but not present on $\phi = 0$; $\sigma_{r\phi} = 0$ on $\phi = 0$, but not present on $\theta = \pi/2$), allows the formation of the $(\theta\text{-}\phi)$-plane, otherwise, the radial component of the unit normal vector, n_r, on the surfaces would be present in Eq. (1.11a-c). In the second derivation they come out as a result of the application of Gauss theorem, but vanish due to the reasons just presented.

c.) The first derivation makes use of the differential equations, while the second starts from the total potential energy. Both procedures end with the same variational equation after some intuitive manipulations.

The lack of symmetry and the non-existance of a minimum principle for the variational equation corresponds to the fact that both real and complex eigenvalues must be associated with this variational equation.

It must be stressed, however, that the entire present formulation is contingent upon the assumption of the separated form of the eigenstate (Eq. 1.6, page 10). There exists no proof that the eigenstate ought to have this form, and that other eigenstates, possibly even not separated ones, might exist and might be more severe, even though this seems unlikely.

CHAPTER II

METHOD OF SOLUTION ON A FINITE ELEMENT GRID

2.1 Introduction

The variational equation derived in Chapter I and given by Eq. (1.13) has the tremendeous advantage that the stress boundary conditions are automatically implied whenever a free surface is present. Therefore, compared to a finite difference method where free surfaces would require additional programming, the finite element method is selected to approach the problem. The program is then written in the Fortran IV computer language.

The finite elements are chosen as simple four-node quadrilaterals. The distribution functions for F,G, and H, Eq. (1.6a-c), are considered bilinear in θ and ϕ. The coefficients of the stiffness amatrix, Eq. (2.9), are calculated by the Gaussian numerical integration technique using nine integration points, [25].

The variational equation emerges as a generalized non-linear problem for the eigenvalues. Various methods of numerical solution of this type of problems have been discussed in detail in Ref. [3]. Method B from page 230 of Ref. [3] has been selected to search for the root λ. A method of solution when λ is complex has also been discussed in Ref. [6] in connection with other problems. The root of smallest value, or of smallest $Re(\lambda)$ in the case of complex roots, is of main practical interest.

An extrapolation technique based on the "deferred approach to the limit" [8] is proposed for the final value of root λ as the number of grid subdivisions goes to infinity.

The program is general and capable of handling various situations, such as intersections of crack plane and crack front edge of any orientation, notches of any orientation and of any opening, etc. The program will be also capable of handling cases when the exponent λ is expected to be complex, such as intersections of crack edges with two-material interfaces. This requires a conversion of the Fortran program to complex arithmetic.

2.2 Finite Element Formulation

A.) Treatment of line singularities.

From the three-dimensional singularity point 0, Fig. 1.1, page 11, there usually emanates a stress singularity line, such as the crack front edge shown as line 00' which coincides with the polar ray $\theta = 0$. The displacements near this line usually behave as $(r\rho)^p$ [3,11] such that $r\rho$ represents the distance from the ray $\theta = 0$ when $\theta \to 0$. The exponent p will then represent the exponential behavior for the displacement field near the singularity line. For the crack front edge considered here, the values $p = 0, \frac{1}{2}, 1, 3/2, \ldots$, are possible, and for notch edges other values of p would apply.

From the theory of the finite element method for plane problems it is known, for example, that the rate of convergence in the presence of square-root singularity is only $0(h)$, while in its absence the convergence is quadratic, $0(h^2)$, h being the element size [26].

It is conceivable that the functions F, G, and H, Eq. (1.6a-c), may exhibit gradient singularities at the point where the crack front edge 00' (a singularity line) emanates from point 0, Fig. 1.1; then $p < 1$. Such functions are not suitable for numerical calculations, and if they are approximated numerically, their accuracy and convergence are adversely affected by the presence of singularities. This difficulty can be avoided by using singular finite elements near the singularity line. A more convenient method has been proposed and used with success in Ref. [3]. In this method, the displacements in the r,θ, and ϕ directions are expressed as

$$u(r,\theta,\phi) = r^n r_1^p f(\theta,\phi) = r^\lambda \rho^p f(\theta,\phi) \tag{2.1a}$$

$$v(r,\theta,\phi) = r^n r_1^p g(\theta,\phi) = r^\lambda \rho^p g(\theta,\phi) \tag{2.1b}$$

$$w(r,\theta,\phi) = r^n r_1^p h(\theta,\phi) = r^\lambda \rho^p h(\theta,\phi) \tag{2.1c}$$

in which, p is the exponent for the displacement field near the singularity line; $\lambda = n + p$; $r_1 = r\rho$; ρ is any chosen smooth continuous function of θ and ϕ which is non-zero everywhere except on the singularity line $\theta = 0$, and which represents the distance measured on a unit sphere. Possible choices are $\rho = \theta$, $\rho = \sin\theta$, etc. The second suggestion will be used for numerical calculations, since $\rho = \sin\theta$ will then represent the exact distance from the ray not only for $\theta \to 0$, but everywhere in the domain. (Note, however, that $\rho = \sin\theta$ cannot be used when the angle $\theta = \pi$ is part of the domain and where

no line of singularity exists, i.e., at $\theta = \pi$). Thus, it is convenient to introduce the notations:

$$F(\theta,\phi) = \rho^p \, f(\theta,\phi) \tag{2.2a}$$

$$G(\theta,\phi) = \rho^p \, g(\theta,\phi) \tag{2.2b}$$

$$H(\theta,\phi) = \rho^p \, h(\theta,\phi) \tag{2.2c}$$

$$\rho^p = (\sin\theta)^p \tag{2.2d}$$

If the field near the singularity line varies as $\rho^{\frac{1}{2}}$ when p is set to $\frac{1}{2}$, then functions f,g, and h may be expected to be free of gradient singularities. This would make the convergence rate quadratic, $O(h^2)$, [26]. On the other hand, if components of types p^1, p^0, and possibly other components of different exponents were present in the solution [9], the rate of convergence would not be quadratic, but slower than quadratic [26].

When several exponents p are present, the lowest one must be used. This is shown as follows. Consider that an exponent p^*, which differs from the actual value of p, is used. Then, the displacement and stress fields would behave as:

$$u_i \sim r^\lambda \, \theta^p \, F(\theta,\phi) \tag{2.3a}$$

$$\sigma_{ij} \sim \partial u/\partial\theta \sim r^{\lambda}\theta^{p-1}F(\theta,\phi) \tag{2.3b}$$

for the exact solution, and

$$u_i \sim r^{\lambda}\ \theta^{p^*}F^*(\theta,\phi) \tag{2.4a}$$

$$\sigma_{ij} \sim \partial u/\partial\theta \sim r^{\lambda}\theta^{p^*-1}F^*(\theta,\phi) \tag{2.4b}$$

for the numerical solution.

Equating the two critical expressions, for the stresses σ_{ij}, one obtains:

$$F^*(\theta,\phi) = \theta^{p-p^*}F(\theta,\phi) \tag{2.5}$$

where the function $F(\theta,\phi)$ is bounded. If one chooses $p^* > p$, function $F^*(\theta,\phi)$ can obviously become unbounded as $\theta \to 0$; and it cannot be adequately represented numerically. Thus,

$$p^* \leq p \tag{2.6}$$

is necessary. The best choice would naturally be to make p^* equal to the lowest exponent p present.

Under these considerations, there is still the restriction that along the crack front edge, $\theta \to 0$, the displacement field must exhibit the behavior

$$\theta^q, \quad \text{such that } q > 0 \tag{2.7}$$

for the strain energy to remain bounded. Note that q is not the exponent for the singularity function ρ.

B.) Displacement distribution in an element.

Choosing a finite element grid in the (θ-φ)-plane, Fig. 2.1, the unknown functions F,G, and H may be represented within each finite element, Fig. 2.1, in the form

$$F(\theta,\phi) = \sum_{i=1}^{M} X_i F^i , \quad F^i = \rho^p f^i(\theta,\phi) \tag{2.8a}$$

$$G(\theta,\phi) = \sum_{i=1}^{M} X_i G^i , \quad G^i = \rho^p g^i(\theta,\phi) \tag{2.8b}$$

$$H(\theta,\phi) = \sum_{i=1}^{M} X_i H^i , \quad H^i = \rho^p h^i(\theta,\phi) \tag{2.8c}$$

in which X_i, $i = 1,2,\ldots,M$, are the nodal values of $f(\theta,\phi)$, $g(\theta,\phi)$ and $h(\theta,\phi)$; and $f^i(\theta,\phi)$, $g^i(\theta,\phi)$ and $h^i(\theta,\phi)$ are given distribution functions within the finite elements, usually chosen as polynomials in θ and φ [25].

Denoting (θ_m,ϕ_m) as the coordinates of the m^{th} node, the distribution functions must be chosen such that

$$f^i(\theta_m,\phi_m) = \begin{cases} 1, & i = 3m-2 \\ 0, & i \neq 3m-2 \end{cases} \tag{2.9a}$$

$$g^i(\theta_m,\phi_m) = \begin{cases} 1, & i = 3m-1 \\ 0, & i \neq 3m-1 \end{cases} \tag{2.9b}$$

$$h^i(\theta_m,\phi_m) = \begin{cases} 1, & i = 3m \\ 0, & i \neq 3m \end{cases} \tag{2.9c}$$

in order to accomodate three degrees of freedom at each node $m = 1,2,\ldots,M$, [25].

The variations of functions F,G, and H and their respective derivations may now be expressed as

$$\delta F = \sum_{j=1}^{M} F^j \delta X_j, \quad \delta F_\theta = \sum_{j=1}^{M} F_\theta{}^j \delta X_j, \quad \delta F_\phi = \sum_{j=1}^{M} F_\phi{}^j \delta X_j \tag{2.10a}$$

$$\delta G = \sum_{j=1}^{M} G^j \delta X_j, \quad \delta G_\theta = \sum_{j=1}^{M} G_\theta{}^j \delta X_j, \quad \delta G_\phi = \sum_{j=1}^{M} G_\phi{}^j \delta X_j \tag{2.10b}$$

$$\delta H = \sum_{j=1}^{M} H^j \delta X_j, \quad \delta H_\theta = \sum_{j=1}^{M} H_\theta{}^j \delta X_j, \quad \delta H_\phi = \sum_{j=1}^{M} H_\phi{}^j \delta X_j \tag{2.10c}$$

C.) Variational equation in an element.

Substituting Eqs. (2.6a-c) and (2.8a-c) in to Eq. (1.14), it follows that

$$\Phi_F = \sum_i \Phi_F^i X_i, \quad \Phi_{F_\theta} = \sum_i \Phi_{F_\theta}^i X_i, \ldots, \Phi_{H_\phi} = \sum_i \Phi_{H_\phi}^i X_i \qquad (2.11)$$

in which

$$\Phi_F^i = [Q(1-\lambda)+2][(\lambda+2)\rho^p f^i + (\rho^p)_\theta g^i + \rho^p g_\theta^i + \rho^p g^i \cot\theta + \frac{\rho^p}{\sin\theta} h_\phi^i]$$

$$- 2\lambda(\lambda+2)\rho^p f^i, \quad \Phi_{F_\theta}^i = \ldots,\ldots$$

$$\Phi_{H_\phi}^i = \frac{1}{\sin\theta}\{[Q(\lambda+2)\rho^p f^i + (\rho^p)_\theta g^i + \rho^p g_\theta^i + \rho^p g^i \cot\theta + \frac{\rho^p}{\sin\theta} h_\phi^i]$$

$$+ 2[\frac{\rho^p}{\sin\theta} h_\phi^i + \rho^p g^i \cot\theta + \rho^p f^i]\} \qquad (2.12)$$

Finally, substitution of Eqs. (2.7a-c) and (2.11) into variational equation (1.13) yields a discrete variational equation of the form

$$\sum_{j=1}^{M} (\sum_{i=1}^{M} k_{ij} X_j)\delta X_i = 0 \qquad (2.13)$$

in which k_{ij} are stiffness coefficients expressed as follows

$$k_{ij} = \iint_A \{\Phi_F^i F^j + \Phi_{F_\theta}^i F_\theta^j + \Phi_{F_\phi}^i F_\phi^j + \Phi_G^i G^j + \Phi_{G_\theta}^i G_\theta^j + \Phi_{G_\phi}^i G_\phi^j + \Phi_H^i H^j$$

$$+ \Phi_{H_\theta}^i H_\theta^j + \Phi_{H_\phi}^i H_\phi^j\} \sin\theta \, d\theta d\phi \qquad (2.14)$$

Note that the stiffness matrix $[k_{ij}]$ is non-symmetric; i.e., $k_{ij} \neq k_{ji}$ in general. The variational equation (2.12) must hold for any choice of δX_i $(i = 1,\ldots,M)$, and this requires that

$$\sum_{i=1}^{M} k_{ij} X_j = 0 \qquad (i = 1,\ldots,M). \qquad (2.15)$$

This is a system of M linear homogeneous algebraic equations, representing an eigenvalue problem. All stiffness coefficients k_{ij}, not just the diagonal ones, depend on singularity exponent λ, and so the eigenvalue problem is of the generalized type. Furthermore, it is easy to see that k_{ij} are polynomials in λ, as well as in Poisson ratio ν (when multiplied by $1-2\nu$);

$$k_{ij} = k_{ij}(\lambda,\nu). \qquad (2.16)$$

D.) Integration for the stiffness matrix.

The finite elements are chosen as four-node quadrilaterals in the $(\theta-\phi)$-plane. Three degrees of freedom are placed at each node in order to

accomodate the displacement field (f,g,h). The basic distribution shape function $f^i(\theta,\phi)$, $g^i(\theta,\phi)$, and $h^i(\theta,\phi)$ on the original rectangle are considered as bilinear in θ and ϕ, i.e., $a + b\theta + c\phi + d\theta\phi$*.

Following the conventional methods found in finite element techniques [25,27], the finite element stiffness matrix is obtained by mapping a general quadrilateral, Fig. (2.1), into a unit square, Fig. (2.2), given by the transformation

$$\begin{Bmatrix} \theta \\ \phi \end{Bmatrix} = \begin{bmatrix} \underset{\sim}{B} & , & \underset{\sim}{0} \\ \underset{\sim}{0} & , & B \end{bmatrix} \begin{Bmatrix} \underset{\sim}{T} \\ \underset{\sim}{F} \end{Bmatrix} \tag{2.17}$$

where

$$\underset{\sim}{B} = (B_1, B_2, B_3, B_4) \tag{2.18a}$$

$$B_i = \tfrac{1}{4}(1+\theta^*\theta_i^*)(1+\phi^*\phi_j^*),\ i = k,l,m,n \tag{2.18b}$$

$$\underset{\sim}{T} = (\theta_K, \theta_L, \theta_M, \theta_N)^T \tag{2.18c}$$

$$\underset{\sim}{F} = (\phi_K, \phi_L, \phi_M, \phi_N)^T \tag{2.18d}$$

in which the subscript T denotes a transpose; (θ_i^*, ϕ_i^*) are the corners $(\pm 1, \pm 1)$ of the unit square numbered clockwise beginning at (-1,-1); (θ_I, ϕ_I) are the corresponding corner coordinates of the quadrilateral

*In retrospect, it appears that much more accurate results could have been obtained with higher-order finite elements.

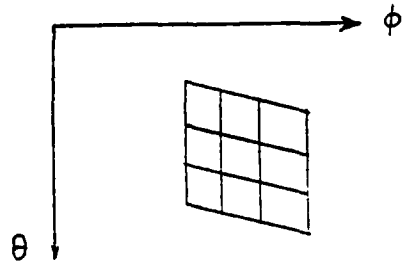

Fig. 2.1: Finite element grid in the $(\theta\text{-}\phi)$-plane.

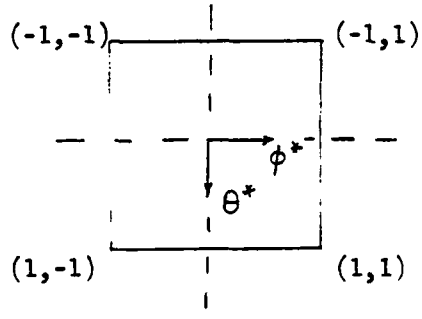

Fig. 2.2: Unit square, obtained by mapping a general element from Fig. 2.1, using Eq. (2.17).

element; (θ^*,ϕ^*) are the coordinates of a general point within the unit square; and (θ,ϕ) are the coordinates of the corresponding point on the quadrilateral element.

Carrying out the foregoing transformation of variables θ and ϕ into θ^* and ϕ^*, the stiffness coefficients given by Eq. (2.14) may be expressed in the well-known manner [25]:

$$k_{ij} = \iint_A \Psi(\theta,\phi)d\theta d\phi = \int_{-1}^{1}\int_{-1}^{1} \Psi^*(\theta^*,\phi^*)d\theta^* d\phi^* \tag{2.19}$$

in which $\Psi(\theta,\phi)$ is the integrand of Eq. (2.14); and where

$$\Psi^*(\theta^*,\phi^*) = |J|\ \Psi(\theta^*,\phi^*) \tag{2.20a}$$

$$J = \begin{bmatrix} \partial\theta/\partial\theta^* & , & \partial\phi/\partial\theta^* \\ \partial\theta/\partial\phi^* & , & \partial\phi/\partial\phi^* \end{bmatrix} \tag{2.20b}$$

J being the Jacobian of the transformation given in Eq. (2.16).

The integration of the second term in Eq. (2.18) is carried out numerically by the Gaussian quadrature formula [25], over nine points a_i of weights H_i:

$$k_{ij} = \sum_{p=1}^{3}\sum_{q=1}^{3} H_p H_q\ \Psi^*(a_p,a_q) \tag{2.21}$$

in which $a_3 = -a_1 = 0.7745966692414 93$; $a_2 = 0$; $H_1 = H_3 = 5/9$; $H_2 = 8/9$.

A (12 x 12) stiffness matrix is thus obtained for all elements, which are then incorporated element by element into the final global stiffness matrix k_{ij}. A detailed Fortran program is given in Appendix B.

E.) Comment.

The treatment of line singularities described in Section 2.2A may be thought of in a different light. The representation of the displacements with the approximate form $[u,v,w] = r^{\lambda}\rho^{p}[f(\theta,\phi),g(\theta,\phi),h(\theta,\phi)]$, Eqs. (2.1a-c) can be expanded further in the series

$$[u,v,w] = \sum_{p=0,\frac{1}{2},1,\ldots}^{\infty} r^{\lambda}\rho^{p}[f(\theta,\phi),g(\theta,\phi),h(\theta,\phi)]$$

where $f(\theta,\phi)$, $g(\theta,\phi)$, $h(\theta,\phi)$ and λ can be obtained for each value of p, for a properly chosen function ρ (such as $\rho = \sin\theta$). Thus, forming a more general represention of the displacement field which is easily accessible to numerical methods for its solution as shown in Section 2.2 B-D. Indeed, the above equation is not the most general expression because there exists the possibility of some other representation for the displacement which might be intuitively obtained. However complicated, general, or exact series representation one may choose, the most interesting and practical term in the proposed series is that whose stress field dominates over all other possible terms

present in the complete solution. Since displacements behave like r^{λ} and stresses like $r^{\lambda-1}$ as $r \to 0$, the smallest value for λ must be sought.

2.3 Methods for the Eigenvalue Search

The problem is to find the smallest eigenvalue λ such that $Re(\lambda) > -\frac{1}{2}$. Again, λ is limited to $Re(\lambda) > -\frac{1}{2}$ for the strain energy to be bounded near the point of singularity. Various methods might be available for the eigenvalue search connected with Eq. (2.14) [3,28]. Two methods are presented, but only the most efficient one is chosen to solve the problem.

A.) Quadratic polynomial on the eigenvalue problem.

It is interesting to note that the stiffness coefficients of $k_{ij}(\lambda)$, Eq. (2.13) are quadratic polynomials in λ, see Eq. (2.11). Hence, the matrix $k_{ij}(\lambda)$ may be written as

$$[k_{ij}] = \underset{\sim}{k} = \underset{\sim}{a} + \underset{\sim}{b}\lambda + \underset{\sim}{c}\lambda^2 \tag{2.22}$$

where $\underset{\sim}{a}$, $\underset{\sim}{b}$, and $\underset{\sim}{c}$ are real square matrices independent of λ and of size (M x M), M being the number of nodes. So, Eq. (2.14), $\underset{\sim}{k}\,\underset{\sim}{X} = 0$, takes the form:

$$\underset{\sim}{a}\,\underset{\sim}{X} + \lambda\,\underset{\sim}{b}\,\underset{\sim}{X} + \lambda^2\,\underset{\sim}{c}\,\underset{\sim}{X} = 0 \tag{2.23}$$

where $\underset{\sim}{X}$ is the column matrix of X_i. This expression is a nonsymmetric quadratic eigenvalue problem on λ

In an iterative eigenvalue search, k_{ij} would have to be repeatedly evaluated for various λ-values. Obviously, Eq. (2.22) allows reduction in the number of computations needed to obtain k_{ij}, since it sufficies to determine three matrices of sizes (M x M) independent of λ, and then evaluate $\underline{k}$ given λ till Eq. (2.14) is satisfied.

Furthermore, it is useful to observe that complex eigenvalues of Eq. (2.14) or (2.22) can occur only in conjugate pairs, because

$$\overline{\underline{k}(\lambda)\underline{X}} = \overline{\underline{k}(\lambda)}\ \overline{\underline{X}} = \underline{k}(\bar{\lambda})\ \overline{\underline{X}} \tag{2.24}$$

so that if $\underline{k}(\lambda)\underline{X} = 0$, then also

$$\underline{k}(\bar{\lambda})\overline{\underline{X}} = 0 \tag{2.25}$$

where a superposed bar denotes a complex conjugate.

B.) *Conversion to non-homogeneous system of equations.*

The method for the eigenvalue search described in this section has been used with success in connection with other problems which lead to the equations of the type of Eq. (2.14), for the real case in Ref. [3,4] and for the complex case [6]. The method used herein will be explained in complex arithmetic which can easily be converted to real arithmetic by ignoring all the imaginary components.

Eq. (2.14) represents a large system of M homogeneous linear algebraic equations for the values X_j which belong to the nodes $j = 1,2,\ldots,M$.

$$\sum_{i=1}^{M} k_{ij}(\lambda,\nu)X_j = 0,\ i = 1,2,\ldots,M. \tag{2.26}$$

For a given value of Poisson's ratio ν, the root λ and the corresponding eigenvector $X_n(n = 1,2,\ldots,M)$, is evaluated by the following technique:

First, the matrix $k_{ij}(\lambda,\nu)$ is calculated for one chosen value of $\lambda = \lambda_R + i\lambda_I$, where $\lambda_R = Re(\lambda)$ and $\lambda_I = Im(\lambda)$. Then, the equation belonging to one of the unknowns X_n, e.g., for the m^{th} term X_m, at the surface node, is deleted from the matrix k_{ij}, and stored separately. This equation is then replaced by the equation $X_m = (1,1)$ which makes the equation system non-homogeneous.

This matrix, for the new system of equations, is non-singular, because λ is a simple root when $Im(\lambda) \neq 0$. Thus, all $X_n,(n = 1,2,\ldots,M)$ can be solved by converting standard library subroutines for banded real matrices to complex arithmetic, see Appendix C. In the case of real roots, the new matrix is normally non-singular.

Once the unknowns, X_n, are solved, the right-hand side, Q_m, of the original m-th equation is evaluated. The quantity Q_m may be regarded as a function of λ_R and λ_I, i.e.:

$$\sum_{j}^{M} k_{mj}X_j = Q_m(\lambda_R,\lambda_I) \tag{2.27}$$

After a second quantity of Q_m is evaluated for another value of λ, chosen at the beginning of this procedure, the iterative "regula falsi" method is applied to λ_R and λ_I separately, in order to find the value of λ such that Q_m will be zero, i.e., $Re(Q_m) = Im(Q_m) = 0$, thus, satisfying Eq. (2.14). Computationally, Eq. (2.14) will obviously not be satisfied exactly. In the program the iterative "regula falsi" method is used until the difference of two consecutive values of λ is of order $0(10^{-5})$, and to whose last value yielded $|Q_m| = 0(10^{-6})$*.

Accuracy and convergence can be improved when the m-th equation is chosen such that $\sum_j^M |k_{mj}|$ is the largest of all $\sum_j^M |k_{ij}|, i = 1,\ldots,M$, [6]. The search for this value was not necessary here since all of them were found to be of the same order. Nonetheless, the convergence of the iteration method is sometimes quite slow. To obtain a good initial guess, λ must be scanned in small steps, usually of about 0.05 and 0.005 for the real and imaginary parts of λ, respectively. Fig. (3.6) gives an indication of the sharply varying slope of Q_m v.s. λ for an example whose solution is real. Thus, much care is required to avoid missing the smallest root and to keep the computational time to a minimum.

The root search subroutine can be generalized further for various cases which will be used in later chapters. Note that the search for root λ may be geometrically interpreted as the intersection of the line of solution for a constant number of finite elements, N, with the vertical line ν = constant, see Eq. (2.15) and Fig. (3.5). For

*The difference in initial guesses for λ is in the order $0(h^{-2})$ and their corresponding Q_m values usually range in the order $0(h^2)$ to $0(h^4)$.

regions when this curve, λ v.s. ν, turns sharply upwards (or downwards), the subroutine converges poorly or not at all, i.e., either the intersections occur at very small angles or no intersection seems to exist. To circumvent this difficulty, Eq. (2.16) may be considered as an eigenvalue problem for ν at a fixed λ. Then, the solution represents an intersection of the line of contant N with the horizontal line λ = constant.

Similarly, when the problem is to find orientation angles β and γ for their crack front edges and planes, or notches with opening α and orientation β and γ, for which the values of λ and ν are desired, as fixed then k_{ij} will be a function of these angles:

$$k_{ij} = k_{ij}(\lambda,\nu;\ \alpha,\beta,\gamma) \tag{2.28}$$

and Eq. (2.27) may be considered as an eigenvalue problem for α,β, and γ.

In the case of complex roots the search method is more complicated than that for the real roots. First, one must scan a region of complex $\lambda = (\lambda_R,\lambda_I)$. At each point the quantity $[\mathrm{Re}(Q_m)^2 + \mathrm{Im}(Q_m)^2]^{-1}$ is computed and a plot is constructed. Once a peak is noticed in the plot, then the "regula falsi" method is performed in the following manner:

> Two values for λ_R, chosen inside the region of the peak, are fixed. For each of the two λ_R, λ_I is iterated with respect to $\mathrm{Im}(Q_m)$ and when it converges $\mathrm{Re}(Q_m)$ is stored. The third λ_R value is iterated with respect to the two previous $\mathrm{Re}(Q_m)$.

Again, it is fixed and λ_I is iterated untill λ_I converges. And so on. Once λ_R has converged, a final iteration is performed on λ_I. Thus, a complex root is approximately computed.

C.) Eigenvalue convergence.

Interesting results can be obtained when the convergence rate of the numerical eigenvalues, computed for different number of grid subdivisions, is studied carefully. Indeed, convergence studies can at times be questionable, especially when sophisticated manipulations are needed to obtain numerical values. However, its use is justified when a convergence method constantly agrees with exact, or nearly exact, solutions to the same problem based on a completely independent approach.

For example, it is well known that the ordinary finite element method exhibits quadratic convergence (or it has an error of the order $O(h^2)$), provided that there are no singularities within the domain [26]. That is, functions f, g, and h and their gradients are non-singular, $p = \frac{1}{2}$, see Section (II-2). So, the convergence of the eigenvalue λ should also be quadratic. When singularities are present, e.g., $p = 0$, then the convergence is less than quadratic and the error E is of the order $O(h^m)$, where h is the size of the element and m the convergence rate. Then, noting that ($\sim$denoting proportionality)

$$h^2 \sim 1/N \tag{2.29}$$

and

$$E \sim k/N \tag{2.30}$$

where N is the number of finite elements and k a constant, possibly dependent on Q

$$Q = 2\nu/(1-2\nu) \tag{2.31}$$

These relations should hold accurately when N is sufficiently large. Hence,

$$E = \lambda_N - \lambda_e \sim k/N \tag{2.32}$$

where, λ_N is the computed value using N finite elements and λ_e the exact solution. Then, Eq. (2.30) can be written as

$$\log E = \log k + m \log \sqrt{N} \tag{2.33}$$

If a quadratic convergence is present, expression (2.31) must exhibit a straight line of slope m = 2 for sufficiently large N when log E is plotted versus log $\sqrt{N}$. Otherwise, $|m| < 2$. This observation can be used to advantage in extrapolating the convergence pattern and estimating the results for $N \to \infty$, or $h \to 0$.

D.) An extrapolation technique.

Many extrapolation techniques exist in the literature, most referring to particular problems [23,24] based on the h^m extrapolation.

This idea was first suggested by Richardson [29] and a fuller treatment was later given by Richardson and Grant [8]. The latter deviced an extrapolation formula, better known as the "deferred approach to the limit", in which h represents the average size of the interval divisions. This method may be extended here to suit the problems in question.

If λ, is the solution at the end of an interval obtained by using $h = h_1 \sim 1//N_1$ and λ_2 is the solution at the end of the same interval using the same formula but with $h = h_2 \sim 1//N_2$, the extrapolation

$$\lambda_{extrap.} = \frac{\lambda_1 h_2^m - \lambda_2 h_1^m}{h_2^m - h_1^m} \tag{2.34}$$

gives an improved approximation over the linear extrapolation ($m = 1$) provided that:

i.) the total round-off error is negligible

ii.) both h are small enough for the error to be proportional to h^m, i.e. $E = O(h^m)$.

When N is too large, there is a danger that round-off error will build-up to substantial proportions. Thus far, this error has not yet been detected, even with largest system of equations used here: 975 simultaneous equations belonging to 288 elements. Hence, condition (i.) may be considered to hold for the large computers available today.

The convergence rate m, in condition (ii.) is a seldomly known value, yet, it is of most importance for extrapolation studies. Then, the question arises for its value which would apply to these problems. Its assessment will now be analyzed.

Extending the Richardson's h^m extrapolation formula, Eq. (2.32), which is based on the two conditions mentioned earlier, the convergence pattern can be exploited further to greatly improve the accuracy of the results with the additional provision that the grids for various subdivisions are all similar and generated according to the same rule imposed at the beginning of the problem. Let λ_N be the root obtained when N number of finite elements is used. The following extrapolation technique is proposed.

Plot the values of root λ_N versus $1000/N^{n/2}$ for various chosen values of n. The convergence rate m = n which gives the best straight-line fit, as indicated by the least sum of absolute deviations, is selected. Then, a regression line is passed to obtain the extrapolated value as $N \to \infty$, or $h \to 0$.

Obviously, this technique must work if the assumption that the error is of the order $0(h^m) = 0(N^{-m/2})$ holds. Note that all eigenvalues λ_N are included, not just two, as in Eq. (2.32). Hence, the value m, obtained in such manner, is the effective convergence rate.

This technique can be interpreted in the following manner:

Let $\lambda_i, i = 1,2,\ldots,K$, be the roots obtained by using the finite element method, e.g., N = 128,72,32,18; then i = 1,2,3,4. Let

$$X_i = h_i^n = 1000/N^{n/2} \tag{2.35}$$

be the X-coordinate of the λ_i-root for a convergence rate n, where n can vary continuously. Construct a rectangular coordinate system $\lambda - x$, as shown in Fig. 3.4. The data points in Fig. 3.4 are from a typical example to be studied in the next chapter.

The best-fit straight-line $\lambda = a + bx$ through the data points is determined by the minimum value of the sum of squares of the diviations δ_i:

$$S(n) = \sum_{i=1}^{K} (\delta_i)^2 = \sum_{i=1}^{K} [\lambda_i - a(n) - b(n)X_i(n)] \tag{2.36}$$

where $a = a(n)$ and $b = b(n)$ are the coefficients of the straight-line. Henceforth, the subscript i will be dropped because the summations are understood to be over all K data points. For S to be a minimum for a particular n-value:

$$\frac{\partial S}{\partial a} = \frac{\partial S}{\partial b} = 0 \tag{2.37}$$

which yields

$$b = \frac{K\sum X_i\lambda_i - \sum X_i \sum \lambda_i}{K\sum X_i^2 - \sum X_i \sum X_i} \tag{2.38a}$$

$$a = \frac{1}{K} \left(\sum \lambda_i - b \sum X_i \right) \tag{2.38b}$$

The optimum value of n, for which S(n) is a total minimum is obtained by

$$\frac{\partial}{\partial n} S(n) = 0, \quad \text{at } n = m \tag{2.39}$$

from which m, the effective convergence rate, is intuitively chosen. Clearly, the extrapolated value will be a(m). The proofs that:

$$E = O(h^m) = \frac{\partial}{\partial n} S(n) = 0, \text{ at } n = m \tag{2.40}$$

or vice versa

$$\frac{\partial}{\partial n} S(n) = 0, \text{ at } n = m \;=\; E = O(h^m) \tag{2.41}$$

are beyond the scope of this work, if such theorem does indeed exist.

Unfortunately, the literature on this technique is not available. Its servicability can only be supported if it concurs with known solutions, as it will be shown to be true in the succeeding chapter.

E.) Comment.

The application or a regular finite element method to the variational equation, Eq. (1.14), is straight-forward, with the only implication being computational errors. The technique used to search

for the smallest complex eigenvalue has been proved to work successfully in [6]. An extrapolation technique based on convergence patterns is proposed. A rigorous proof that such technique must work is not given.

CHAPTER III

NUMERICAL SOLUTIONS

3.1 Introduction

The finite element method developed on the $(\theta\text{-}\phi)$-plane and applied to the variational equation derived on the unit sphere is of general applicability. This method can now be used to obtain the solution for a crack whose front edge and plane inclination angles are of arbitrary values, see Fig. 3.18, page 103; a notch of arbitrary opening and orientation, see Fig. 3.26, page 101, and for the solution of a crack or notch with two dissimilar materials.

The analytical solution for a Mode I crack whose front edge and plane are normal to the surface, see Fig. 3.1, page 68, has been obtained by Benthem [9] and Kawai, Fugitaui, and Kumagai [10]. Significant advances, which led to highly accurate analytical solutions, have recently been made in potential theory problems by Morrison and Lewis [11] and by Keer and Parihar [12]. The former authors succeeded in obtaining a tractable differential equation by virtue of using special coordinates (conical coordinates) suited for the particular problem of charge singularities. Keer and Parihar's method, utilizing spherical coordinates, appears to have broader application and involves the use of Green's functions to formulate the problem in terms of a singular integral. The crucial step is to differentiate this integral equation to get rid of a constant right-hand side and obtain an eigenvalue problem, which is then solved numerically by Erdogan and Gupta's

method, and thus obtaining the solution for crack corner in an infinite elastic space in Mode I opening; also obtained numerically by Bazant [3], who used finite difference methods as an approach to the problem. Parihar and Keer have extended their very effective, original and elegant method to the same problem for Modes II and III singularities which is irreducible to potential theory [14a]. They have also obtained the solution for shear on a rigid corner stamp on a semi-infinite elastic body for which the solution is complex [14b]. These solutions and those of plane problems provide valuable check cases for the accuracy and correctness of the present method. In a more recent private communication,* Benthem has obtained numerical solutions not yet published of an arbitrary crack using finite difference methods applied to the differential equations of equilibrium. His solutions agree reasonably well with the results to be presented.

In the progress of this work certain limitations to the finite element method have been found. The obvious one is that for which the Poisson ratio is close to 0.5 and the term $Q = 2\nu/1-2\nu$ increases without bounds, and for which it was noted that Modes II and III are more susceptible than Mode I. Also, when the angle of inclination β for the crack front edge is close to 0 or π, see Figs. 3.10 and 3.11, page 84, numerical inaccuracies were seen; because when these domains are mapped in the $(\theta-\phi)$-plane they are distorted considerably and one would need to increase the number of finite elements until the domains are reasonably represented. A final limitation is that whenever the eigenvalue is real and larger than unity in the interation routine, λ will

*April, 1978, Delft, Netherlands

converge to exactly unity, the reason being that rotational effects will dominate, i.e., $\lambda = 1$.

3.2 Check Cases

As a first step, the program is checked for its correctness and accuracy. Various simple cases of known solution, usually given in terms of displacements in the Cartesian coordinate system, are transformed to the spherical coordinate system [7, page 37]. This is done by letting the y-axis coincide with the crack plane $\phi = 0, \pi$ at $\theta = \pi/2$; the z-axis coincide with the crack front edge, $\theta = 0$; and the x-axis being perpendicular to both, y- and z-axis, i.e., at $\phi = \pm \pi/2$, $\theta = \pi/2$, see Fig. (3.1) page 68. Then, the following transformation is allowed:

$$\begin{Bmatrix} u \\ v \\ w \end{Bmatrix} = \begin{bmatrix} \sin\theta \sin\phi & \sin\theta \cos\phi & \cos\theta \\ \cos\theta \sin\phi & \cos\theta \cos\phi & -\sin\theta \\ \cos\phi & -\sin\phi & 0 \end{bmatrix} \begin{Bmatrix} u_x \\ u_y \\ u_z \end{Bmatrix} \qquad (3.1)$$

where (u_x, u_y, u_z) is the Cartesian displacement field of the known solution.

The spherical displacement field, (u,v,w), in the domain $0 \leq \theta \leq \pi/2$, $0 \leq \phi \leq \pi$ is checked for i) continuity, ii) existence of at most first order derivatives, and iii) boundary condition requirements. Then, the field is substituted into the program by calculating the displacements at each nodal point, i.e., obtaining X_i, Eq. (2.14).

The stiffness matrix k_{ij} is subsequently computed; and Eq. (2.14) must be approximately satisfied. As an error indicator, the right-hand sides for all i were compared to the sum of their absolute terms as indicated by the condition

$$\left| \sum_{i=1}^{M} k_{ij} X_j \right| \Big/ \sum_{i=1}^{M} |k_{ij} X_j| < 10^{-4} \tag{3.2}$$

at all nodal points i, i = 1,2,...,M; for a mesh of only 32 elements. The elementary solutions for the various special cases considered here were first analyzed for their dependence on λ and ρ^p, Eqs. (2.1a-c), in order to obtain the λ and p values.

A.) Rigid body rotations.

The three body rotations allowed imply that $\lambda = 1$ and $p = 0$. For example, the rotation about the z-axis, $\theta = 0$, implies that

$$u = v = 0, \quad w = r \sin \theta \tag{3.3}$$

for which $\lambda = 1$, $p = 0$, $H(\theta,\phi) = \sin \theta$; and $F(\theta,\phi) = G(\theta,\phi) = 0$. Note that it is also possible to have $\lambda = 1$, $p = 1$, and $h(\theta,\phi) = 1$ for this particular example. Table 3.1 shows the print-out of Eqs. (2.14) and (3.2) using Eq. (3.3).

B.) Homogeneous strain field.

The only homogeneous stress field that will satisfy the free surface conditions is that which belongs to $\sigma_{yy} = 1$ (or constant), i.e.,

RHS FORCES IN R-DIRECTION

2.776E-17	2.776E-17	4.163E-17	2.776E-17	2.776E-17	2.776E-17	2.776E-17	2.776E-17	2.776E-17
7.772E-16	6.661E-16	1.332E-15	6.661E-16	6.661E-16	6.661E-16	6.661E-16	6.661E-16	6.661E-16
8.882E-16	8.882E-16	1.554E-15	1.776E-15	0.	0.	0.	0.	8.882E-16
2.887E-15	4.219E-15	2.665E-15	4.219E-15	2.442E-15	2.442E-15	2.442E-15	2.442E-15	2.442E-15
8.882E-16	8.882E-16	0.	0.	0.	0.	0.	0.	0.

RHS FORCES IN THE-DIRECTION

-8.327E-17	0.	8.327E-17	-1.110E-16	0.	0.	0.	0.	2.220E-16
4.441E-16	3.553E-15	1.554E-15	3.553E-15	1.776E-15	1.776E-15	1.776E-15	1.776E-15	4.441E-16
3.553E-15	-8.882E-16	8.882E-16	0.	0.	0.	0.	0.	0.
0.	8.882E-16	-8.882E-16	4.441E-15	1.776E-15	1.776E-15	1.776E-15	1.776E-15	2.665E-15
0.	-2.665E-15	8.882E-16	-4.441E-15	-2.665E-15	-2.665E-15	-2.665E-15	-2.665E-15	1.776E-15

RHS FORCES IN PHI-DIRECTION

4.441E-16	0.	-8.882E-16	-8.882E-16	-8.882E-16	-8.882E-16	-8.882E-16	-8.882E-16	1.000E+50
-7.994E-15	-8.882E-16	-4.441E-15	-8.882E-16	-7.994E-15	-7.994E-15	-7.994E-15	-7.994E-15	1.000E+50
-2.842E-14	-2.309E-14	-1.776E-14	-3.020E-14	-2.309E-14	-2.309E-14	-2.309E-14	-2.309E-14	1.000E+50
-1.066E-14	-1.599E-14	-1.954E-14	-1.599E-14	-1.599E-14	-1.599E-14	-1.599E-14	-1.599E-14	1.000E+50
-7.105E-15	-7.105E-15	0.	0.	0.	0.	0.	0.	1.000E+50

RHS/ABS(RHS) FORCES IN R-DIRECTION

2.807E-15	2.807E-15	4.210E-15	2.807E-15	2.807E-15	2.807E-15	2.807E-15	2.807E-15	2.807E-15
6.024E-15	5.164E-15	1.033E-14	5.164E-15	5.164E-15	5.164E-15	5.164E-15	5.164E-15	5.164E-15
2.262E-15	2.262E-15	3.958E-15	4.523E-15	0.	0.	0.	0.	2.262E-15
4.398E-15	6.427E-15	4.059E-15	6.427E-15	3.721E-15	3.721E-15	3.721E-15	3.721E-15	3.721E-15
2.320E-15	2.320E-15	0.	0.	0.	0.	0.	0.	0.

RHS/ABS(RHS) FORCES IN THE-DIRECTION

-1.671E-15	0.	1.671E-15	-2.227E-15	0.	0.	0.	0.	4.455E-15
1.292E-15	8.913E-15	3.899E-15	8.913E-15	4.456E-15	4.456E-15	4.456E-15	4.456E-15	1.292E-15
4.713E-15	-1.000E-15	1.008E-15	0.	0.	0.	0.	0.	0.
0.	7.792E-16	-7.792E-16	3.896E-15	1.558E-15	1.558E-15	1.558E-15	1.558E-15	2.625E-15
0.	-2.735E-15	9.110E-16	-4.558E-15	-2.735E-15	-2.735E-15	-2.735E-15	-2.735E-15	1.822E-15

RHS/ABS(RHS) FORCES IN PHI-DIRECTION

1.709E-15	0.	-1.709E-15	-1.709E-15	-1.709E-15	-1.709E-15	-1.709E-15	-1.709E-15	1.000E+00
-5.290E-15	-2.939E-16	-1.469E-15	-2.939E-16	-2.645E-15	-2.645E-15	-2.645E-15	-2.645E-15	1.000E+00
-1.010E-14	-4.135E-15	-3.101E-15	-5.407E-15	-4.135E-15	-4.135E-15	-4.135E-15	-4.135E-15	1.000E+00
-2.921E-15	-2.191E-15	-2.678E-15	-2.191E-15	-2.191E-15	-2.191E-15	-2.191E-15	-2.191E-15	1.000E+00
-3.549E-15	-1.799E-15	0.	0.	0.	0.	0.	0.	1.000E+00

Table 3.1: Numberical values at nodal points for rigid body rotation

in the y-axis direction ($\theta = \pi/2$, $\phi = 0$). Ignoring rigid body displacements already considered in Section A, this field yields:

$$(u_x, u_y, u_z) = (-\nu x, y, -\nu z) \tag{3.4}$$

Then, after using the transformation forumla, Eq. (3.2), the spherical displacement field is:

$$u(r,\theta,\phi) = r[\sin^2\theta(\cos^2\phi - \nu \sin^2\phi) - \nu \cos^2\theta] \tag{3.5a}$$

$$v(r,\theta,\phi) = r[\sin\theta \cos\theta(\cos^2\phi - \nu \sin^2\phi + \nu)] \tag{3.5b}$$

$$w(r,\theta,\phi) = r[-\sin\theta \sin\phi \cos\phi(1 + \nu)] \tag{3.5c}$$

for which $\lambda = 1$ and $p = 0$. The functions $F(\theta,\phi)$, $G(\theta,\phi)$ and $H(\theta,\phi)$ would then be the expressions inside the brackets of u,v, and w, respectively. If Poisson's ratio $\nu = 0$, then $\lambda = 1$ and $p = 1$ can be considered, and

$$f(\theta,\phi) = \sin\theta \cos^2\phi \tag{3.6a}$$

$$g(\theta,\phi) = \cos\theta \cos^2\phi \tag{3.6b}$$

$$h(\theta,\phi) = -\sin\phi \cos\phi \tag{3.6c}$$

RHS FORCES IN R-DIRECTION

-1.359E-05	-4.411E-05	-8.498E-05	-1.259E-04	-1.428E-04	-1.259E-04	-8.498E-05	-4.411E-05	-1.359E-05
-3.576E-04	-9.037E-04	-1.359E-03	-1.814E-03	-2.002E-03	-1.814E-03	-1.359E-03	-9.037E-04	-3.576E-04
1.201E-03	1.185E-03	-1.752E-03	-4.689E-03	-5.905E-03	-4.689E-03	-1.752E-03	1.185E-03	1.201E-03
6.092E-03	9.013E-03	1.359E-03	-6.295E-03	-9.466E-03	-6.295E-03	1.359E-03	9.013E-03	6.092E-03
4.547E-03	6.968E-03	1.837E-03	-3.295E-03	-5.420E-03	-3.295E-03	1.837E-03	6.968E-03	4.547E-03

RHS FORCES IN THE-DIRECTION

-2.733E-04	-5.752E-04	-6.441E-04	-7.129E-04	-7.414E-04	-7.129E-04	-6.441E-04	-5.752E-04	-2.733E-04
-9.399E-05	-7.568E-04	-2.130E-03	-3.504E-03	-4.072E-03	-3.504E-03	-2.130E-03	-7.568E-04	-9.399E-05
4.641E-03	7.150E-03	2.006E-03	-3.139E-03	-5.269E-03	-3.139E-03	2.006E-03	7.150E-03	4.641E-03
6.657E-03	1.087E-02	4.967E-03	-9.349E-04	-3.380E-03	-9.349E-04	4.967E-03	1.087E-02	6.657E-03
-1.094E-02	-1.894E-02	-1 183E-02	-4.729E-03	-1.785E-03	-4.729E-03	-1.183E-02	-1.894E-02	-1.094E-02

RHS FORCES IN PHI-DIRECTION

3.067E-03	-1.746E-03	-2.470E-03	-1.746E-03	1.012E-12	1.746E-03	2.470E-03	1.746E-03	-4.102E+40
1.709E-02	-1.007E-02	-1.424E-02	-1.007E-02	5.834E-12	1.007E-02	1.424E-02	1.007E-02	-4.102E+40
3.160E-02	-1.855E-02	-2.623E-02	-1.855E-02	1.075E-11	1.855E-02	2.623E-02	1.855E-02	-4.102E+40
4.130E-02	-2.416E-02	-3.417E-02	-2.416E-02	1.399E-11	2.416E-02	3.417E-02	2.416E-02	-4.102E+40
2.236E-02	-1.306E-02	-1.847E-02	-1.306E-02	7.571E-12	1.306E-02	1.847E-02	1.306E-02	-4.102E+40

RHS/ABS(RHS) FORCES IN R-DIRECTION

-5.091E-04	-9.656E-04	-2.777E-03	-9.346E-03	-1.826E-02	-9.346E-03	-2.777E-03	-9.656E-04	-5.091E-04
-1.036E-03	-1.530E-03	-3.430E-03	-1.048E-02	-2.004E-02	-1.048E-02	-3.430E-03	-1.530E-03	-1.036E-03
1.045E-03	6.032E-04	-1.351E-03	-8.561E-03	-2.003E-02	-8.561E-03	-1.351E-03	6.032E-04	1.045E-03
2.902E-03	2.514E-03	5.815E-04	-6.612E-03	-1.994E-02	-6.612E-03	5.815E-04	2.514E-03	2.902E-03
3.476E-03	3.120E-03	1.270E-03	-5.689E-03	-1.963E-02	-5.689E-03	1.270E-03	3.120E-03	3.476E-03

RHS/ABS(RHS) FORCES IN THE-DIRECTION

-2.148E-03	-2.646E-03	-4.434E-03	-1.135E-02	-2.060E-02	-1.135E-02	-4.434E-03	-2.646E-03	-2.148E-03
-1.171E-04	-5.550E-04	-2.310E-03	-8.798E-03	-1.700E-02	-8.798E-03	-2.310E-03	-5.550E-04	-1.171E-04
2.856E-03	2.600E-03	1.081E-03	-4.029E-03	-1.141E-02	-4.029E-03	1.081E-03	2.600E-03	2.856E-03
3.527E-03	3.413E-03	2.298E-03	-1.037E-03	-6.174E-03	-1.037E-03	2.298E-03	3.413E-03	3.527E-03
-1.112E-02	-1.151E-02	-9.798E-03	-8.311E-03	-3.993E-03	-8.311E-03	-9.798E-03	-1.151E-02	-1.112E-02

RHS/ABS(RHS) FORCES IN PHI-DIRECTION

3.020E-02	-7.519E-03	-9.078E-03	-9.598E-03	9.498E-12	9.598E-03	9.078E-03	7.519E-03	-1.000E+00
2.682E-02	-7.451E-03	-8.997E-03	-9.512E-03	9.408E-12	9.512E-03	8.997E-03	7.451E-03	-1.000E+00
2.486E-02	-7.160E-03	-8.782E-03	-9.335E-03	9.234E-12	9.335E-03	8.782E-03	7.160E-03	-1.000E+00
2.430E-02	-6.841E-03	-8.541E-03	-9.134E-03	9.029E-12	9.134E-03	8.541E-03	6.841E-03	-1.000E+00
2.224E-02	-6.474E-03	-8.261E-03	-8.903E-03	8.811E-12	8.903E-03	8.261E-03	6.474E-03	-1.000E+00

Table 3.2: Numerical values at nodal points to homogeneous strain field

would apply. Table 3.2 shows the print-out of Eqs. (2.14) and (3.2) using Eqs. (3.6a-c).

C.) Plane-strain solutions.

The solutions for near-tip plane-strain fields may be found in references [ ] for opening I mode, shear mode II, and antiplane mode III. Obviously the antiplane mode field cannot satisfy all stress boundary conditions at the surface $\theta = \pi/2$, or the nodes which belong to the body surface in Eq. (2.14). In this case only the fulfillment of the equilibrium equations for the interior nodes was checked. As an example, the displacement field for mode I opening is [12]:

$$u = C\sqrt{r}\,[\sin\theta(A + B)] \tag{3.7a}$$

$$v = C\sqrt{r}\,[\cos\theta(A + B)] \tag{3.7b}$$

$$w = C\sqrt{r}\,[A-B] \tag{3.7c}$$

where $C = -K_I\sqrt{2}\,(1+\nu^1)/E^1$; $E^1 = E/(1-\nu^2)$; $\nu^1 = \nu/(1-\nu)$

$$A = [2(1-\nu^1) - \cos^2\alpha]\sin\alpha\sin\phi$$

$$B = [1 - 2\nu^1 + \sin^2\alpha]\cos\alpha\sin\phi \tag{3.8}$$

$$\alpha = (\phi - \pi)/2$$

RHS FORCES IN R-DIRECTION

-2.714E-02	-1.283E-02	-1.212E-02	-1.220E-02	-1.227E-02	-1.232E-02	-1.236E-02	-1.238E-02	-6.195E-03
-5.162E-02	-2.798E-05	-2.836E-05	-2.860E-05	-2.895E-05	-2.915E-05	-2.930E-05	-2.939E-05	-1.471E-05
-6.361E-02	-2.055E-06	-2.266E-06	-2.446E-06	-2.593E-06	-2.709E-06	-2.791E-06	-2.841E-06	-1.429E-06
-7.161E-02	2.210E-05	2.206E-05	2.202E-05	2.199E-05	2.197E-05	2.195E-05	2.194E-05	1.097E-05
-3.721E-02	1.594E-05	1.596E-05	1.597E-05	1.598E-05	1.598E-05	1.599E-05	1.599E-05	7.995E-06

RHS FORCES IN THE-DIRECTION

-2.441E-02	-1.192E-02	-1.201E-02	-1.209E-02	-1.216E-02	-1.221E-02	-1.225E-02	-1.227E-02	-6.138E-03
-3.414E-02	5.679E-05	5.714E-05	5.743E-05	5.767E-05	5.786E-05	5.799E-05	5.807E-05	2.905E-05
-2.611E-02	7.029E-05	7.077E-05	7.117E-05	7.151E-05	7.177E-05	7.195E-05	7.207E-05	3.605E-05
-1.413E-02	4.774E-05	4.808E-05	4.836E-05	4.860E-05	4.878E-05	4.891E-05	4.899E-05	2.451E-05
-2.617E-03	-3.777E-04	-3.807E-04	-3.833E-04	-3.854E-04	-3.870E-04	-3.882E-04	-3.889E-04	-1.946E-04

RHS FORCES IN PHI-DIRECTION

-6.676E-03	-2.904E-03	-2.502E-03	-2.095E-03	-1.682E-03	-1.265E-03	-8.450E-04	-4.230E-04	1.103E+37
-1.131E-02	1.834E-05	1.580E-05	1.323E-05	1.062E-05	7.987E-06	5.336E-06	2.671E-06	1.103E+37
-1.257E-02	2.034E-05	1.753E-05	1.467E-05	1.178E-05	8.859E-06	5.918E-06	2.963E-06	1.103E+37
-1.335E-02	2.157E-05	1.858E-05	1.556E-05	1.249E-05	9.394E-06	6.275E-06	3.141E-06	1.103E+37
-6.803E-03	1.099E-05	9.470E-06	7.927E-06	6.365E-06	4.787E-06	3.198E-06	1.601E-06	1.103E+37

RHS/ABS(RHS) FORCES IN R-DIRECTION

-6.200E-03	-1.372E-03	-1.372E-03	-1.372E-03	-1.373E-03	-1.373E-03	-1.374E-03	-1.374E-03	-1.374E-03
-4.837E-03	-1.308E-06	-1.316E-06	-1.323E-06	-1.328E-06	-1.332E-06	-1.335E-06	-1.337E-06	-1.338E-06
-4.836E-03	-7.798E-08	-8.535E-08	-9.153E-08	-9.655E-08	-1.004E-07	-1.032E-07	-1.049E-07	-1.054E-07
-4.836E-03	7.450E-07	7.379E-07	7.320E-07	7.272E-07	7.236E-07	7.211E-07	7.196E-07	7.191E-07
-4.836E-03	1.034E-06	1.027E-06	1.021E-06	1.017E-06	1.013E-06	1.011E-06	1.009E-06	1.009E-06

RHS/ABS(RHS) FORCES IN THE-DIRECTION

-6.229E-03	-1.534E-03	-1.537E-03	-1.539E-03	-1.542E-03	-1.545E-03	-1.548E-03	-1.551E-03	-1.551E-03
-4.736E-03	3.963E-06	3.962E-06	3.962E-06	3.963E-06	3.965E-06	3.968E-06	3.972E-06	3.972E-06
-4.668E-03	6.353E-06	6.360E-06	6.368E-06	6.377E-06	6.387E-06	6.398E-06	6.410E-06	6.410E-06
-4.489E-03	7.783E-06	7.809E-06	7.835E-06	7.863E-06	7.892E-06	7.922E-06	7.953E-06	7.953E-06
-3.710E-03	-3.084E-04	-3.146E-04	-3.211E-04	-3.277E-04	-3.347E-04	-3.418E-04	-3.493E-04	-3.493E-04

RHS/ABS(RHS) FORCES IN PHI-DIRECTION

-2.524E-03	-6.215E-04	-6.077E-04	-5.893E-04	-5.639E-04	-5.260E-04	-4.639E-04	-3.425E-04	1.000E+00

-2.056E-03	1.852E-06	1.821E-06	1.781E-06	1.723E-06	1.635E-06	1.483E-06	1.160E-06	1.000E+00
-2.071E-03	1.850E-06	1.820E-06	1.779E-06	1.722E-06	1.634E-06	1.483E-06	1.161E-06	1.000E+00
-2.107E-03	1.860E-06	1.832E-06	1.793E-06	1.739E-06	1.655E-06	1.510E-06	1.196E-06	1.000E+00
-2.098E-03	1.853E-06	1.824E-06	1.784E-06	1.728E-06	1.643E-06	1.495E-06	1.177E-06	1.000E+00

Table 3.3: Numerical values at nodal points for near-tip plane strain field

RHS FORCES IN R-DIRECTION

-3.771E-06	-3.573E-10	-3.603E-10	-3.629E-10	-3.650E-10	-3.666E-10	-3.678E-10	-3.685E-10	-1.844E-10
-5.274E-05	-7.460E-09	-7.520E-09	-7.570E-09	-7.612E-09	-7.644E-09	-7.667E-09	-7.681E-09	-3.843E-09
-1.879E-04	-2.737E-08	-2.759E-08	-2.777E-08	-2.793E-08	-2.804E-08	-2.813E-08	-2.818E-08	-1.410E-08
-4.117E-04	-5.949E-08	-5.996E-08	-6.036E-08	-6.069E-08	-6.095E-08	-6.113E-08	-6.125E-08	-3.064E-08
-1.297E-04	3.471E-04	3.498E-04	3.522E-04	3.541E-04	3.556E-04	3.567E-04	3.573E-04	1.788E-04

RHS FORCES IN THE-DIRECTION

-1.536E-04	-2.166E-08	-2.164E-08	-2.179E-08	-2.191E-08	-2.201E-08	-2.208E-08	-2.212E-08	-1.107E-08
-9.200E-04	-1.369E-07	-1.380E-07	-1.389E-07	-1.396E-07	-1.402E-07	-1.406E-07	-1.409E-07	-7.050E-08
-1.831E-03	-2.672E-07	-2.693E-07	-2.711E-07	-2.726E-07	-2.737E-07	-2.745E-07	-2.750E-07	-1.376E-07
-2.724E-03	-3.845E-07	-3.876E-07	-3.902E-07	-3.923E-07	-3.940E-07	-3.952E-07	-3.959E-07	-1.981E-07
-7.864E-04	1.745E-03	1.759E-03	1.771E-03	1.780E-03	1.788E-03	1.793E-03	1.797E-03	8.988E-04

RHS FORCES IN PHI-DIRECTION

-3.023E-05	5.466E-09	4.710E-09	3.942E-09	3.165E-09	2.381E-09	1.590E-09	7.961E-10	-4.101E+40
-1.815E-04	3.198E-08	2.756E-08	2.307E-08	1.852E-08	1.393E-08	9.305E-09	4.658E-09	-4.101E+40
-3.625E-04	6.389E-08	5.505E-08	4.608E-08	3.700E-08	2.783E-08	1.859E-08	9.305E-09	-4.101E+40
-5.427E-04	9.564E-08	8.241E-08	6.898E-08	5.538E-08	4.166E-08	2.783E-08	1.393E-08	-4.101E+40
-1.663E-04	3.085E-04	2.658E-04	2.225E-04	1.787E-04	1.344E-04	8.977E-05	4.494E-05	-4.101E+40

RHS/ABS(RHS) FORCES IN R-DIRECTION

-4.837E-03	-2.288E-07	-2.289E-07	-2.291E-07	-2.292E-07	-2.293E-07	-2.295E-07	-2.295E-07	-2.296E-07
-4.837E-03	-3.415E-07	-3.416E-07	-3.417E-07	-3.418E-07	-3.419E-07	-3.421E-07	-3.422E-07	-3.422E-07
-4.836E-03	-3.516E-07	-3.517E-07	-3.518E-07	-3.519E-07	-3.521E-07	-3.522E-07	-3.523E-07	-3.523E-07
-4.835E-03	-3.487E-07	-3.488E-07	-3.489E-07	-3.490E-07	-3.491E-07	-3.492E-07	-3.493E-07	-3.493E-07
-2.070E-03	2.765E-03	2.766E-03	2.767E-03	2.768E-03	2.768E-03	2.769E-03	2.770E-03	2.770E-03

RHS/ABS(RHS) FORCES IN THE-DIRECTION

-4.839E-03	-3.374E-07	-3.376E-07	-3.378E-07	-3.380E-07	-3.382E-07	-3.383E-07	-3.384E-07	-3.384E-07
-4.834E-03	-3.590E-07	-3.591E-07	-3.593E-07	-3.595E-07	-3.596E-07	-3.598E-07	-3.599E-07	-3.599E-07
-4.824E-03	-3.516E-07	-3.518E-07	-3.521E-07	-3.523E-07	-3.525E-07	-3.527E-07	-3.529E-07	-3.529E-07
-4.813E-03	-3.398E-07	-3.400E-07	-3.403E-07	-3.405E-07	-3.408E-07	-3.410E-07	-3.413E-07	-3.413E-07
-2.270E-03	2.533E-03	2.536E-03	2.538E-03	2.541E-03	2.544E-03	2.546E-03	2.549E-03	2.549E-03

RHS/ABS(RHS) FORCES IN PHI-DIRECTION

-2.372E-03	2.317E-07	2.291E-07	2.256E-07	2.206E-07	2.127E-07	1.985E-07	1.654E-07	-1.000E+00
-2.345E-03	2.261E-07	2.236E-07	2.201E-07	2.152E-07	2.075E-07	1.937E-07	1.614E-07	-1.000E+00
-2.299E-03	2.245E-07	2.218E-07	2.181E-07	2.128E-07	2.045E-07	1.897E-07	1.560E-07	-1.000E+00
-2.240E-03	2.214E-07	2.182E-07	2.140E-07	2.079E-07	1.985E-07	1.821E-07	1.459E-07	-1.000E+00
-1.058E-03	1.179E-03	1.164E-03	1.143E-03	1.113E-03	1.066E-03	9.837E-04	7.987E-04	-1.000E+00

Table 3.4: Numerical values at nodal points for near-tip plane-strain field in smaller domain

Then, $\lambda = \frac{1}{2}$ and $p = 0$. These values also hold for the two remaining modes and need not be discussed further. A print-out of Eqs. (2.14) and (3.2) is shown in Table 3.3 using Eqs. (3.7a-b) and (3.8).

D.) Checks on smaller domains.

For the sake of accuracy for the method, cases B and C were rerun for domains of small notches, but still containing 32 elements. Table 3.4 shows the print-out for the example given in Section C for a notch of boundaries $0 \leq \theta \leq \pi/16$, $15\pi/16 \leq \phi \leq \pi$. As expected, the accuracy increases inside the domain but not at the boundaries, since the boundaries of the actual problem are not those of a notch.

E.) Comment.

Note that, if Eq. (2.14) is satisfied computationally, i.e., its righthand sides are small, then alternatively, the variational equation, Eq. (1.13), must be satisfied exactly. In all check cases studied above substitution of Eqs. (3.7a-c), (3.5a-c), and (3.3) into Eq. (1.13) yielded zero after long hand algebraic manipulations

3.3 Crack Plane and Front Edge Normal to Surface

The finite element computer program derived in Chapter II and outlined in Appendix B is now applied. The first problem is that of a crack whose plane and front edge are normal to the halfspace, as depicted in Fig. 3.1. Recently, Benthem [9] and Kawai, Fujitani, and Kumagai [10,30] presented analytical solutions for this problem but only for Mode I opening. A comparison of their results with the ones obtained in this chapter is made.

A.) Symmetric opening, Mode I; $p = \frac{1}{2}$.

To analyze the field near the terminal point 0, Fig. 3.1, in Mode I opening for the problem just presented it is sufficient to consider only half the domain, because there exists symmetry with respect to $\phi = \pi$. The new domain will continue to be rectangular in the $(\theta\text{-}\phi)$-plane with boundaries $0 \leq \theta \leq \pi/2$, $0 \leq \phi \leq \pi$, Fig. 3.2, or, as indicated by the domain enclosed by the slashed lines in Fig. 3.1. The stress boundary conditions on the crack surface ($\phi = 0$) and on the half-space surface ($\theta = \pi/2$) are automatically satisfied by the finite element method. The boundary conditions of $\theta = 0$ (the pole, top side of the $(\theta\text{-}\phi)$-domain in Fig. 3.2), are irrelevant and none have been imposed.

The boundary conditions on the symmetry plane ($\phi = \pi$) must properly reflect the symmetries of displacements and stresses with respect to $\phi = \pi$. Therefore, for the symmetric crack (Mode I) opening, one must impose for all nodes at $\phi = \pi$ the condition $w = 0$, i.e., $h = 0$, Eqs. (1.6c) and (2.1c). The symmetry conditions for stresses, namely $\sigma_{\phi r} = \sigma_{\phi\theta} = 0$, will be also be automatically satisfied by the finite element method as natural boundary conditions. Thus, these considerations ensure a statically determinate support for the body and at the same time properly reflect the symmetry properties.

From the work previously done on potential-related problems [3], it was expected that the displacement field should exhibit a behavior of the form

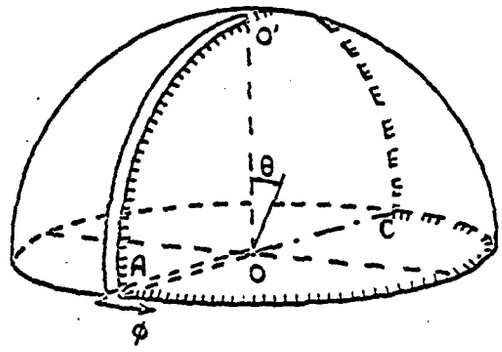

Fig. 3.1: Orthogonal crack. Spherical coordinate system at termination of crack front edge 00'at body surface, pointO. (The unit sphere is shown only to visualize the coordinate; the body is semi-infinite).

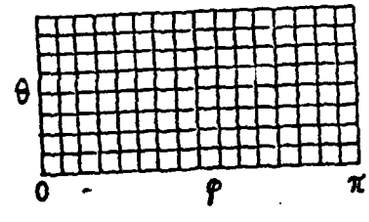

Fig. 3.2: Finite element grids used for orthogonal crack. Domain O'ACO' from Fig. 3.1 visualized in the (θ-φ)-plane.

ν/N	18	32	72	128	Benthem [9]
0.0	0.565263	0.537891	0.517198	0.50973	0.50
0.15	0.648844	0.611861	0.582320	0.570591	0.5164
0.30	0.756772	0.704681	0.662787	0.645832	0.5477
0.40	no conver.	0.826392	0.756209	0.721745	0.5868

λ/N	18	32	72	128
0.905	0.390605	0.423676	0.453383	0.466796

Table 3.5: Numerical results. Eigenvalues for orthogonal crack using N finite elements; Mode I, $p = \frac{1}{2}$.

$$u(r,\theta,\phi) = r^{\lambda}\sin^{p}\theta \; F\,(\theta,\phi) \qquad (3.8b)$$

In Ref. [3], p was suitably taken as $p = \frac{1}{2}$. This choice was motivated by the fact that the term ρ^{p}, Eq. (3.86) is dominant at finite r and as $\theta \to 0$. Unfortunately, the literature related to the method of solution used here to treat elasticity problems is non-existent. Therefore, expecting similar behaviors, p was chosen to be $p = \frac{1}{2}$ as a first attempt to solve the problem.

Symmetric opening is acquired in the program by forcing any of the nodes belonging to the crack surface ($\phi = 0$) in the ϕ-direction. Table 3.5 gives the numerical results of λ for various values of Poisson's ratio ν. For values of ν which exceed 0.4, the root search surbroutine converged very poorly, or not at all. For these cases, λ was fixed and ν was considered the root, as explained in Section 2.3 B. Some results are given at the bottom of Table 3.5. However, when ν becomes very close to 0.5, the present formulation breaks down, because the value $Q = 2/(1 - 2\nu)$, Eq. (1.8), increases without bounds. A special program would have to be written for ν close to 0.5 and for incompressible materials, $\nu = 0.5$.

Note that for the case of Poison's ratio $\nu = 0$ the computed value of the root for the finest grid used (128 elements, 459 simultaneous equations), was 0.50973. The exact solution is known to be 0.5 [9]. Thus, the computed value is still within 1.9% error. Closer estimates for the exact solution with these values, Table 3.5, can be gotten with the extrapolation technique explained in Section 2-C. Eq. (2.33)

should hold for m = -2, since p = $\frac{1}{2}$ will not introduce gradient singularity near $\theta \to 0$, [26]. The plot of log E versus log $\sqrt{N}$, Eq. (2.33), is shown in Fig. 3.3 for the case $\nu = 0$, where the exact solution is known, $\lambda_e = 0.5$. Indeed, the plot is a straight line with a slope indicating m = -2.0. Thus, for $\nu = 0$, the present formulation, p = $\frac{1}{2}$, seems to follow a systematic pattern of quadratic convergence.

This observation can be used to advantage in extrapolating the convergence pattern and estimating the results for $N \to \infty$, $h \to 0$; even for $\nu > 0$, where no error analysis can be made, since no exact solution is available. Thus, a plot of λ versus 1000/N, i.e., m = 2, is constructed in Fig. 3.4. Again, for quadratic convergence these plots should be straight lines for sufficiently large N. According to Fig. 3.4 this seems indeed to be true. Therefore, regression lines (straight lines) are extended to obtain estimates of the values as $N \to \infty$, i.e., estimates of the exact solution, as shown in Fig. 3.4. The extrapolated values, along with the numerical results of Table 3.4, are shown in Fig. 3.5 and are compared with Benthem's solution [9]. Note, however, that for the case $\nu = 0$, the extrapolation point, $N \to \infty$, falls on 0.5 ± 0.002, $\lambda = 0.5$ being the exact solution.

The fact that estimates, $N \to \infty$, significantly deviate from Benthem's results [9], as shown in Fig. 3.5, can be attributed to the <u>case p = $\frac{1}{2}$</u>: i.) The solution presents eigenvalues which are in the order of those obtained by Benthem, but unfortunately for the case p = $\frac{1}{2}$, the exact or numerical solution is unlikely to be available for comparison purposes. ii.) In light of the results to be presented in the subsequent section, this solution is correct within 1%. iii.) From (ii.),

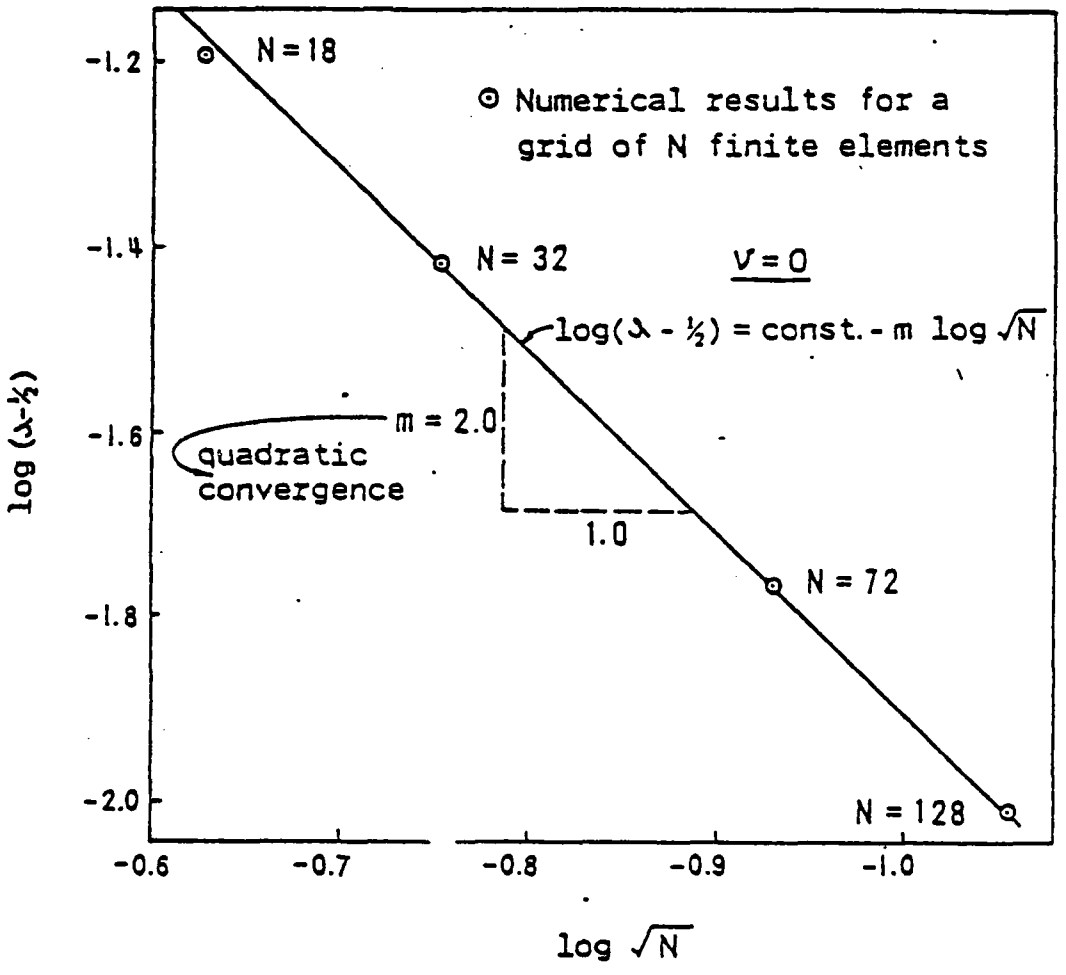

Fig. 3.3: Determination of the rate of convergence with increasing number of elements. Use of Eq. (2.33); Mode I, $p = \frac{1}{2}$.

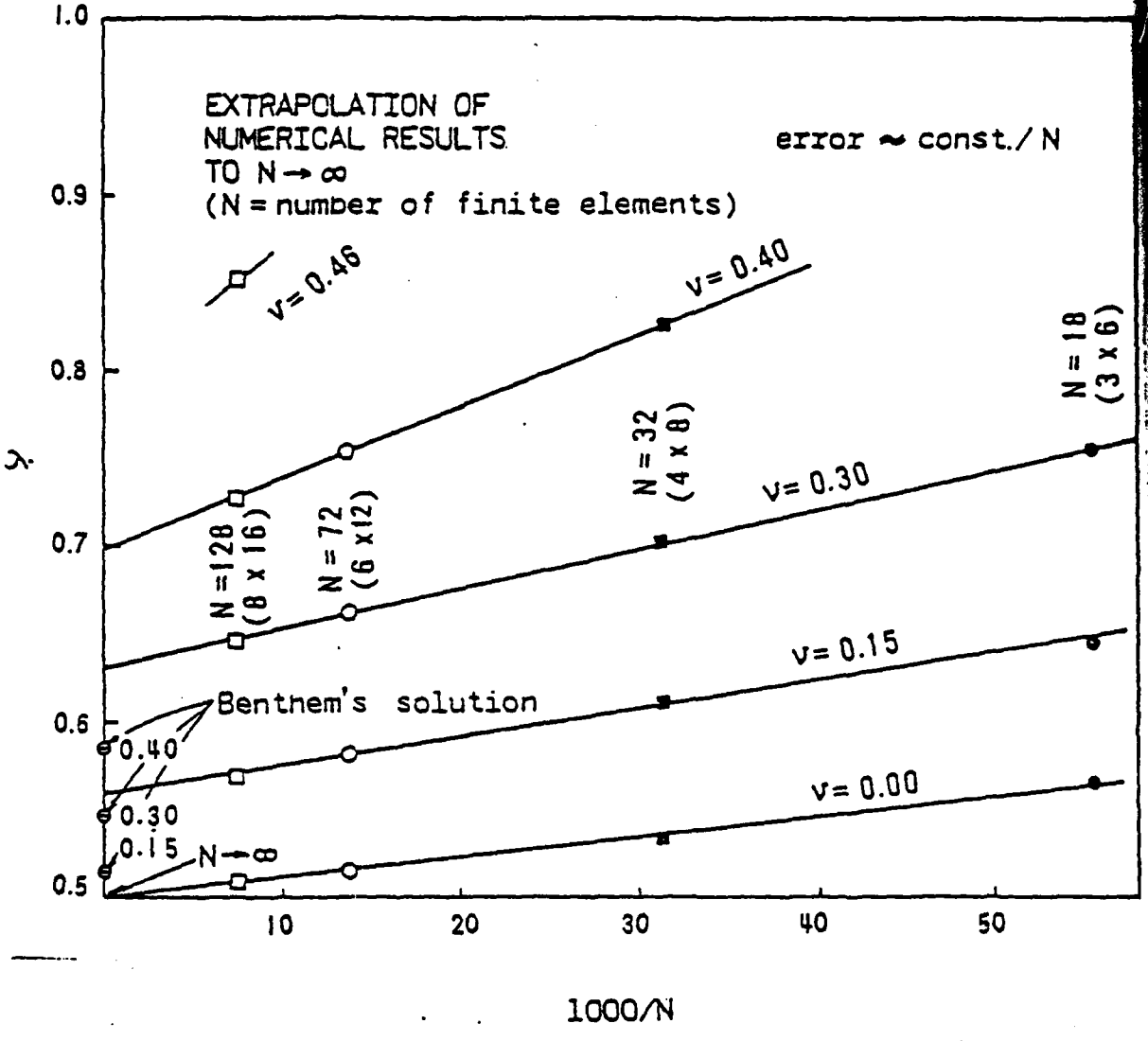

Fig. 3.4: Extrapolation of numerical results to infinite number of elements, using Eq. (2.31); Mode I, $p = \frac{1}{2}$.

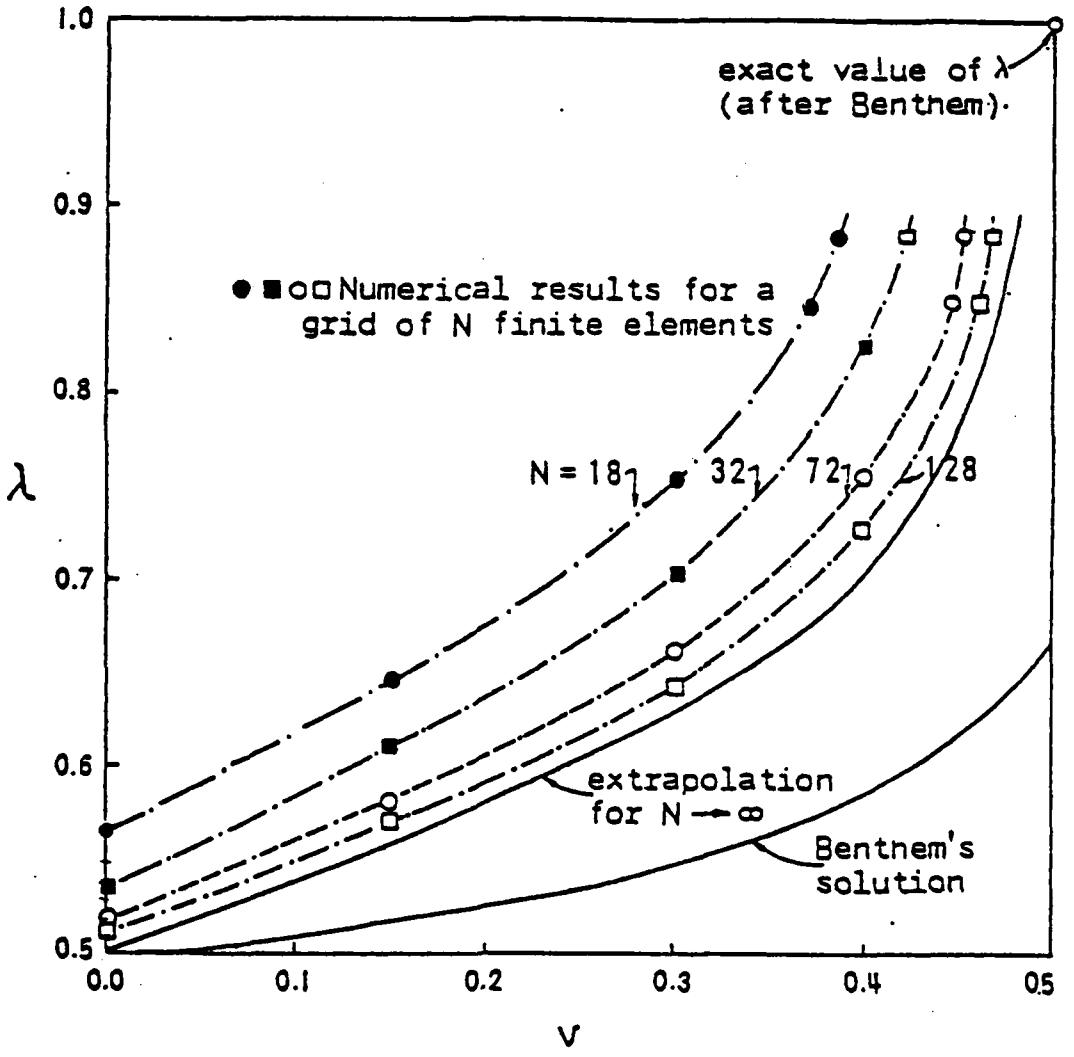

Fig. 3.5: Singularity exponent λ for various values of Poisson ratio; Mode I, $p = \frac{1}{2}$.

this solution assures the existence of an infinite enumerable eigenvalues for the problem, e.g., other solutions can be gotten for $p = 0, \frac{1}{2}, 1, \ldots,$. Hence, Fig. 3.5, is not a complete solution, unless $\nu = 0$.

B.) Symmetric opening, Mode I, $p = 0$.

The author is obliged to John P. Benthem, Professor at Delft University of Technology, for clarifying, in a private communication, the value for p from the implications of his analytical solution.

The choice $p = \frac{1}{2}$ in previous computations, Fig. 3.5, was inappropriate for the complete solution, because a restriction is prescribed to the displacements, similar to that of a generalized Fourier series which would represent the displacements, thus, limiting their complete and natural dependence on the angle θ for which the smallest eigenvalue should exist. Let $(r\rho)^p$, Eqs. (2.1a-c) be the term with the lowest exponent in the field near the singularity line, (crack front edge $\rho = \theta = 0$). Indeed, $p = \frac{1}{2}$ is the lowest p corresponding to the deformed states for crack front singularity, but where the displacement field behaves like:

$$u,v,w \sim \theta^{\frac{1}{2}} \; ; \quad \theta \to 0 \quad , \quad 0 < r < \infty \quad . \tag{3.9}$$

and stresses (displacement gradients), like:

$$\sigma \sim \theta^{-\frac{1}{2}} \; ; \; \theta \to 0 \quad , \quad 0 < r < \infty \; . \tag{3.10}$$

However, in the neighborhood of the singularity line (crack front edge, $\theta = 0$) one may have values of $p = 0, \frac{1}{2}, 1, \ldots$ etc., as was proven in Section 2.2A, Eq. (2.6). In otherwords, Eq. (3.9) does not mean that there are no displacement fields starting with the stronger exponent $p = 0$,

$$u,v,w \sim \theta^{0} \; ; \; \theta \to 0, \quad 0 < r < \infty \quad . \tag{3.11}$$

The exponent $p = 0$ does <u>not</u> give rise to stresses

$$\sigma \sim \theta^{-1} \; ; \; \theta \to 0 \; , \quad 0 < r < \infty \; . \tag{3.12}$$

In otherwords, the term $(\rho)^{p}$ does not cause any singulatiry as $p \to 0$, or $\theta \to 0$, at a finite fixed r. However, this may cause functions $F(\theta,\phi)$, and $H(\theta,\phi)$ to have gradient singularity of the type θ^{p+q}, or θ^{q}, as $r \to 0$, where $q > -1$. This singularity would be more severe than the singularity $\theta^{-\frac{1}{2}}$ associated with the planar near tip field. That terms of θ^{q}, $q > -1$ as $r \to o$ should indeed be present is indicated by Benthem's solution [9]. This will still satisfy the restriction that along the crack front edge the strain energy must remain finite, i.e., the behavior θ^{q} of the stresses along the crack front edge be such that $q > -1$.

Therefore, all finite element solutions were rerun with the exponent $p = 0$. The numerical results are given in Table 3.6, and are compared with Benthem's results. Again, as expected, the error de-

creases considerably by using larger number of elements. Also, the more Poisson's ratio ν deviates from zero the larger the error, due to the value of $Q = 2/(1 - 2\nu)$, Eq. (1.17a). Obviously, Q will induce numerical inaccuracies which are well known to occur in all numerical methods of this type.

It was fortunate that for the results obtained in the previous section, $p = \frac{1}{2}$, the convergence rate m was known "a priori' and proved grafically to be quadratic by employing Eq. (2.31). For the case $p = 0$, for which

$$f(\theta,\phi) = F(\theta,\phi),\ g(\theta,\phi) = G(\theta,\phi),\ h(\theta,\phi) = H(\theta,\phi) \qquad (3.13)$$

while $p = \frac{1}{2}$ is also present, the convergence rate must be less than quadratic. But, since the exact, or nearly exact solution is available [9], Eq. (2.31) can again be used grafically to find the value of m, as shown in Fig. 3.6. The extrapolation points (or regression lines $N \to \infty$), are shown in Fig. 3.7. These points are then compared with Benthem's solution in Fig. 3.8, showing both solution coinciding with each other within a 0.002 deviation.

Because the gradient of $F(\theta,\phi)$, $G(\theta,\phi)$ and $H(\theta,\phi)$ might tend to infinity as $\theta \to 0$, it seems appropriate to refine the grid step $\Delta\theta$ as θ decreases. Irregular rectangular net works in which $\Delta\phi$ was constant and in which $\Delta\theta$ was refined so as to keep $\Delta\theta$ roughly equal $(\sin\theta)\Delta\phi$, have been tried, using same numbers of subdivisions in both θ and ϕ directions, as shown in Fig. 3.9. Although the numerical results for the same maximum size element (regular grids)

ν/N	18	32	72	128	Eq. (2.37) m	Eq. (2.37) $\lambda_{extrap.}$	Benthem [9]
0.0	0.599526	0.557464	0.526630	0.515518	1.92	0.50048	0.50
0.15	0.633718	0.584418	0.547803	0.534580	1.90	0.51639	0.5164
0.30	0.694607	0.633701	0.587553	0.570735	1.84	0.54624	0.5477
0.40	0.785317	0.705110	0.642422	0.619050	1.76	0.58289	0.5868
0.45	0.906749	0.788391	0.701023	0.66702	1.86	0.62164	0.625*
0.48	no conver.	no conver.	0.790455	0.734952			0.66*

*Obtained graphically from Benthem's Figure [9].

Table 3.6: Numerical Results. Eigenvalues for orthogonal crack using N finite elements; Mode I, p = 0.

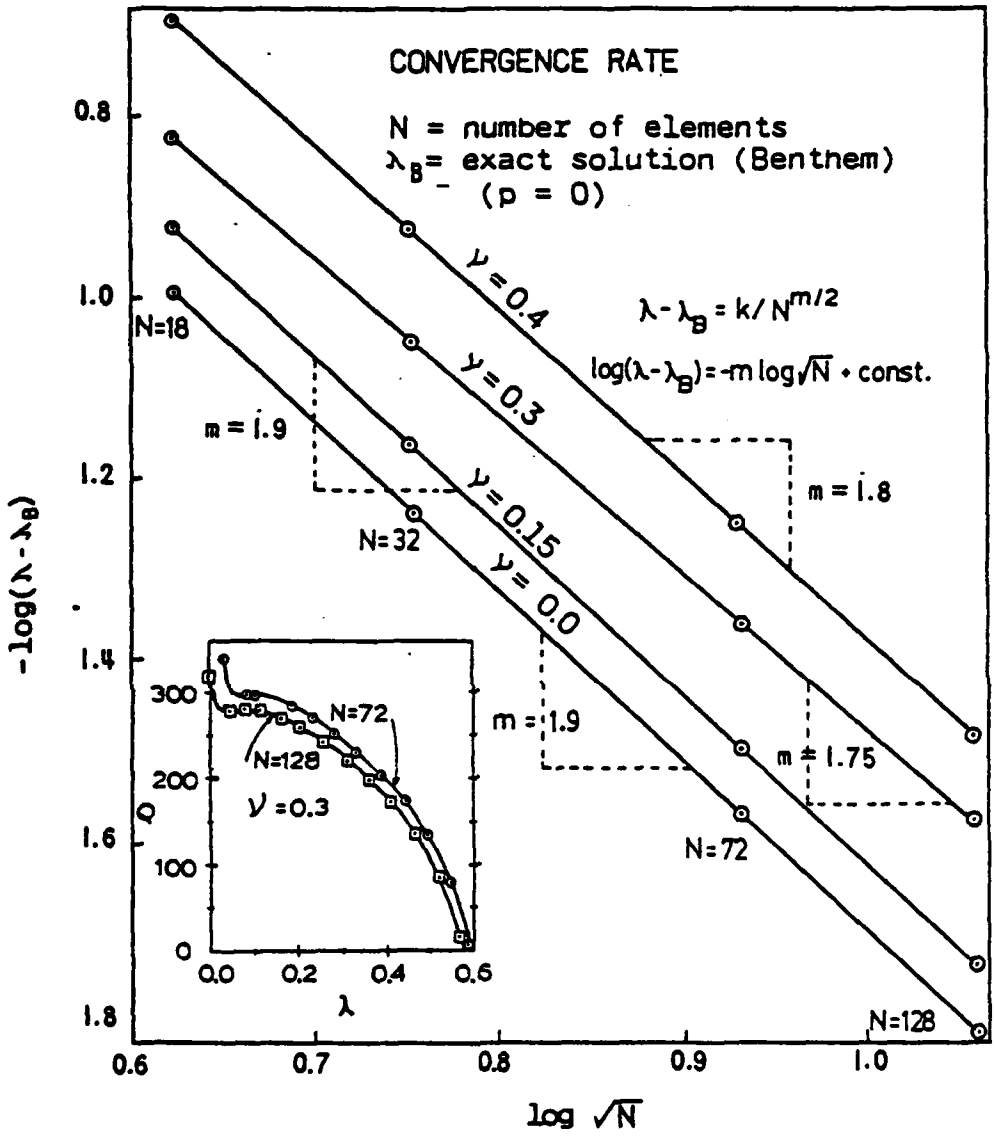

Fig. 3.6: Determination of the rate of convergence with increasing number of elements. Use of Eq. (2.31). Insert: Search of eigenvalue using Eq. (2.26). Mode I, p = 0.

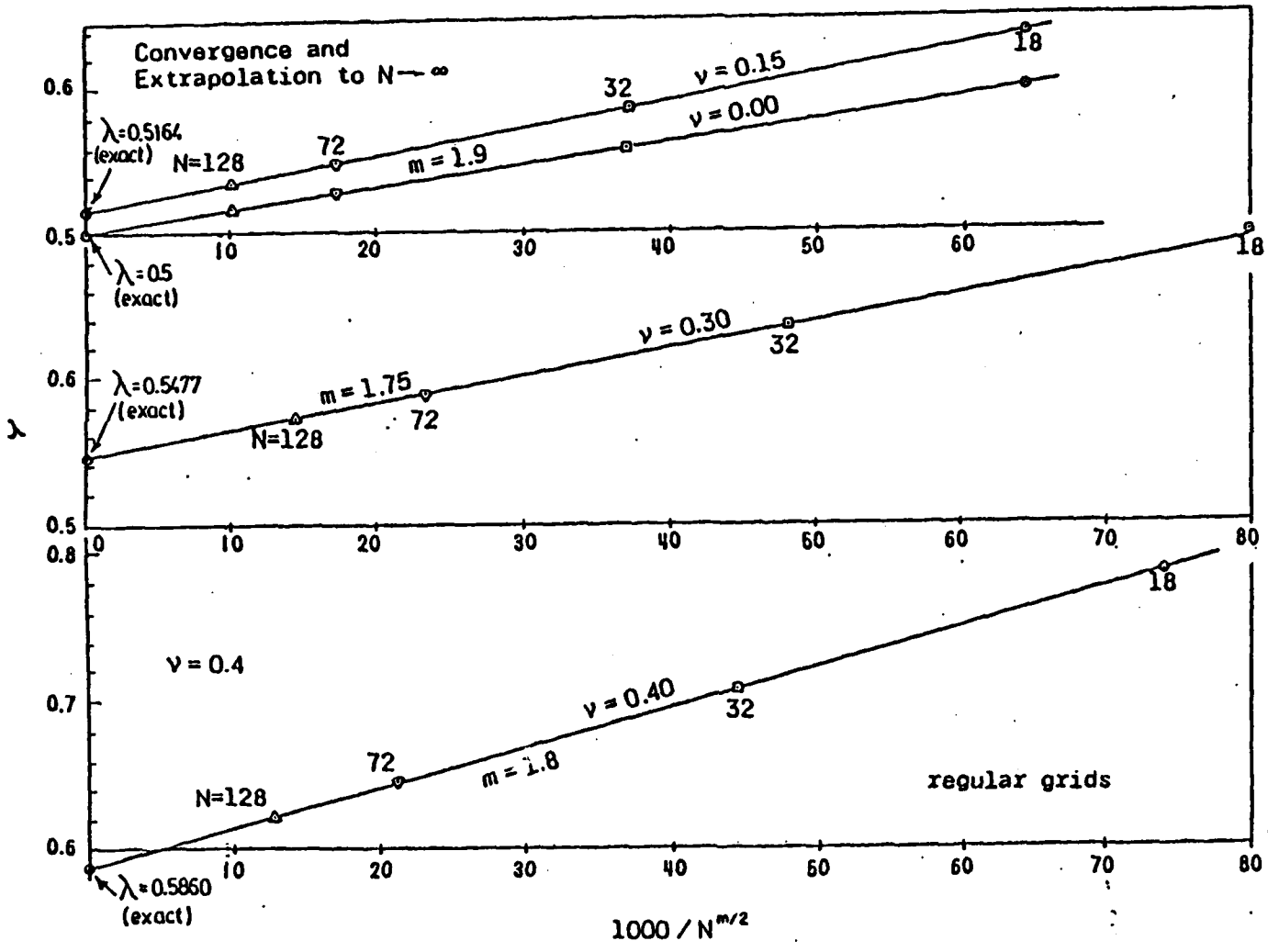

Fig. 3.7: Extrapolation of numerical results from Fig. 3.6 to N = ∞. Mode I, p = 0.

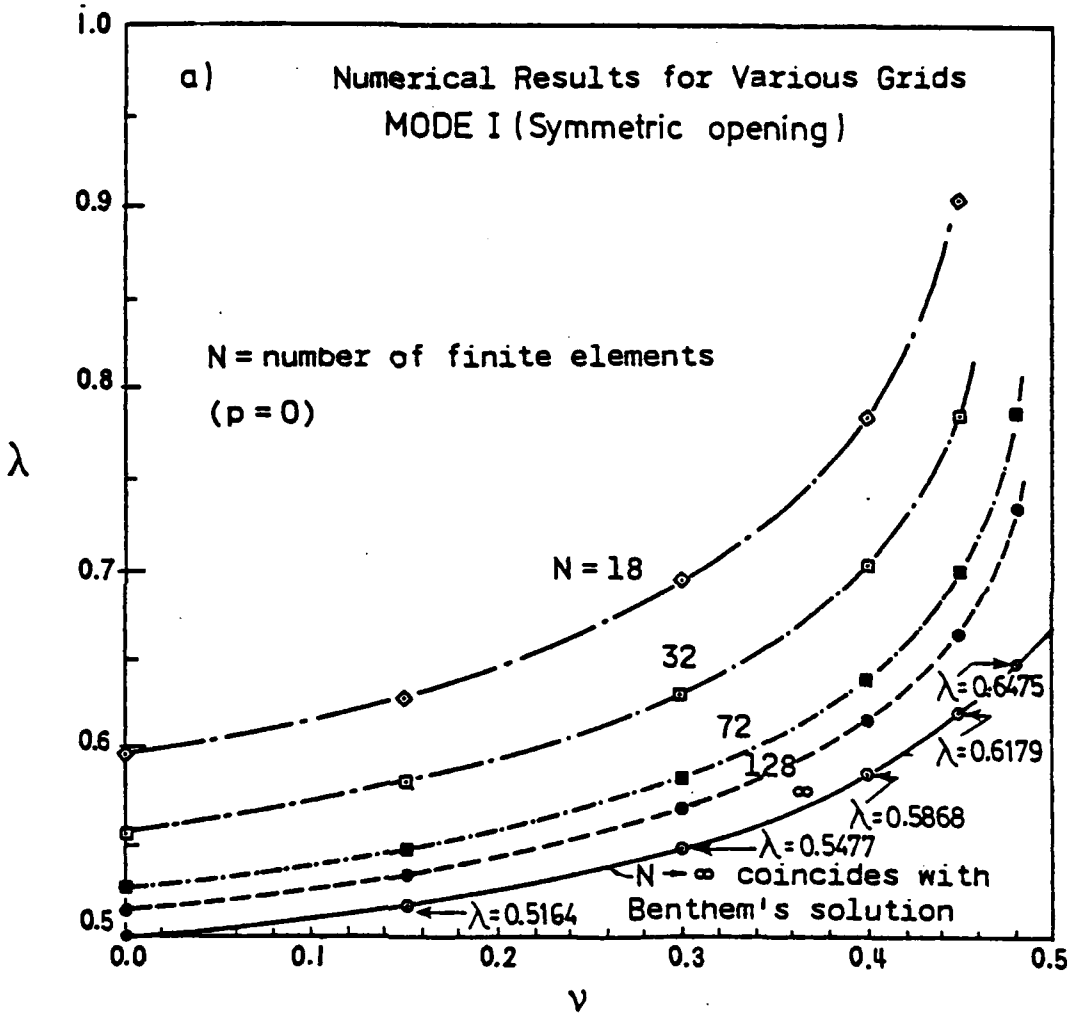

Fig. 3.8: Numerical results for orthogonal crack; Mode I, p = 0.

were better than those for the refined (irregular grids), the extrapolated values for the refined grids were no better than those for uniform subdivisions. So, non-uniform subdivisions of the meridians would be ineffective.

Recently, Kawai, Fujitani, and Kumagai [10] also presented analytical solutions for the same problem (orthogonal crack). They obtain three roots for all Poison ratios which disagree with Benthem [9] as well as the present work. For example, the smallest root [10] for $\nu = 0.3$ is approximately $\lambda = 0.3$. The insert of Fig. 3.6 shows the value of Q, which must be zero in the search of the eigenvalue, Eq. (2.26). The curve that Q versus λ traces is smooth and continuous Therefore, no eigenvalue near $\lambda = 0.3$ for $Q = 0$ could have been missed.

Furthermore, the program was checked against the analytical and numerical solutions for a sharp corner of angle 2α on the crack front edge of a planar crack whose complement is the wedge-shaped punch of angle 2β within an infinite elastic solid, see Fig. 3.10. The solution for this symmetric opening (Mode I) of such a crack was given in [3], where a finite difference solution was based on a reduction to potential theory. Very accurate solutions, by means of singular integral equations, have recently been obtained by Keer and Parihar [13]. Both solutions [3,13] have found that for symmetric opening, the eigenvalue is independent of Poison ratio for a fixed angle 2α.

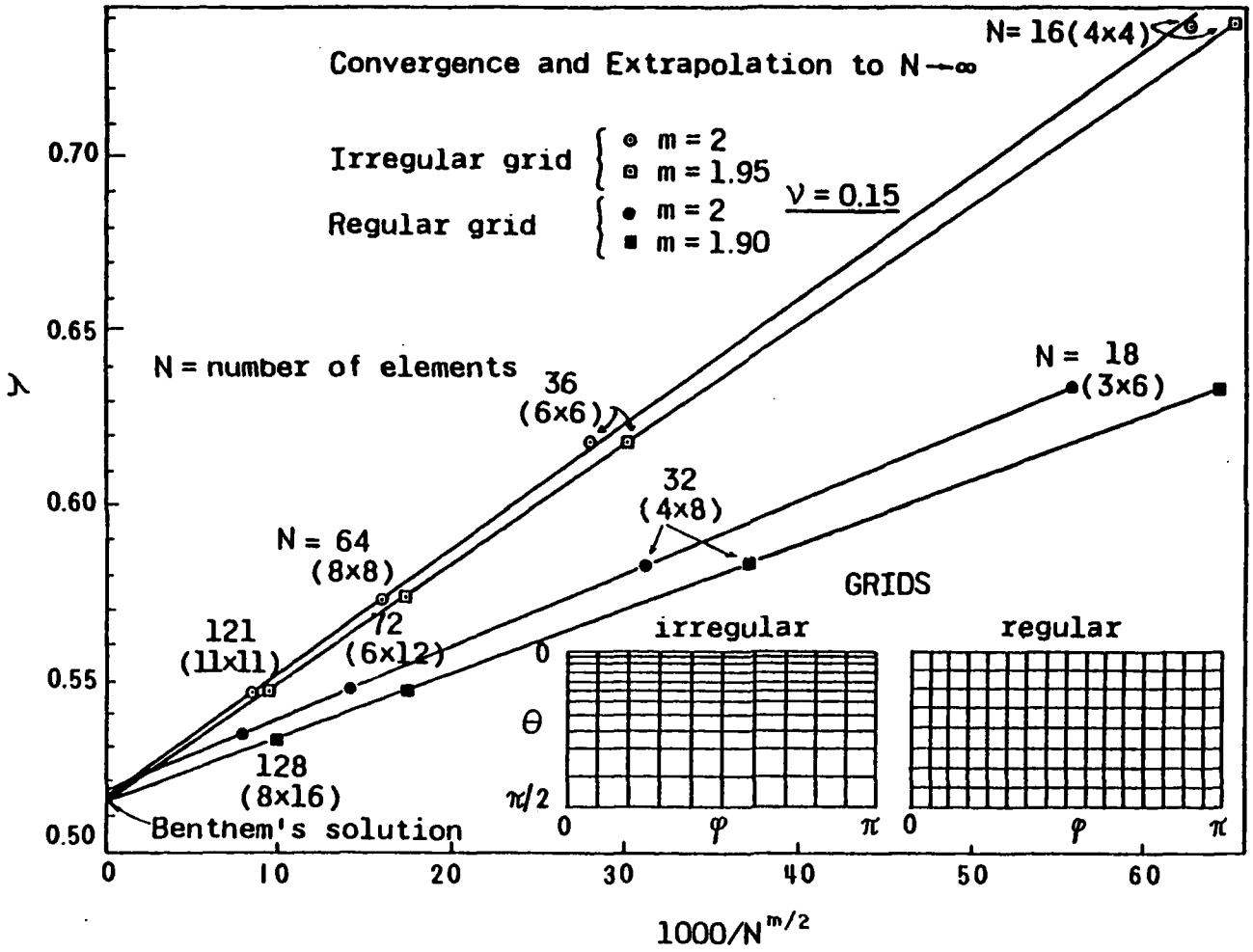

Fig. 3.9: Extrapolation of numerical results for orthogonal crack with grid refinement for Poisson ratio $\nu = 0.15$; Mode I, p = 0.

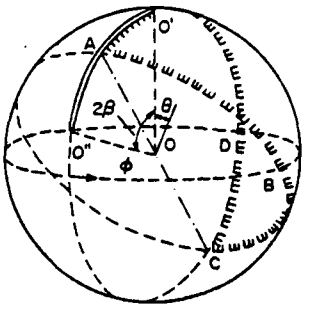

Fig. 3.10: Crack corner in an infinite elastic space. (The unit sphere is not the body surface; it is used to visualize the spherical coordinates; the body is infinite.)

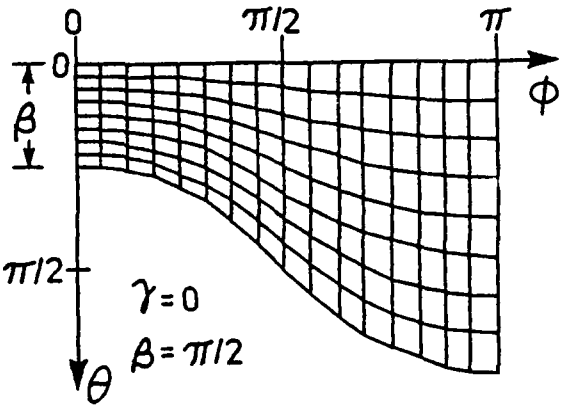

Fig. 3.11: Finite element grid used for the crack corner in an infinite elastic space. Domain O'ACO' from Fig. 3.10 visualized in the (θ-φ)-plane.

AD-A086 491 NORTHWESTERN UNIV EVANSTON IL DEPT OF CIVIL ENGINEERING F/G 20/11
THE SURFACE SINGULARITY OF CRACKS.(U)
OCT 79 Z P BAZANT, L F ESTENSSORO AFOSR-75-2859
UNCLASSIFIED 79-10/2515 AFOSR-TR-80-0457 NL

2 OF 2
AD A 086491

END
DATE FILMED
8-80
DTIC

ν/N	18	32	72	128	Eq. 2.39 m	Eq. 2.39 $\lambda_{extrap.}$	Keer, Bazant
0.0	0.405092	0.367277	0.334316	0.320938	1.46	0.29531	0.2966
0.3	0.390271	0.357526	0.328774	0.317036	1.44	0.29425	0.296

Table 3.7: Numerical results. Eigenvalues for crack corner of angle $\beta = 3/2\pi$ in an infinite elastic space using N finite elements; Mode I, p = 0.

Because of symmetry about $\phi = \pi$ and $\theta = \beta$, one needs only to consider one quarter of the unit sphere as shown by the dashed lines of Fig. 3.10. The bottom side of the domain, $\theta_b = \alpha/2$, is a great circle around the unit sphere, which in the $(\theta$-$\phi)$-plane is given by the equation

$$\theta = \theta_b = \arctan(\tan\beta/\cos\phi);\ \text{if } \theta < 0,\ \text{then } \theta \leftarrow \theta + \pi \quad (3.14)$$

where $\beta = \alpha/2$. The θ-coordinates of the nodal points on the r-th curved row, Fig. 3.11, are calculated as

$$\theta = \theta_b(r-1)/(r_b-1) \quad (3.15)$$

where r_b is the number of the last row, $\theta = \theta_b$, and $r = 1$ corresponds to $\theta = 0$. Eq. (3.15) describes a uniform subdivision of each meridian, as shown in Fig. 3.11.

The stress and displacement conditions at $\phi = \pi$ have already been discussed in the previous section. The displacement conditions at the bottom boundary (θ_b), must be replaced by displacement boundary conditions of symmetry:

$$v\cos\eta - w\sin\eta = 0, \quad \text{at } \theta = \theta_b \quad (3.16)$$

where η is the angle that the bottom boundary makes with the ϕ-axis in the $(\theta$-$\phi)$-plane, i.e., the normal displacement of the bottom nodal points is zero. The stress boundary conditions $\sigma_{\theta\theta} = \sigma_{\theta r} = 0$ at

$\theta = \theta_b$ will be automatically satisfied by the finite element method.

Table 3.7 gives the numerical results for the cases of $\nu = 0$ and 0.3 for $\alpha = \pi/4$, chosen for examples. Using Eq. (2.31) the values of m are graphically calculated in Fig. 3.12. Finally, the extrapolation point are obtained in Fig. 3.13, and compared to the values $\lambda = 0.296$, calculated in [3] and $\lambda = 0.2966$ in [13]. Indeed, the eigenvalues are independent of Poisson ratio for a fixed α. The fact that all three values ($\lambda = 0.296$ obtained by different researchers, using independent methods of solution), are the same, further confirms that the present solution is correct.

Now, the question arises for the value of the convergence rate m when no exact solution is available and hence Eq. (2.31) cannot be used as before. For such cases, the extension of Richardson's h^m technique, described in Section 2.3D, was found to work exceptionally well. All numerical results were run in a simple subroutine, which is included in the program, Appendix B. The m-values are given in the preceding Tables, next to their corresponding numerical values. The extrapolation values for all cases thus far studied came within 0.4% error, as shown in the tables. Again, reaffirming the present method of solution and justifying the use of the extrapolation technique proposed in Section 2.3D. For the sake of brevity, whenever an extrapolated value is mentioned herein it will refer to this technique, unless otherwise specified.

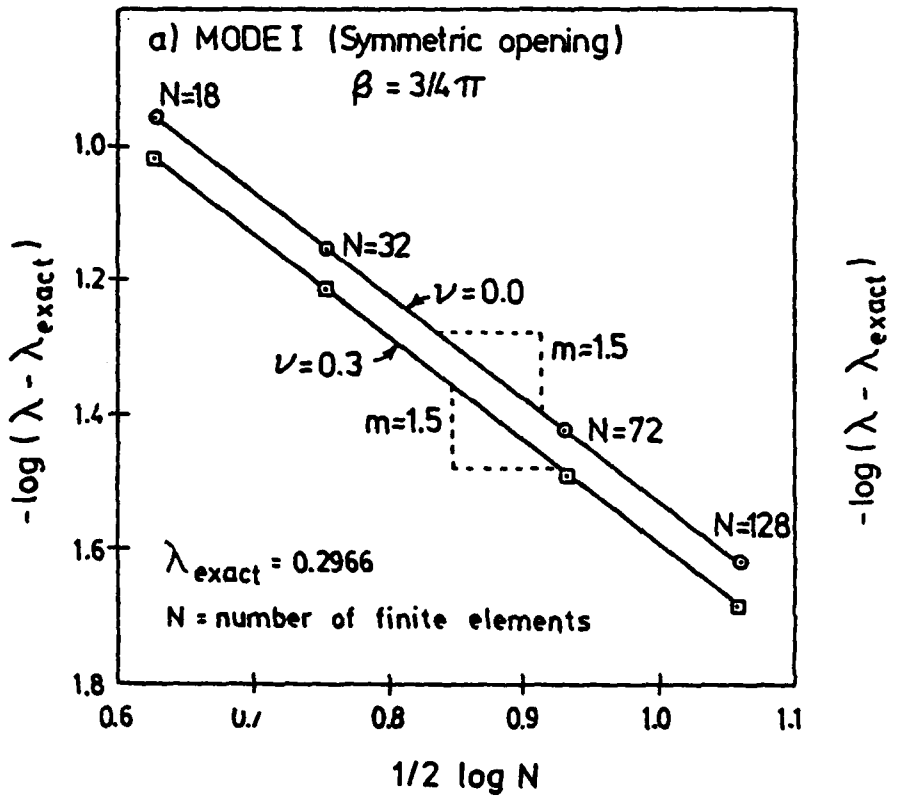

Fig. 3.12: Finite element convergence pattern for right angle corner at front edge of planar crack inside elastic body. Mode I, p = 0.

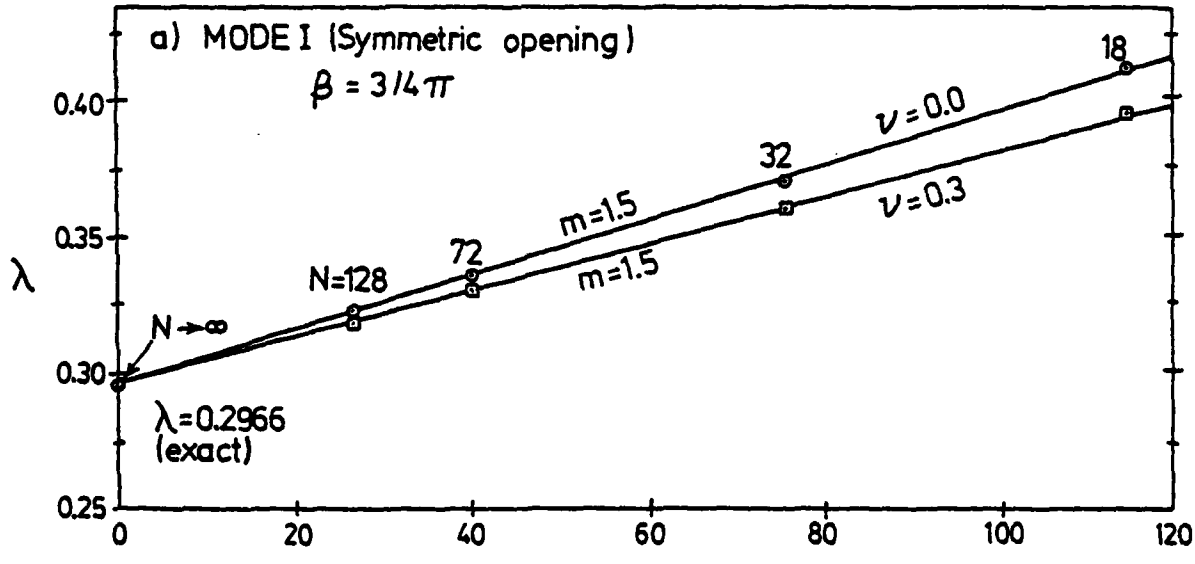

Fig. 3.13: Extrapolation of numerical results to $N \to \infty$ for the case in Fig. 3.12. Mode I, p = 0.

Note that the extrapolation value in the subroutine corresponds to the first coefficient of the straight-line with optimum slope m, i.e., the value of the regression line at $h = 0$, $N \to \infty$.

A final check was performed on the orthogonal crack in Fig. 3.1, for Mode I opening. It consisted of including the entire $(\theta\text{-}\phi)$-domain of the unit, sphere, i.e., $0 \leq \theta \leq \pi/2$, $0 \leq \phi \leq 2\pi$; where no symmetry considerations need be made. One node may be fixed in the ϕ-direction to prevent rotation and thus implement a statically determinate support for the body. However, since rotation implies $\lambda = 1$, see Section 3.2A, the support is normally not necessary unless $\lambda = 1$. This also means that in this finite element method it is sufficient to impose only one force at a nodal point to achieve the mode required, and not two forces of opposite direction applied at two opposite nodal points.

The numerical results are given in Table 3.8 along with the convergence rate m and the extrapolated value for the case $\nu = 0.15$, but excluding the value for $N = 18$. If this last value were to be included one would obtain $m = 2.6$ and $\lambda_{extrap.} = 0.5267$. However, note that $N = 18$ in the domain $0 \leq \theta \leq \pi/2$, $0 \leq \phi \leq 2\pi$ is a very coarse mesh, thus, inducing an error which would not be of the order $0(h^m)$, $m < 2$. Since the convergence rate is to be limited by $m \leq 2$, as mentioned earlier in Section 2.3C the value for $N = 18$ has to be excluded, even though the extrapolated value using all four points is within a 2% error. And as a rule of hand, so will future values for $N = 18$ when the entire domain is included. For such cases, the number of finite elements will be raised to 200 and 288, where

one would again expect a convergence rate less than quadratic and more accurate results.

C.) Antisymmetric openings, Mode II and III.

For antisymmetric crack openings the question of proper antisymmetric conditions at $\phi = \pi$ and at the free surface $\theta = \pi/2$ are more complicated than for the symmetric opening. It appears that Modes II and III cannot exist seperately at the surface point (which was first suggested by Professor L. M. Keer of Northwestern University in an uncontested $5.00 bet). Indeed, it is impossible to imagine conditions of zero stress state at the half-space surface ($\theta = \pi/2$) to be satisfied by a displacement field which would exhibit either Mode II or Mode III antisymmetry. The finite element claculations confirmed this also; i.e., when the full domain $\theta\varepsilon(0,\pi/2)$, $\phi\varepsilon(0,2\pi)$ was used and Mode II antisymmetric displacements were forced in two symmetrically opposite nodes at the crack surface ($n = 1$ at $\phi = \pi/2$ and $n = -1$ at $\phi = 3\pi/2$, both at $\theta = \pi/2$), the v displacements at $\theta = \pi/2$ were found to be nonzero and exhibit perfect antisymmetry about $\phi = \pi$; which is characteristic of Mode III. Furthermore, a surface nodal displacement was forced such that Mode III opening would be obtained, i.e., the v displacement at the crack surface. However, the eigenvalue slowly converged to the same eigenvalue when Mode II opening was forced. Thus, the antisymmetric Modes II and III are always combined at the surface point.

Therefore, one may impose at $\phi = \pi$, the symmetry plane, either

Mode II-type condition: $u \sin\theta - v \cos\theta = 0$, or (3.17)

Mode III-type condition: $u \cos\theta - v \sin\theta = 0$, (3.18)

or any linear combination of these two conditions, among which the simplest choice is

$$u(\theta,\pi) = v(\theta,\pi) = 0. \tag{3.19}$$

The antisymmetry condition for stress in both modes is $\sigma_{\phi\phi} = 0$ at $\phi\phi = \pi$, which is again automatically satisfied by the finite element method as a natural boundary condition.

The singularity exponent λ in either case is the same, and because it belongs to a combination of two modes, λ is a double root.

Table 3.9 gives the numerical results when Eq. (3.17) is used and Table 3.10 gives the numerical results when the full domain $\theta\epsilon(0,\pi/2)$, $\phi\epsilon(0,2\pi)$ is used where no symmetry analysis is made. The extrapolated values in Table 3.10 differ significantly from those of Table 3.9. Hence, at this point it was necessary to increase the number of finite elements to 288 for the domain $\phi\epsilon(0,2\pi)$, as shown in Table 3.10 for the case $\nu = 0.3$. This case yielded the same extrapolated value as that obtained from the domain $\phi\epsilon(0,\pi)$. Fig. 3.14 shows the numerical results of Table 3.10 with the extrapolated values of Table 3.10. Note that for the case $\nu = 0$ the eigenvalue

ν/N	18	32	72	128	m	$\lambda_{extrap.}$	Benthem
0.15	0.789175	0.639575	0.572169	0.549754	1.99	0.5234	0.5164

Table 3.8: Numerical results. Eigenvalues for orthogonal crack with full body; $0 \le \theta \le \pi/2$, $0 \le \phi \le 2\pi$; using N finite elements. Mode I, p = 0.

ν/N	18	32	72	128	m	$\lambda_{extrap.}$
0.0	0.612712	0.564782	0.529639	0.517067	1.926	0.50001
0.15	0.551476	0.500448	0.463557	0.450516	1.966	0.43533
0.3	0.521529	0.466533	0.426113	0.411730	1.922	0.40207
0.4	0.530050	0.465491	0.415043	0.398513	1.860	0.39591

Table 3.9: Numerical results. Eigenvalues for orthogonal crack; $0 \le \theta \le \pi/2$, $0 \le \phi \le \pi$; using N finite elements. Modes II and III.

ν/N	32	72	128	200	288	m	$\lambda_{extrap.}$
0.0	0.698366	0.597145	0.555897			1.580	0.48432
0.1	0.653992	0.545166	0.504840			1.842	0.44715
0.15	0.639572	0.528586	0.487784			1.862	0.43030
0.3	0.616785	0.498913	0.454053	0.432559	0.420677	1.880	0.40202
0.4	0.635112	0.506881	0.452256			1.842	0.34790

Table 3.10: Numerical results. Eigenvalues for orthogonal crack with full body; $0 \le \theta \le \pi/2$, $0 \le \phi \le 2\pi$; using N finite elements. Modes II and III.

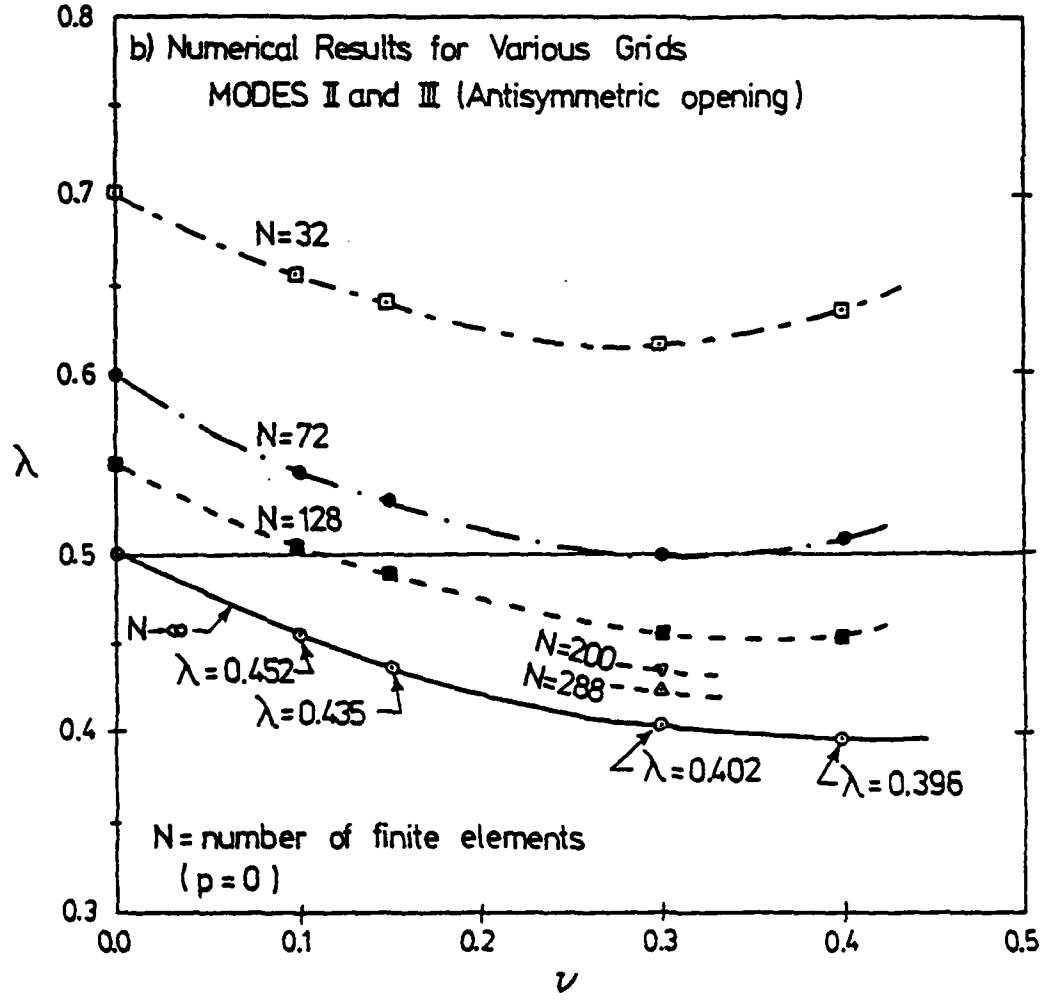

Fig. 3.14: Numerical results for orthogonal crack, Modes II and III.

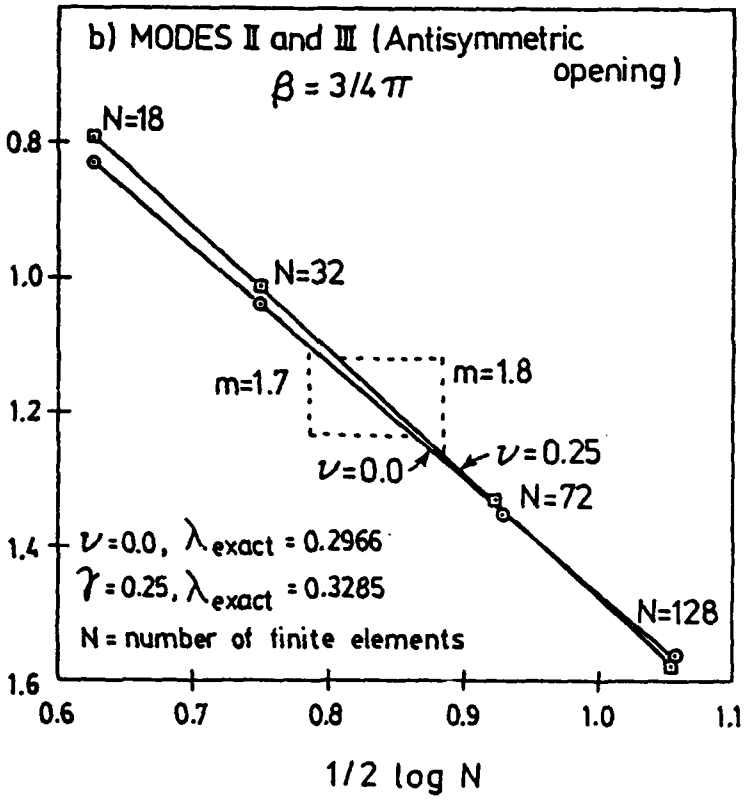

Fig. 3.15: Finite element convergence pattern for right angle corner at front edge of planar crack inside elastic body. Modes II and III.

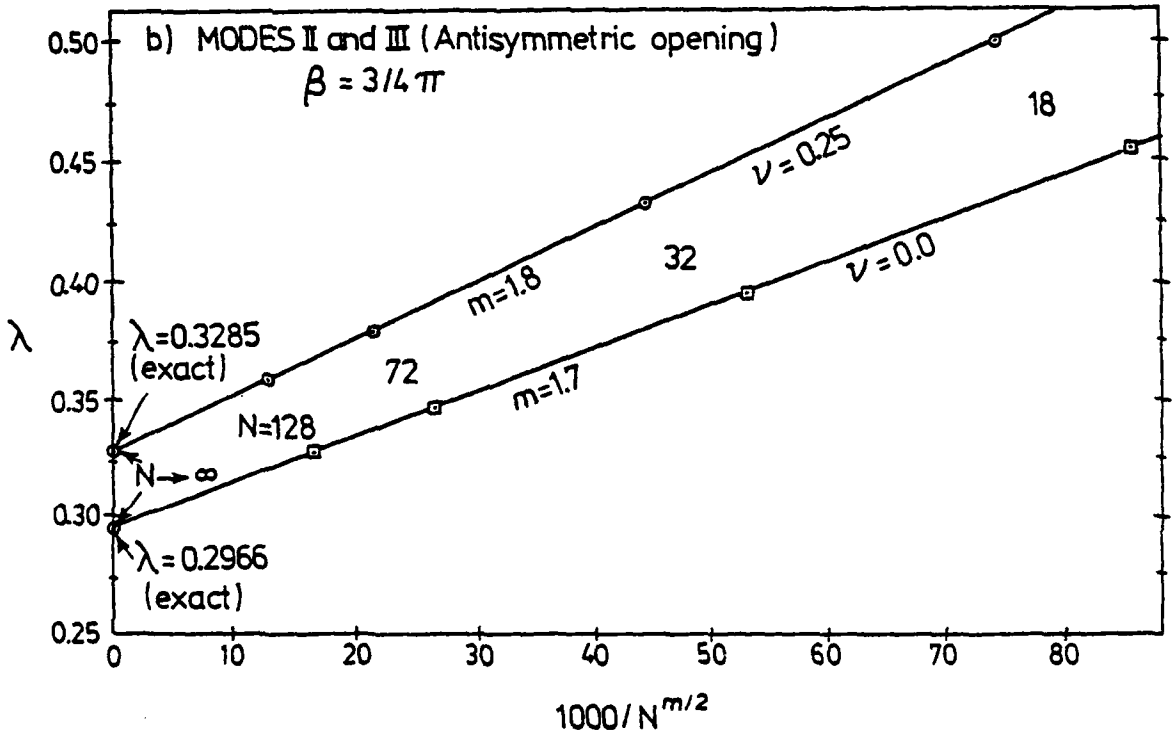

Fig. 3.16: Extrapolation of numberical results to $N \to \infty$ for case in Fig. 3.15. Modes II and III.

is exactly $\lambda = 0.5$, which was again expected. No solution seems to exist in the literature concerning Modes II and III for comparison in Fig. 3.14.

The antisymmetric opening, Modes II and III, was also checked against the known analytical solution of a crack corner in an infinite elastic space, Fig. 3.10, page 84 solved by Keer and Parihar [14a]. They found that the solution for these modes to be irreducible to potential theory and to depend on Poisson ratio ν. For example, for a crack corner of angle $\alpha = \pi/4$ the eigenvalues $\lambda = 0.2966$ and 0.3285 were obtained for Poisson's ratio $\nu = 0.0$ and 0.25, respectively. Table 3.10a gives the numerical results for both cases. Figs. 3.15 shows the convergence pattern using Eq. 2.33 and Fig. 3.16 the extrapolated values using the convergence rate m obtained graphically from Fig. 3.15. The values for m and $\lambda_{extrap.}$ using Eq. 2.39 are also given in Table 3.10a.

3.4 Crack Propagating at the Surface

From the practical point of view, the case of a propagating crack is of main interest. There exist certain physical restrictions for the solution of a propagating crack which can be derived from energy considerations. For cracks that do not propagate, the only restrictions are that the strain energy within a small sphere about point 0, as well as the strain energy per unit length of edge within a small cylinder whose axis coincides with the crack front edge 00', Fig. 3.1, be integrable. Let the strain energy by denoted by E_o, then

ν/N	18	32	72	128	Eq. 2.39 m	Eq. 2.39 $\lambda_{extrap.}$	Keer, Parihar
0.0	0.444118	0.387192	0.34142	0.324126	0.82	0.2950	0.2966
0.25	0.48972	0.425921	0.374182	0.354623	0.84	0.3245	0.3285

Table 3.10a: Numerical results. Eigenvalues for crack corner of angle $2\beta = 3/2\pi$ in an infinite elastic space, using N finite elements, Modes II and III.

$$E_o = \int_v \frac{1}{2} \sigma_{ij} \epsilon_{ij} \, dv. \tag{3.20}$$

The above expression can be simplified by asymptotic analysis. Noting that near the surface terminal point 0, the displacements behave like:

$$u_i \sim r^{\lambda} \tag{3.21a}$$

where $\sim$ denotes proportionality. Hence,

$$\partial_{u_i}/\partial r \sim r^{\lambda-1} \tag{3.21b}$$

$$\epsilon_{ij} \sim r^{\lambda-1} \tag{3.21c}$$

$$\sigma_{ij} \sim r^{\lambda-1} \tag{3.21d}$$

$$dv \sim r^2 dr \tag{3.21e}$$

yields,

$$E_o \sim r^{2\lambda+1} \tag{3.22}$$

For the strain energy to be integrable, or bounded, as $r \to 0$, requires

$$\mathrm{Re}(\lambda) > -\tfrac{1}{2}\ , \quad \text{stationary crack.} \tag{3.23}$$

As the crack propagates, energy flows into all points of the crack front edge and is consumed by the process of separation, i.e., creation of crack surfaces. The energy flux near the points of the crack front edge may generally have two components: (a) The flux E_1 which is parallel to the edge and flows into any point on the crack front edge, including the surface point 0. E_1 must be zero because the trace of the surface point 0 as it moves is a line, and a line can be associated only with a negligible amount of additional surface energy. (b) The flux E_2 of energy into the moving crack front edge per unit length of edge must be finite and non-zero because the surface energy γ is finite and non-zero.

The first condition (a) requires that

$$E_1 = \iint_{\Omega} \sigma_{ij}(\partial u_j/\partial x)\, d\Omega = 0 \tag{3.24}$$

where σ_{ij} is the cartesian stress tensor; u_j are the cartesian displacements; x is the coordinate in the direction of the crack extension; and Ω is a surface of a sufficiently small sphere centered at point 0. Noting that $d\Omega = r^2 \sin\theta\, d\theta d\phi$, and from Eqs. (3.21), it follows that $E_1 \sim r^{2\lambda}$, and for E_1 to be zero as $r \to 0$, it is necessary that

$$\mathrm{Re}(\lambda) > 0\ , \tag{3.25}$$

which is a weak condition on a propagating crack.

The second condition (b) requires that

$$E_2 = \int_L \sigma_{ij} \, (\partial u_i/\partial x) \, r_1 d\phi \tag{3.26}$$

where (r_1,ϕ) is a polar coordinate system in a plane normal to the crack front edge; L is a circle of radius r_1 in this plane centered around the edge; x is the direction of crack propagation; u_i are the cartesian displacements; and σ_{ij} is the cartesian stress tensor. Also, the energy flux E_2 may in general be expressed by Rice's J-integral [23,31] for linear elastic behavior:

$$E_2 = \int_L \left(\tfrac{1}{2} \sigma_{ij} \, \varepsilon_{ij} dy - \sigma_{ij} \, n_i \frac{\partial u_i}{\partial x} \, r_1 d\phi\right) \tag{3.27}$$

in which $dy = r_1 \sin\phi \, d\phi$ and $\partial/\partial x = \cos\phi(\partial/\partial r_1) - (\sin\phi/r_1)(\partial/\partial\phi)$. On physical grounds, the flux E_2 must obviously be positive, non-zero and finite at all points near the surface terminal point 0 of the crack front edge. Furthermore, the flux E_2 may be expected to be constant along the crack edge, assuming that the energy needed for the creation of new surface is the same along these points. However, this last requirement may be simplified by the asymptotic deductions. When Eqs. (3.21) are substituted into Eq. (3.27), it follows that ($\sim$ denotes proportionality)

$$E_2 \sim r_1^{2\lambda-1} \tag{3.28}$$

Thus, for E_2 to be bounded and non-zero as $r_1 \to 0$, it is necessary that $\mathrm{Re}(2\lambda - 1) = 0$, or

$$\mathrm{Re}(\lambda) = \tfrac{1}{2}, \text{ propagating crack} \qquad (2.39)$$

This condition must be satisfied for the terminal surface point of a crack that propagates, but not for a stationary crack, as it is well known [23,31].

According to Eq. (3.29), a crack which propagates, or for which propagation is imminent, must exhibit $\lambda = \frac{1}{2}$ (the exponent being assumed to be real if there are no two dissimilar materials). By far, this case is of the greatest practical interest. Therefore, a meaningful question is to ask whether there exist inclinations β of the crack front edge Fig. 3.17 and γ of the crack plane Fig. 3.18, for which the eigenvalue $\lambda = \frac{1}{2}$ is attained. For the orthogonal crack edge ($\beta = \pi/2$, $\gamma = 0$; Fig. 3.1), propagation is obviously possible only if $\nu = 0$.

Tables 3.11 and 3.12 give the numerical results for the symmetric (Mode I) and antisymmetric (Modes II and III) cracks whose plane is normal to the surface ($\gamma = 0$) and whose edge inclination angle β varies for various values. The extrapolated results are plotted in Fig. 3.20.

It is interesting to note that the solutions presented in Fig. 3.20 agree with the common sense that as the crack "size" defined by the edge inclination angle β decreases, i.e., there is more material that is not cracked, the eigenvalue λ increases; and as the crack "size" increases, i.e., there is more material that is cracked, the eigenvalue λ decreases. In other words, the stress singularity exponent λ-1 increases (weaker singularity) as β decreases and

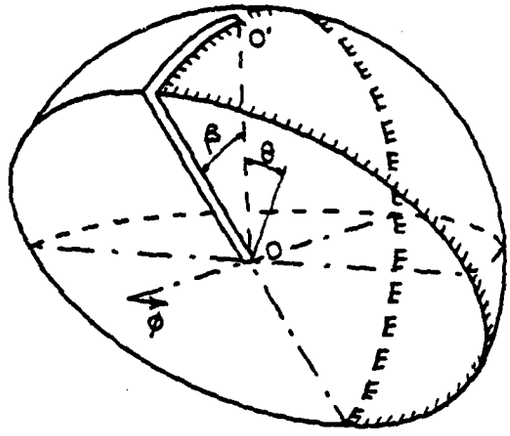

Fig. 3.17: Spherical coordinate system at termination of crack front edge 00' at body surface. Inclined edge. (The unit sphere is shown only to visualize the coordinates; the body is semi-infinite).

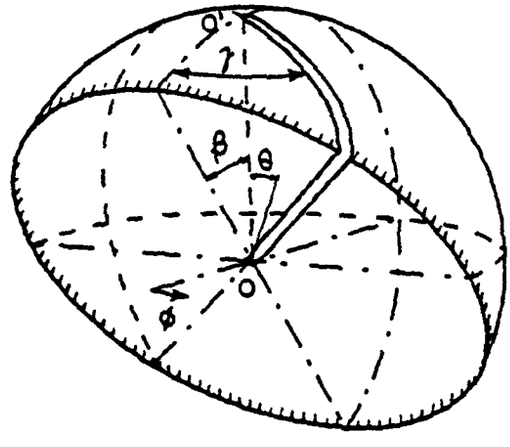

Fig. 3.18: Spherical coordinate system at termination of crack front edge 00' at body surface. Inclined edge and inclined crack plane. (The unit sphere is shown only to visualize the coordinates; the body is semi-infinite).

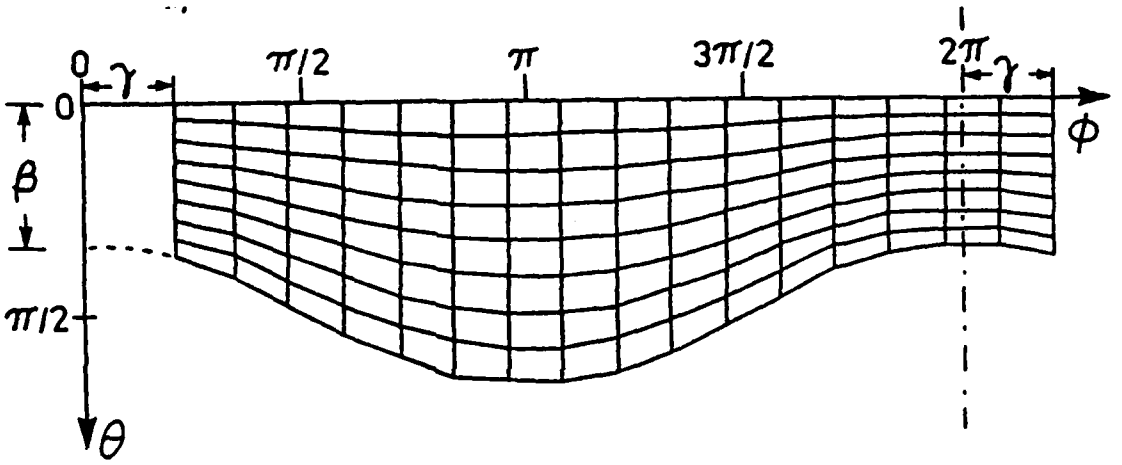

Fig. 3.19: Finite element grids used for cracks whose edge and plane are inclined.

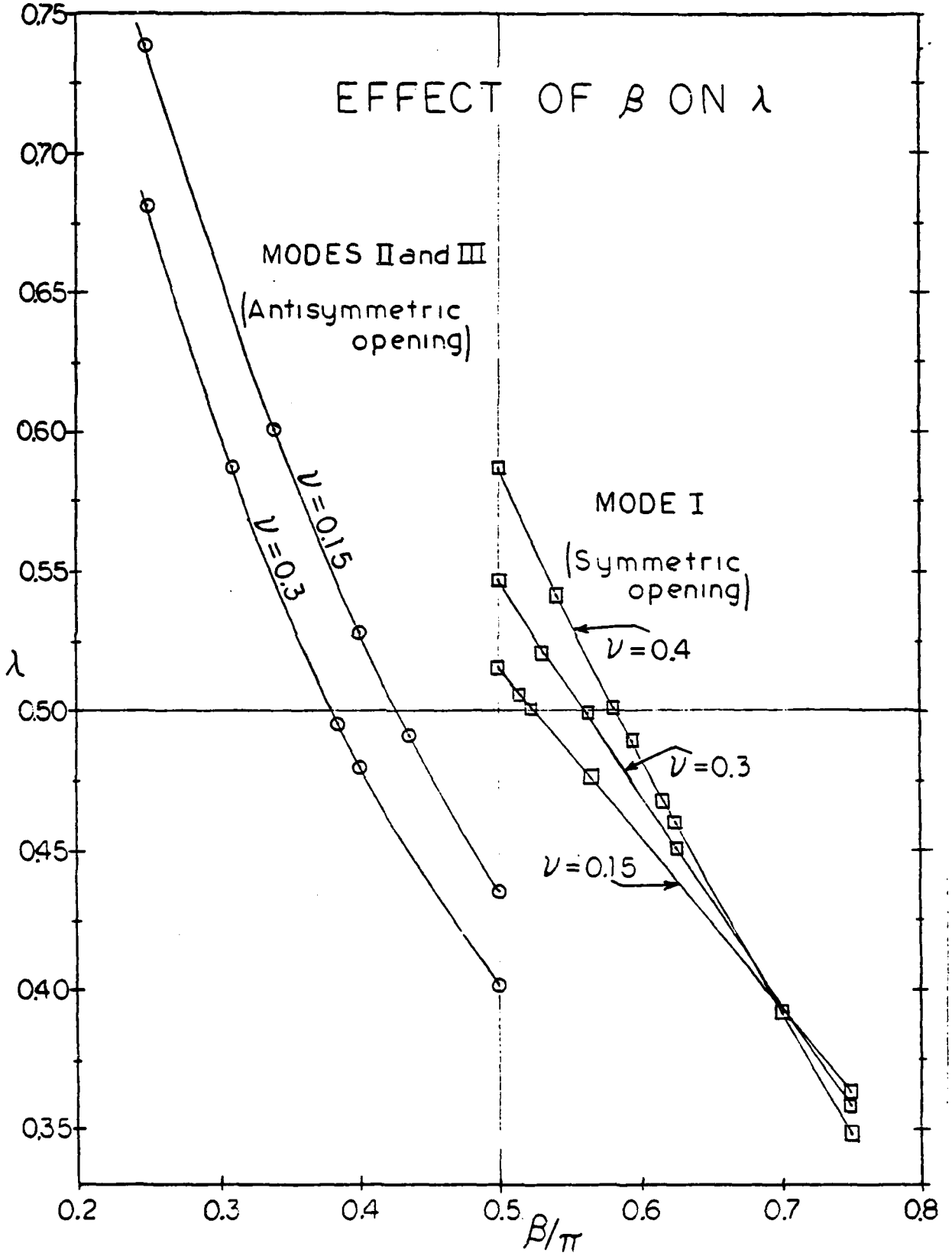

Fig. 3.20: Extrapolated values of λ versus crack inclination angle β.

β/N	18	32	72	128	m	$\lambda_{extrap.}$	ν
0.7500 π	0.516130	0.455535	0.408415	0.390684	1.760	0.36344	0.15
0.5650 π	0.591961	0.543683	0.507719	0.494700	1.882	0.47642	0.15
0.5234 π	0.617518	0.568880	0.532770	0.519731	1.900	0.50178	0.15
0.5156 π	0.622766	0.573944	0.537699	0.524613	1.900	0.50660	0.15
0.7500 π	0.529933	0.462411	0.409619	0.389829	1.740	0.35852	0.30
0.6250 π	0.594414	0.536191	0.491747	0.435444	1.820	0.45131	0.30
0.5625 π	0.639569	0.581339	0.537291	0.521228	1.900	0.49974	0.30
0.5313 π	0.665790	0.606537	0.561731	0.545416	1.840	0.52165	0.30
0.7500 π	0.563350	0.484157	0.418853	0.393608	1.606	0.34888	0.40
0.7000 π	0.590324	0.516101	0.455498	0.432278	1.640	0.39239	0.40
0.6250 π	0.646374	0.574576	0.517118	0.495395	1.688	0.45945	0.40
0.6172 π	0.653335	0.581452	0.524054	0.502385	1.900	0.46702	0.40
0.5938 π	0.675564	0.603046	0.545521	0.523892	1.920	0.48924	0.40
0.5800 π	0.689569	0.616416	0.558597	0.536904	1.922	0.50206	0.40
0.5400 π	0.734456	0.659404	0.598803	0.576551	1.944	0.54152	0.40

Table 3.11: Numerical results. Eigenvalues for crack whose plane is normal to the surface and whose edge inclination angle varies. Mode I.

β/N	18	32	72	128	m	$\lambda_{extrap.}$	ν
0.435π	0.596673	0.550547	0.517672	0.506187	1.99	0.49150	0.15
0.400π	0.628081	0.584022	0.552758	0.541893	1.98	0.52813	0.15
0.340π	0.696749	0.655059	0.625292	0.614992	1.98	0.60163	0.15
0.250π	0.844784	0.803730	0.771322	0.759142	1.79	0.73965	0.15
0.400π	0.587424	0.540269	0.506538	0.494771	2.00	0.47960	0.30
0.385π	0.600785	0.554534	0.521537	0.510055	1.99	0.49531	0.30
0.310π	0.686476	0.643217	0.612274	0.601528	1.98	0.59763	0.30
0.250π	0.784873	0.741345	0.708889	0.697233	1.88	0.68077	0.30

Table 3.12: Numerical results. Eigenvalues for crack whose plane is normal to the surface and whose edge inclination angle varies. Modes II and III.

ν/N	32	72	128	200	288	m	$\beta_{extrap.}$
0.3	0.682082	0.613279	0.590975	0.580683	0.575053	1.99	0.562536

Table 3.13: Numerical results. Eigenvalues for crack front edge angle β of a propagating crack, $\nu = 0.3$. Mode I.

decreases (stronger singularity) as β increases. Also note that the lines in Fig. 3.20 are not straight lines and they seem to approach $\lambda = 1$ for $\beta \to 0$, i.e., there is no crack and one would expect rotational effects to take place, see Section 3.2 A; and they seem to approach $\lambda = 0$ for $\beta \to \pi$, i.e., the semi-infinite body is completely cut in half and one would expect rigid body translations to take place.

In order to substantiate the accuracy of these results, the approach to the eigenvalue problem was modified by treating the stiffness matrix as a function of angle β rather than λ, i.e., λ was fixed to 0.5 and Eq. (2.27) was treated as:

$$\sum_{j=1}^{M} k_{ij}(\beta)\, X_j = 0, \quad j = 1,2,\ldots,M \tag{3.29}$$

The eigenvalue search routine based on the Newton method was easily converted to search for β instead of λ. This alternate method was tried for the case $\nu = 0.3$ in Mode I opening and drawn separately in Fig. 3.21(a). The numerical results obtained by this method and based on up to 288 elements are given in Table 3.13. The convergence pattern of β versus N is shown in Fig. 3.21(b) along with the extrapolated value ($N \to \infty$) which yields the same value as that obtained grafically in Fig. 3.21(a). Therefore, the values of β for each value of Poisson's ratio for which $\lambda = 0.5$ from Fig. 3.20 are drawn in Fig. 3.22.

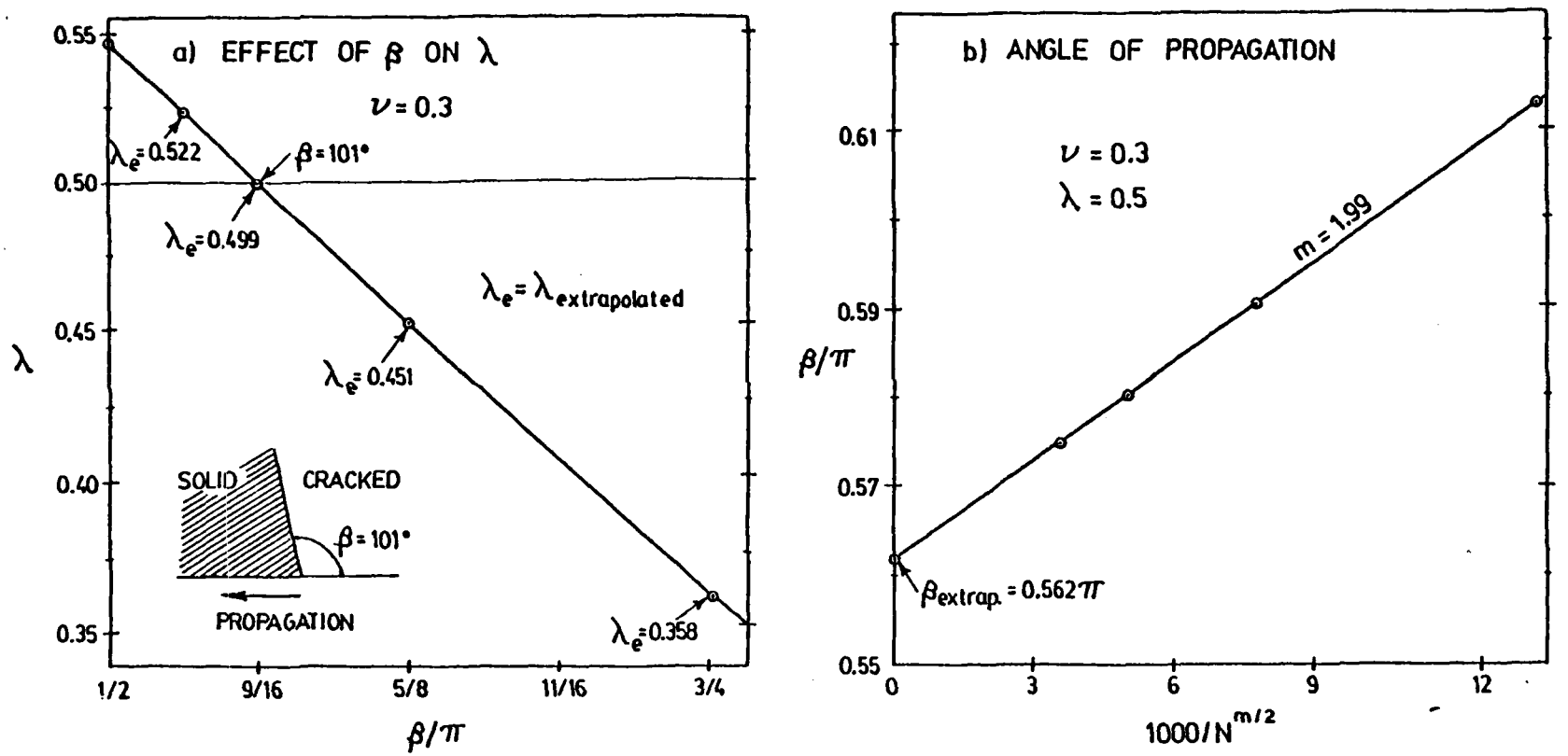

Fig. 3.21: (a) Dependence of singularity exponent λ upon crack front edge angle for normal crack plane (ν = 0.3). Mode I.

(b) Extrapolation of numerical results for crack front edge angle of normal crack plane upon propagation (ν = 0.3). Mode I.

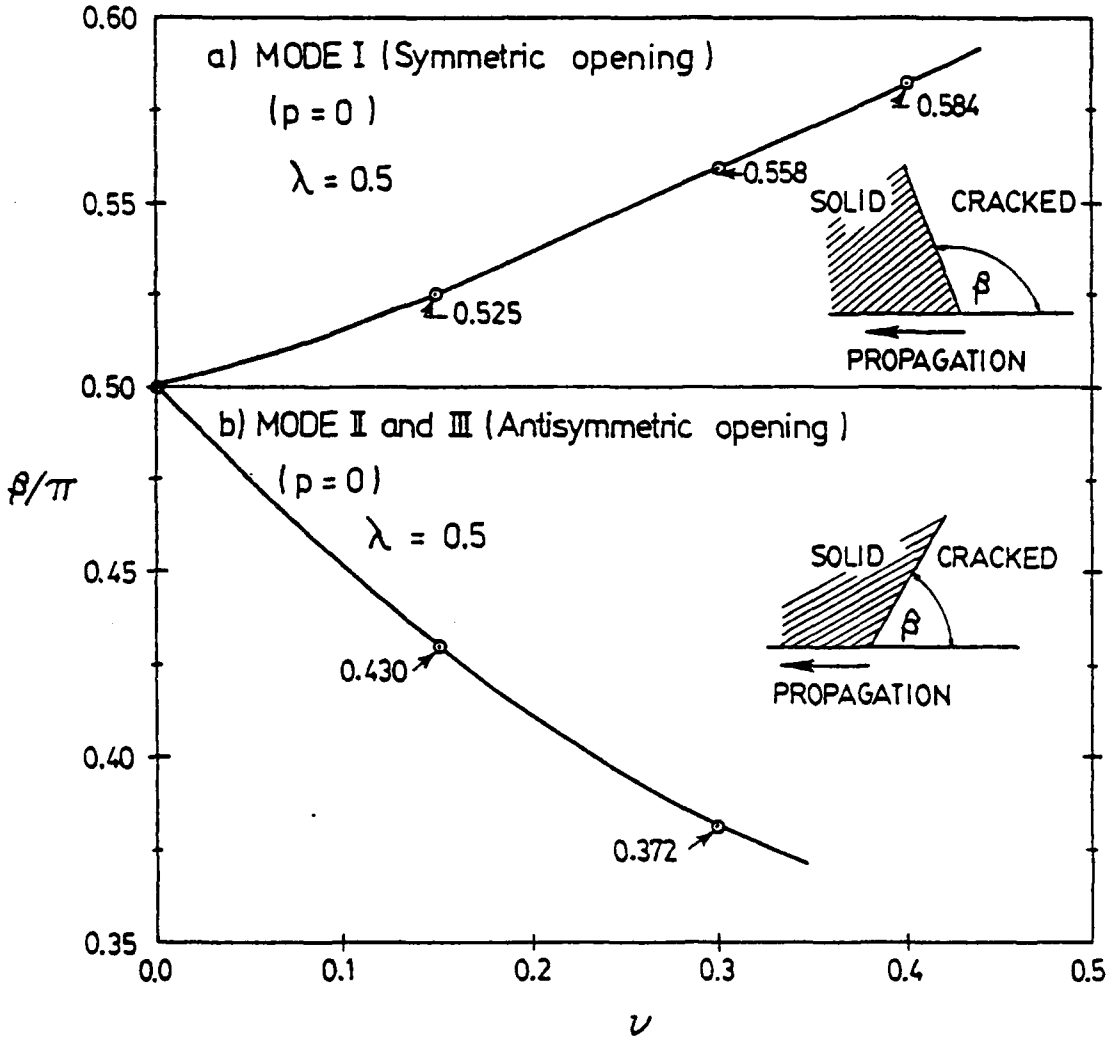

Fig. 3.22: Dependence of crack front edge angles β of a propagating crack upon Poisson's ratio ν. (a) Mode I; (b) Modes II and III. (Normal crack plane).

The physical meaning of the edge inclination angle β for which $\lambda = 0.5$, is that for a propagating crack the symmetric opening, Mode I, gives an obtuse angle ($\beta > \pi/2$), i.e., the surface pont 0 trails behind the interior crack edge; and the antisymmetric opening, Modes II and III, gives an acute angle ($\beta < \pi/2$), i.e., the surface point 0 moves ahead of the interior crack edge. The fact that they are different has an important physical consequence: At the terminal point of a crack whose plane is normal to the surface a combined mode propagation is impossible, i.e., the crack would assume such a shape that its surface terminal point propagates either with a symmetric opening, Mode I, or with an anitsymmetric opening, Mode II and III, but not both combined.

In view of this result, it is natural to ask whether there exist an inclination angle γ of the crack plane for which the β-values for the symmetric and antisymmetric exitation of a propagating crack ($\lambda = 0.5$) would coincide, see Fig. 3.18. However, the numerical results given in Tables 3.14 and 3.15 for the case $\nu = 0.3$ and drawn in Fig. 3.23 indicate that this never occurs, and as the crack plane becomes inclined ($\delta \pm 0$), the β - values for $Re(\lambda) = \frac{1}{2}$ vary as a function of δ. In these cases it is no longer possible to distinguish between symmetric (Mode I) and antisymmetric (Modes II and III) openings, for there is no geometrical symmetry. For each of the two β-values, there exists at point 0 a certain limiting ratio $K_1 : K_2 : K_3$ of the stress intensity factors for Modes I, II and III and no other ratios are possible. So, for cracks of inclined plane, the propagation of the surface point takes place always in a combination of all three modes. Conversely, for a

γ/π	β/π	32	72	128	200	288	m	$\lambda_{extrap.}$
1/12	0.54	0.655505	0.587786	0.560066	0.545999	0.537925	1.666	0.51497
1/12	0.56	0.645284	0.574220	0.546089	0.531843	0.523667	1.680	0.50071
1/12	0.58	0.639213	0.562173	0.533069	0.518399	0.509989	1.690	0.48678
1/6	0.56	0.664311	0.584155	0.554005	0.538982	0.530414	1.728	0.50715
1/6	0.58	0.666197	0.577072	0.544611	0.528637	0.519572	1.780	0.49597
1/6	0.60	0.667235	0.569391	0.536201	0.519018	0.509297	1.792	0.48559
1/4	0.60	0.702632	0.597431	0.558199	0.539102	0.529347	1.820	0.50107
1/4	0.61	0.706619	0.597739	0.556748	0.536780	0.525536	1.820	0.49703
1/4	0.62	0.709921	0.597922	0.555276	0.534450	0.522717	1.808	0.49265

Table 3.14: Numerical results. Eigenvalues for a crack whose plane forms angle γ with the surface and whose edge inclincation angle varies. Mode I.

γ/π	β/π	32	72	128	m	$\lambda_{extrap.}$
1/24	0.36	0.695712	0.599018	0.565533	1.996	0.52306
1/24	0.38	0.679028	0.579920	0.545092	1.990	0.50004
1/24	0.40	0.664473	0.562662	0.526424	1.960	0.47870
1/12	0.36	0.688328	0.594304	0.561267	1.990	0.51852
1/12	0.38	0.672865	0.5755905	0.541554	1.962	0.49622
1/12	0.41	0.653629	0.551960	0.515248	1.920	0.46558
1/8	0.35	0.684789	0.595929	0.564341	1.960	0.52269
1/8	0.37	0.669932	0.577834	0.544835	1.940	0.50077
1/8	0.39	0.657401	0.561800	0.527224	1.910	0.48003
1/6	0.335	0.680817	0.598623	0.59033	1.922	0.52900
1/6	0.365	0.659798	0.572340	0.540572	1.900	0.49695
1/6	0.380	0.651447	0.561084	0.528066	1.882	0.48209
5/24	0.34	0.658234	0.579336	0.550463	1.880	0.51028
5/24	0.36	0.646696	0.563970	0.533513	1.830	0.49048
5/24	0.38	0.637786	0.550840	0.518594	1.840	0.47240
1/4	0.31	0.656844	0.586974	0.561211	1.860	0.52487
1/4	0.335	0.640617	0.566366	0.538845	1.842	0.49948
1/4	0.365	0.627436	0.547054	0.516177	1.820	0.47336

Table 3.15: Numerical results. Eigenvalues for a crack whose plane forms angle γ with the surface and whose edge inclination angle varies. Mode II, Mode III

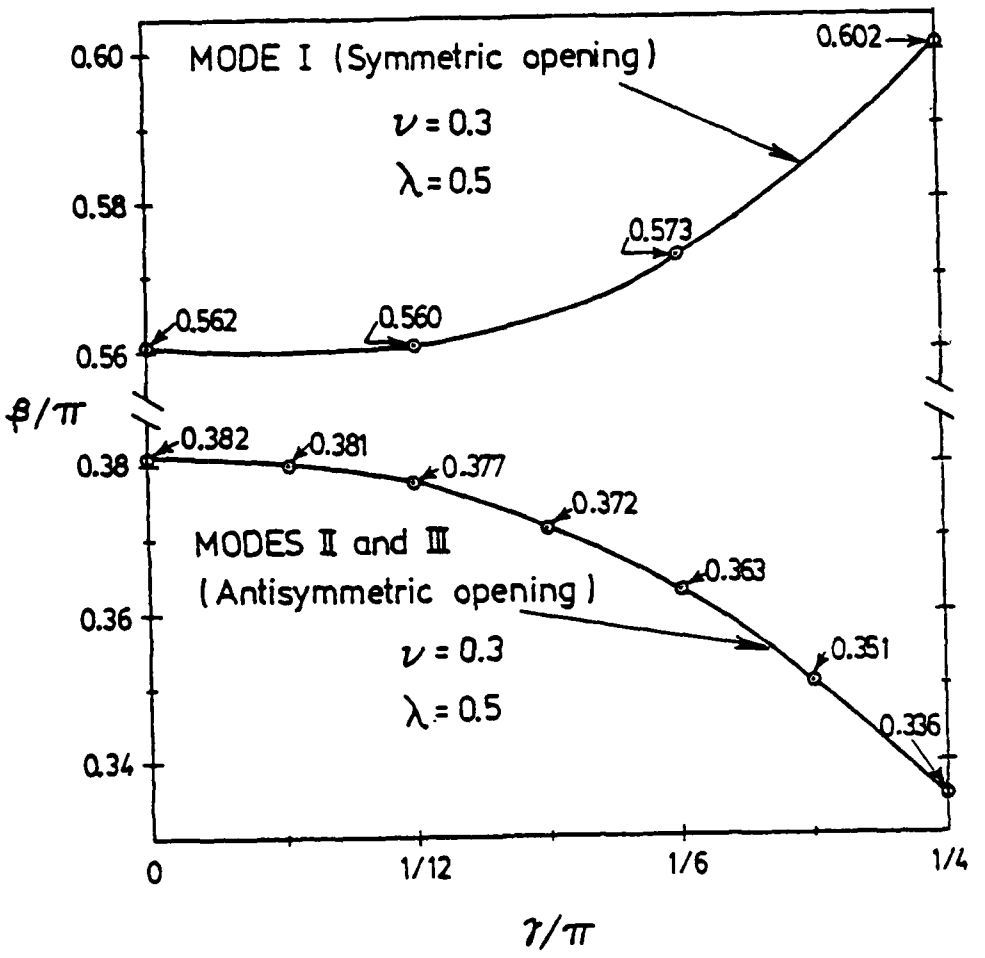

Fig. 3.23: Dependence of crack front edge angle β of a propagating crack upon crack plane angle γ. (a) Mode I; (b) Modes II and III. ($\nu = 0.3$)

given ratio $K_1 : K_2 : K_3$, one can generally find the angles β and δ which must get established at the surface point.

In solving this problem one must take into account the entire domain $0 \leq \theta \leq \theta$, $\gamma \leq \phi \leq 2\pi + \gamma$, because the symmetry is destroyed when $\gamma > 0$. Fig. 3.19 shows a typical finite element grid in the $(\theta\text{-}\phi)$-plane corresponding to the domain enclosed by the dashed curve of Fig. 3.18.

3.5 Experimental Fracture Specimens

Some recently obtained experimental results allow a check on the present numerical results. These are the fatigue loading fracture tests made by P. D. Bell and W. J. Feeney [15], to whom the author is obliged for making their results available, and are reproduced in Figs. 3.24 and 3.25. These photographs show the crack arrest marks observed in fatigue Mode I fracture tests of alluminum alloy and titanium alloy specimens. The Poisson ratios of these materials are (according to material handbooks) about 0.33 and 0.32, respectively, and for which the present solution, Fig. 3.20 gives $\beta \approx 102^\circ$ for both materials. These angles are plotted and compared in Figs. 3.24 and 3.25. Comparatively, the observed trend agrees with the numerical resutls in that the surface point trails behind the interior crack edge (i.e., $\beta > 90^\circ$) rather than moving ahead. The numerical value does not agree too closely with the observed average, but considering that some small scale yielding and inelastic strain reversals occur in the actual tests, and that the plastic "shear lip" phenomenon can along cause $\beta > 90^\circ$, the comparison cannot be qualified as poor. One must also realize the inevitable statistical scatter of the experiment.

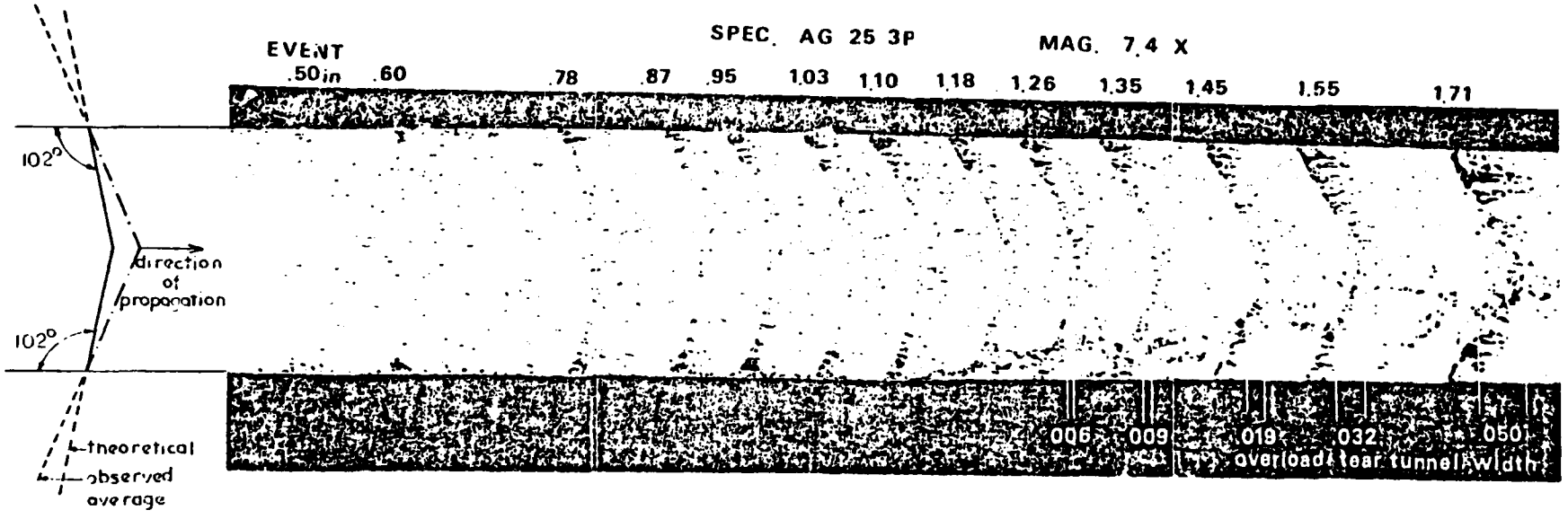

Fig. 3.24: View of fracture face showing fatigue arrest marks on Aluminum Alloy 2219-T5 81 (ν = 0.33, Mode I crack, sheet width 6.35 mm (1/4 in.), magnification 7.4 times, crack propagates to the right). (Reproduced from Fig. A-3, p. 160

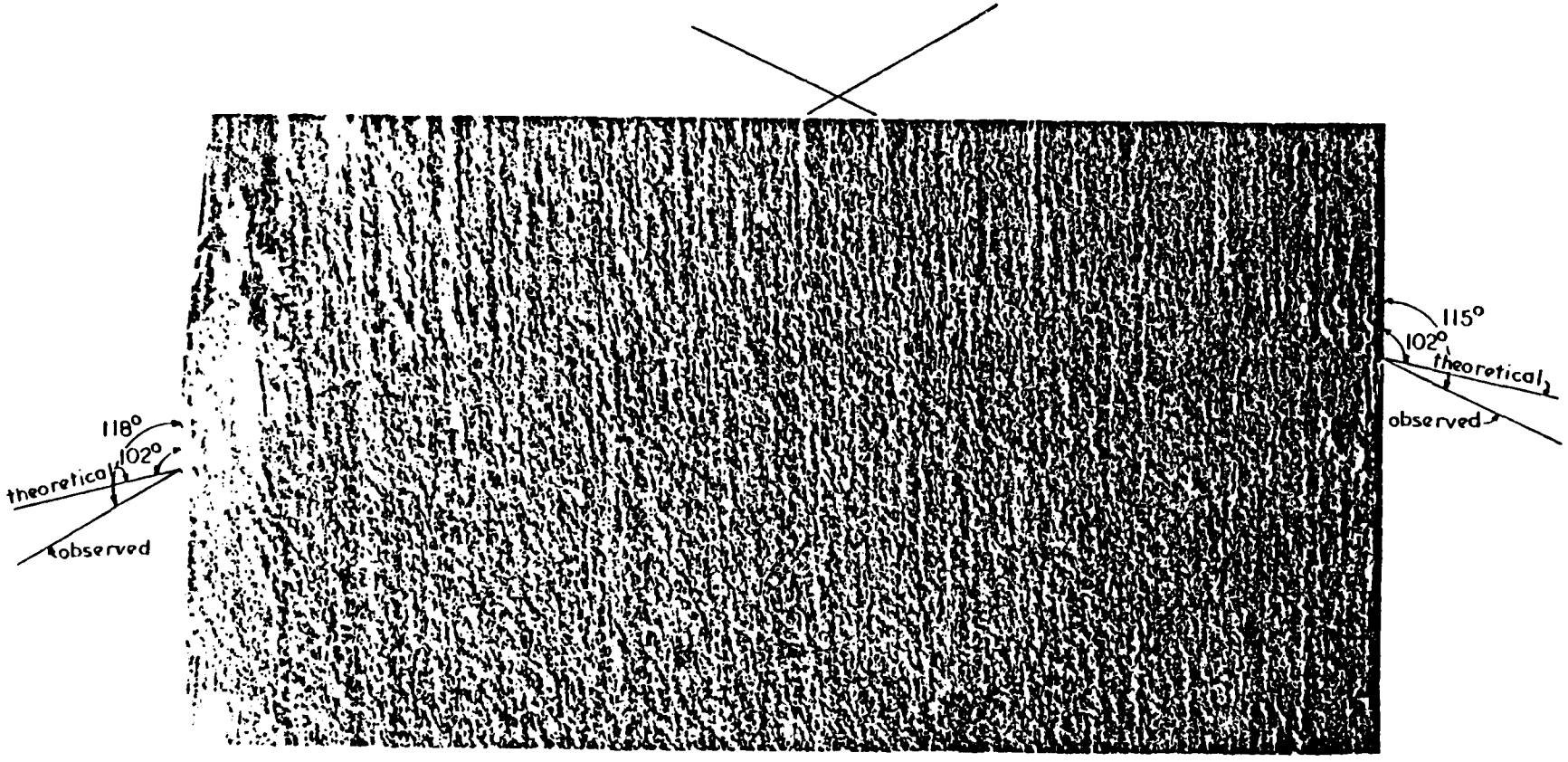

Fig. 3.25: View of fracture face showing crack arrest mark on Titanium Alloy Ti 6A1-4V. (ν = 0.32, Mode I crack, sheet width 6.35 mm (1/4 in.), magnification 33 times, crack propagates upwrads). (Reproduced from Fig. A.6 on p. 167 of P. D. Bell and W. J. Feeney [15]).

The crack arrest marks indicate the line of constant $\lambda = \frac{1}{2}$ for which propagation is established. The curves that these marks trace may be explained in the following manner. Prior to propagation, the two-dimensional theory of fracture mechanics gives $\lambda = \frac{1}{2}$ for the interior of the specimen (plane strain in the middle regions and plane stress near the surface) while $\lambda > \frac{1}{2}$ will hold at the surface point. When propagation is established the interior edge ($\lambda = \frac{1}{2}$) will move perpendicularly to the crack independent of Poisson ratio, while the surface point (weaker singularity, $\lambda > \frac{1}{2}$) will have to reach $\lambda = \frac{1}{2}$ by allowing the crack edge to shift angles and thus moving behind the interior, as predicted in Fig. 3.20.

Even though experimental results are nonexistent for Modes II and III, a similar reasoning may be made. Again, the two-dimensional theory of fracture mechanics gives $\lambda = \frac{1}{2}$ for the interior points while $\lambda < \frac{1}{2}$ will hold at the surface points. When propagation is established, provided the propagation plane remains in the same plane as that of the crack, the surface point (stronger singularity $\lambda < \frac{1}{2}$) will have to reach $\lambda = \frac{1}{2}$ by allowing the crack edge to shift angles and thus move ahead of the interior, as predicted in Fig. 3.20.

3.6 The Two-Material Interface

In plane elasticity, the singularity exponent of an interface crack between two dissimilar materials is complex. Consequently, the displacements in a close enough neighborhood of the crack tip oscillate along the radial ray. This implies an overlap of crack faces which is, of course, physically impossible and is prevented by

contact of crack surfaces. Nevertheless, it is generally believed that the field for complex λ is at least applicable in not too close neighborhood of the crack tip, well beyond the region of oscillations. That this is indeed the case for Mode I cracks has been demonstrated, by Comninou [22]. It must be noted, though, that recently more physically meaningful solutions which take into account the contact stresses on crack surfaces have been developed [22], but their adaptation is beyond the scope of this program. Thus, while extension of these developments to three dimensional singularities should be of high priority, at present we must be content with the less than perfect oscillating singularity.

The foregoing solution applies without any change to cases where λ is complex. Then, of course, k_{ij} and X_j, Eq. (2.15), must be also considered complex and the program must be converted to complex arithmetic, which is easily achieved by proper type declaration of FORTRAN variables. Some difficulties were caused by the need of an equation solving subroutine for complex banded nonsymmetric matrices. Such subroutine has not been available in standard software packages, and so it had to be developed, and it is listed in Appendix C, page 144.

A.) Check cases.

In the first four sections of this chapter it was noted that the convergence of the eigenvalue as the number of finite elements increased was systematic and an extrapolation technique was thus developed. In the check cases where the eigenvalues are complex, the real part

was found to behave equally well, but the complex part did not. Instead, the complex part of λ gave nearly the exact value for any number of finite elements. These check cases were the well known two-dimensional interface crack solutions and the problem of a rigid corner stamp of angle 2β which was solved by Parihar and Keer [14b].

The two-dimensional solution for the exponent is given by [32,33]

$$\lambda = \tfrac{1}{2} \pm i\gamma_1 \tag{3.30}$$

where,

$$\gamma_1 = \frac{\pi}{2} \log \left[\left(\frac{K_1}{\mu_1} + \frac{1}{\mu_2} \right) \Big/ \left(\frac{1}{\mu_2} + \frac{K_2}{\mu_2} \right) \right] \tag{3.31}$$

and $K_i = 3 - 4\nu_i$ for plane strain, (since generalized plane stress cannot be modeled by the program).

For a study case, materials whose Young's moduli have the ratio $E_1/E_2 = 1/40$ and whose Poisson ratios have the same value $\nu_1 = \nu_2 = 0.3$, were chosen. For these values Eq. (3.31) yields $\gamma_1 = 0.0887$. The domain to be considered must be $0 \le \theta \le \pi/2$, $0 \le \phi \le 2\pi$, where the elements in the region $\phi > \pi$ have a Young modulus forty time larger than those in the region $\phi < \pi$, but both regions have the same Poisson ratio $\nu_1 = \nu_2 = 0.3$; and to simulate the two-dimensional problem supports perpendicular to $\theta = \pi/2$ must be placed. The numerical results were: $\lambda = 0.65047 + 0.06548i$; $0.57329 \pm 0.08528i$; $0.54288 + 0.08785i$ for N = 32, 72, and 128 elements, respectively. The extrapolated

value of the real parts gives 0.49709 which is within 0.4% error of the exact value of 0.5. Note that the imaginary part of the eigenvalue using 128 elements is already within 1.5% error. When $\nu = 0$ for both materials, the plane strain solution [33] also applies for the surface singularity with an orthogonal crack edge; for a 2:1 ratio of young moduli this gives $\lambda = 0.5 \pm 0.0535i$; whereas, the program yielded Im $(\lambda) = 0.0514$ for $N = 128$.

For the second study case, a rigid corner stamp of angle $2\beta = 0.2886\pi$ on a semi-infinite body of Poisson ratio $\nu = 0.3$, were chosen from the table in Ref. [14b] where the analytical solution is given by $0.2474 + 0.0409i$. The numerical results for this problem were $\lambda = 0.37044 + 0.04393i$; $0.3128 + 0.04532i$; $0.28804 + 0.04509i$ for $N = 32, 72, 128$ elements, respectively. The extrapolated value of the real parts is 0.241, again within 0.4%; and that the imaginary part using 128 elements is within 10%. There may be two possible reasons for the imaginary part to be in such relatively large error: a.) The representation of the exact domain with finite elements is not very accurate for such angle β, which unfortunately was the largest angle that Parihar and Keer could consider, b.) The analytical solution obtained by Parihar and Keer involves an approximate function substituting a Bessel function, which restricts them to consider only small angles.

In either case, the solutions obtained with the present program show that numerical results can be obtained with reasonable accuracy.

B.) Additional results

Further cases were run using the present program for which no solutions have been given before. These were the results for $\nu > 0$. i.e., the plane strain solution is not applicable.

a.) The singularity for an orthogonal crack edge of an interface of two materials with a Young's moduli ratio of 2:1 and equal Poisson ratio, the program gives $Im(\lambda) = \pm 0.0399$ ($N = 128$) for $\nu = 0.05$ and $Im(\lambda) = \pm 0.006$ ($N = 128$) for $\nu = 0.3$. It can be noted that $Im(\lambda)$ decreases with increasing ν. For $\nu = 0.3$ and a 30:1 ratio of E, the program indicated $Im(\lambda)$ to be 0 or almost 0.

b.) For these cases, the program again showed $Im(\lambda)$ to be close and almost 0. For an interior crack plane of an orthogonal two-material interface, the program indicated that a crack with a front edge orthogonal to the two-material interface has $\lambda = 0.545$, 0.521, and 0.499 for E - rations 1:1, 5:0 and 10:0 for $\nu = 0.3$ ($N \to \infty$).

3.7 The Notch Surface Singularity

Solutions for the surface singularity at notches have not been given before. The present program can readily handle notches with higher accuracy since the material domain decreases with the size of the notch angle. Fig. 3.26 shows the numerical results ($N \to \infty$) for notches terminating at the surface with orthogonal ($\beta = \pi/2$) and symmetrical opening ($\nu = -\alpha$).

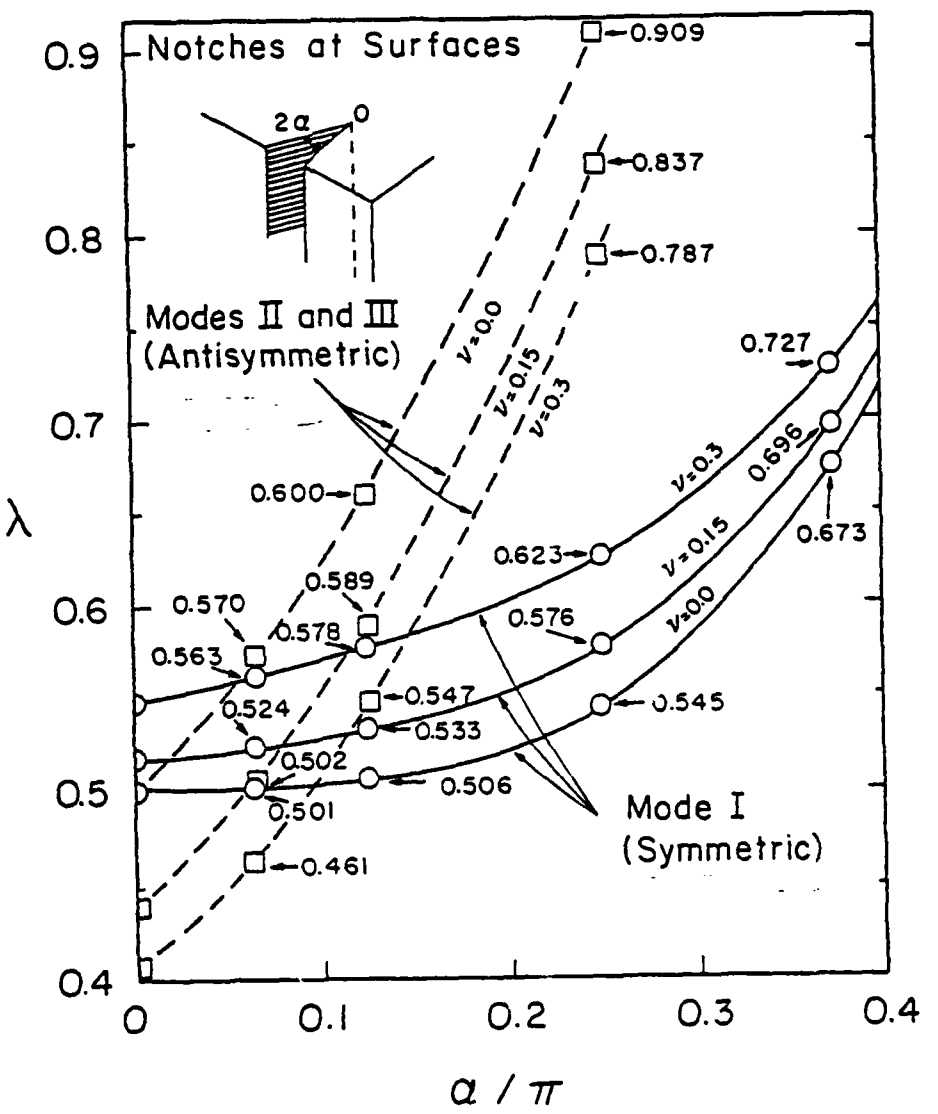

Fig. 3.26: Numerical results for the surface termination of notches having orthogonal front edge ($N \to \infty$).

CONCLUSIONS

The finite element method in angular spherical coordinates provides a powerful general tehcnique for determining three-dimensional elastic stress singularities. The numerical results for cracks whose edge is normal to the surface and for crack corners in an infinite space are in close agreement with the analytical solutions of Benthem, and Keer and Parihar, respectively. The front edge of a propagating crack must terminate at the surface point obliquely. The values of this angle are different for symmetric (Mode I) and antisymmetric (Mode II and III) crack opening; which indicates that a combined mode propagation is impossible at the surface point of a crack whose plane is normal to the surface. For Mode I, the surface point trails behind the interior of the crack; while for Modes II and III, the surface point moves ahead of the interior of the crack. For cracks of inclined plane, the propagation at the surface point takes place in a combination of all three modes.

The numerical results for a rigid corner stamp on a semi-infinite space are also in close agreement with the complex analytical solution of Keer. Some numerical results of complex singularities are obtained, as well as some cases of notches.

REFERENCES

1. KNEIN, M., "Zur Theorie des Druckver suchs", Abhandlungen aus dem Aerodymischen Institut an der Technigchen Hochschule Aachen, Heft 7, 43-62 (1927).

2. WILLIAMS, M. L., "Stress Singularities Resulting from Various Boundary Conditions in Angular Corners of Plates in Extension", Trans. ASME, Ser. E, J. of Appl. Mech., 19, 526-528 (1952).

3. BAŽANT, Z. P., "Three-Dimensional Harmonic Functions Near Termination or Intersection of Gradient Singularity Lines: A General Numerical Method", Int. J. Engng. Sci., 12, 221-243 (1974).

4. BAŽANT, Z. P. and KEER, L. M., "Singularities of Elastic Stresses and of Harmonic Functions at Conical Notches and Inclusions", Int. J. of Solids and Structures, 10, 957-964 (1974).

5. ACHENBACH, J. O. and BAŽANT, Z. P., "Elastodynamic Near-Tip Stress and Displacement Fields for Rapidly Propagating Cracks in Orthotropic Materials", Trans. ASME, Ser. E, J. of Appl. Mech., 42, 183-189 (1975).

6. ACHENBACH, J. D., BAŽANT, Z. P. and KHETA, R. P., "Elastodynamic Near-Tip Fields for a Crack Propagating Along the Interface of Two Orthotropic Solids", Int. J. of Engng. Sci., 14, 811-818 (1976).

7. SWEDLOW, J. L. and KARABIN, M. E., "A Case of Elasto-Plastic Flow Using a New Special Element", Fracture 1977, Proc. 4th Int. Conf. on Fracture, held at Univ. of Waterloo, Ont., Canada in June 1977, Ed. by Taplin, D. M. R., Vol. 1, 117-131.

8. RICHARDSON, L. F. and GAUNT, J. A., "The Deferred Approach to The Limit", Trans. Roy. Soc. London, A226, 299-361 (1927).

9. BENTHEM, J. P., "State of Stress at the Vertex of a Quarter-Infinite Crack in a Half-Space", Int. J. of Solids and Structures, 13, 479-492 (1977).

10. KAWAI, T., FUJITAMI, Y. and KUMAGAI, K., "Analysis of Singularity at the Root of the Surface Crack Problem", Proc. of an Int. Conf. on Fracture Mech. and Tech. held in Hong Kong in March 1977, Ed. by Sih, G. C. and Chow, C. L., Vol. II, pp. 1157-1163.

11. MORRISON, J. A. and LEWIS, J. A., "Charge Singularity at the Corner of a Flat Plate", SIAM (Soc. of Industr. and Appl. Math.) J. of Appl. Math., 31, 233-250 (1976).

12. KEER, L. M. and PARIHAR, K. S., "Singularity at the Apex of Pyramidal Notches with Three Equal Angles", Quart. Appl. Math., 30, 401-405 (1977).

13. KEER, L. M. and PARIHAR, K. S., "Singularity at the Corner of a Wedge-Shaped Punch or Crack", SIAM J. of Appl. Math., 34, No. 2, 297-302 (1978).

14a. PARIHAR, K. S. and KEER, L. M., "Stress Singularity at the Corner of a Wedge-Shaped Crack or Inclusion", Trans. ASME, J., Appl. Mech., Vol. 45, No. 4, December 1978.

14b. KEER, L. M. and PARIHAR, K. S., "The Singularity at the Apex of a Bonded Wedge-Shaped Stamp", Trans. ASME, J. Appl. Mech., Vol. 46, April 1979.

15. BELL, P. D. and FEENEY, W. Y., "Fractographic Evaluation of Fracture Specimens", Tech. Rep. AFFDL-TR-75-152 (to Air Force Flight Dynamics Laboratory, Wright-Patterson Base, Dayton, Ohio), Grumman Aerospace Corporation, Bethpage, N.Y. (1976).

16. KARP, S. N. and KARAL F. C., "The Elastic-Field Behavior in the Neighborhood of a Crack of Arbitrary Angle", Communications on Pure and Appl. Math., 15, 413-421 (1962).

17. LOVE, A. E. H., "A Treatise on the Mathematical Theory of Elasticity", 4th Ed., Dover Publ., New York (1944).

18. FUNG, Y. C., "Founcations of Solid Mechanics", Prentice-Hall International, Inc., Englewood Cliffs, N. J. (1965).

19. SOKOLNIKOFF, I. S., "Mathematical Theory of Elasticity", McGraw-Hill Inc. (1956).

20. TRANTER, C. J., "The Use of the Mellin Transform in Finding the Stress Distribution in an Infinite Wedge", Quart. J. Mech. Appl. Math., Vol. 1, 125 (1948).

21. BENTHEM, J. P., "On the Stress Distribution in Anisotropic Infinite Wedges", Quart. Appl. Math., Vol. XXI, No. 3, p. 189 (1963).

22. COMMINOU, M., "The Interface Crack", Trans. ASME, Ser. E., J. of Applied Mechanics, 44, 631-636 (1977).

23. KNOTT, J. F., "Fundamentals of Fracture Mechanics", Butterworth Publ., London (1973).

24. WILLIAMS, M. L., "Surface Stress Singularities Resulting from Various Boundary Conditions in Angular Corners of Plates Under Bending", Proc., First U.S. Nat.-Congress of Applied Mechanics. Held in Chicago, June 1951, Publ. by ASME.

25. ZIENKIEWICZ, O. C., "The Finite Element Method in Engineering Science", McGraw-Hill, London (1971).

26. STRANG, W. G. and FIX, G. J., "An Analysis of the Finite Element Method", Prentice-Hall International, Inc., Englewood Cliffs, N.J. (1973).

27. DESAI, C. S. and ABEL, J. F., "Introduction to the Finite Element Method", Van Nostrand Reinhold Co., N.Y., N.Y. (1972).

28. CANAHAN, B., LUTHER, H. A. and WINKS, J. O., "Applied Numerical Methods", John Wiley and Sons, Inc. (1969).

29. RICHARDSON, L. F.,"The Approximate Arithmetical Solution by Finite Differences of Physical Problems", Trans. Roy. Soc., London, 307-357 (1910).

30. KAWAI, T., FUJITANI, Y. and KUMAGAI, K., "On the Singular Solution of Three Dimensional Crack Problems", Proc. 2nd Inter. Conf. on Mechanical Behavior of Materials, held in Boston, Mass., Aug. 1976, 230-234 (1976).

31. RICE, J. R., "A Path Independent Integral and the Approximate Analysis of Strain Concentration by Notches and Cracks", Trans. ASME, J. of Appl. Mech., 379-386 (1968).

32. DUNDURS, J., DISCUSSION, Journal of Applied Mechanics, Vol. 36, Trans. ASME, Vol. 91, Ser. E., 150-652 (1969).

33. ERGODAN, F., "Stress Distribution in Bonded Dissimilar Materials With Cracks", Trans. ASME, J. of Appl. Mech., Vol. 32, Ser. E., 418-423 (1965).

34. FOLIAS, E. S., "On the Three-Dimensional Theory of Cracked Plates", Trans. ASME Series E., J. of Appl. Mech., Vol. 42, 663-674 (1975).

35. BAŽANT, Z. P. and ESTENSSORO, L. F., "General Numerical Method for Three-Dimensional Singluarities in Cracked or Notched Elastic Solids", Fracture 1977, Proc. 4th Int. Conf. on Fracture, held at Univ. of Waterloo, Ont., Canada inJune 1977, Ed. by Taplin, D. M. R., Vol. 3, 371-385.

36. BAŽANT, Z. D. and ESTENSSORO, L. F., "Stress Singularity and Propagation of Cracks at their Intersection with Surfaces", Int. J. of Solids and Structures, June, 1978. To be published.

37. BOGY, D. B., "On the Problem of Edge-Bonded Elastic Quarter-Planes Loaded at the Boundary", Int. J. of Solids and Structures, Vol. 6, 1287-1313 (1970.

APPENDIX A

DERIVATION OF THE VARIATIONAL EQUATION

The combination of the equations of equilibrium, Eqs. (1.7a-c) with the boundary conditions, Eqs. (1.11a-c) is given by the variational statement Eq. (1.12). With the intention of using the finite element method, Eq. (1.12) has to be reduced to an equation which involves no higher than first order derivatives and which automatically includes the boundary conditions. In the following derivation the asterisk * indicates terms, or term, which have been added and substracted.

Substituting X_r, X_θ, and X_ϕ from Eqs. (1.7a-c) into the surface integral of Eq. (1.12) yields

$$\iint \{[Q(\lambda - 1) - 2 + 2\lambda](\lambda F + 2F + G_\theta + G \cot \theta + \frac{1}{\sin \theta} H_\phi) +$$

$$- [(\lambda + 1)G_\theta - F_{\theta\theta}] - \cot \theta[(\lambda + 1)G - F_\theta] +$$

$$+ \frac{1}{\sin \theta} (\frac{1}{\sin \theta} F_{\phi\phi} - H_\phi - \lambda H_\phi)\} \sin \theta \, \delta F$$

$$+ [2\lambda G_\theta + 2\lambda G \cot \theta + \frac{2\lambda}{\sin \theta} H_\phi - (2\lambda G_\theta + 2\lambda G \cot \theta +$$

$$+ \frac{2\lambda}{\sin \theta} H_\phi)]^* \sin \theta \, \delta F + \{(Q+2)(\lambda F_\theta + 2F_\theta + G_{\theta\theta} + G_\theta \cot \theta -$$

$$- \frac{1}{\sin^2 \theta} G + \frac{1}{\sin \theta} H_{\theta\phi} - \frac{\cos \theta}{\sin^2 \theta} H_\phi) - \frac{1}{\sin \theta} (H_{\theta\phi} + H_\phi \cot \theta -$$

$$- \frac{1}{\sin\theta} G_{\phi\phi}) + \lambda[(\lambda+1)G - F_\theta]\} \sin\theta\,\delta G + [\frac{2}{\sin\theta} H_{\theta\phi} - 2G\cot^2\theta -$$

$$- (\frac{2}{\sin\theta} H_{\theta\phi} - 2G\cot^2\theta)]^* \sin\theta\,\delta G + \{\frac{1}{\sin\theta} (Q+2)(\lambda F_\phi + 2F_\phi +$$

$$+ G_{\theta\phi} + G_\phi \cot\theta + \frac{1}{\sin\theta} H_{\phi\phi}) - \lambda(\frac{1}{\sin\theta} F_\phi - H - \lambda H) + (H_{\theta\theta} +$$

$$+ H_\theta \cot\theta - \frac{1}{\sin^2\theta} H + \frac{\cos\theta}{\sin^2\theta} G_\phi - \frac{1}{\sin\theta} G_{\theta\phi})\}\,\delta H + [-2H_\theta\cot\theta +$$

$$+ \frac{2}{\sin^2\theta} H + \frac{2}{\sin\theta} G_{\theta\phi} - \frac{2\cos\theta}{\sin^2\theta} G_\phi - 2\lambda H - (-2H_\theta\cot\theta +$$

$$+ \frac{2}{\sin^2\theta} H + \frac{2}{\sin\theta} G_{\theta\phi} - \frac{2\cos\theta}{\sin^2\theta} G_\phi - 2\lambda H)]^* \sin\theta\,\delta H \Big]\Big] d\theta d\phi$$

(A. 1)

Arranging some terms and cancelling others (a light slash indicates terms which cancel), Eq. (A. 1) is reduced to:

$$\int\int\Big[\Big[\{[Q(\lambda-1)-2](\lambda F + 2F + G_\theta + G\cot\theta + \frac{1}{\sin\theta} H_\phi)$$

$$+ 2\lambda(\lambda F + 2F + G_\theta + G\cot\theta + \frac{1}{\sin\theta} H_\phi) - 2\lambda(G_\theta + G\cot\theta + \frac{1}{\sin\theta} H_\phi)$$

$$+ (\lambda G_\theta - G_\theta + F_{\theta\theta}) + \cot\theta(\lambda G - G + F_\theta) +$$

$$+ \frac{1}{\sin\theta}\left(\frac{1}{\sin\theta} F_{\phi\phi} + \lambda H_{\phi} - H_{\phi}\right)\}\sin\theta\,\delta F$$

$$+ \{Q(\lambda F_{\theta} + 2F_{\theta} + G_{\theta\theta} + G_{\theta}\cot\theta - \frac{1}{\sin^2\theta} G + \frac{1}{\sin\theta} H_{\theta\phi} - \frac{\cos\theta}{\sin^2\theta} H_{\phi})$$

$$+ 2(\lambda F_{\theta} + (1+1)F_{\theta} + G_{\theta\theta} + G_{\theta}\cot\theta - \frac{1}{\sin^2\theta} G + \frac{1}{\sin\theta} H_{\theta\phi} - \frac{\cos\theta}{\sin^2\theta} H_{\phi})$$

$$+ \frac{1}{\sin\theta}\left(H_{\theta\phi} - H_{\phi}\cot\theta + \frac{1}{\sin\theta} G_{\phi\phi}\right) + \lambda(\lambda+1)G - \lambda F_{\theta}$$

$$- 2G\cot^2\theta - \frac{2}{\sin\theta} H_{\theta\phi} + 2G\cot^2\theta$$

$$+ [-Q\cot\theta(\lambda F + 2F + G_{\theta} + \frac{1}{\sin\theta} H_{\phi} + G\cot\theta)$$

$$+ Q\cot\theta(\lambda F + 2F + G_{\theta} + \frac{1}{\sin\theta} H_{\phi} + G\cot\theta)]^{*}\}\sin\theta\,\delta G$$

$$+ \{\frac{Q}{\sin\theta}\left(\lambda F_{\phi} + 2F_{\phi} + G_{\theta\phi} + G_{\phi}\cot\theta + \frac{1}{\sin\theta} H_{\phi\phi}\right)$$

$$+ \frac{2}{\sin\theta}\left(\lambda F_{\phi} + (1+1)F_{\phi} + G_{\theta\phi} + G_{\phi}\cot\theta + \frac{1}{\sin\theta} H_{\phi\phi}\right)$$

$$+ \left(H_{\theta\theta} - H_{\theta}\cot\theta + \frac{1}{\sin^2\theta} H + \frac{1}{\sin\theta} G_{\theta\phi} - \frac{\cos\theta}{\sin^2\theta} G_{\phi}\right)$$

$$- \frac{\lambda}{\sin\theta} F_{\phi} + \lambda(\lambda-1)H + \cot\theta\left(H_{\theta} - H\cot\theta + \frac{1}{\sin\theta} G_{\phi}\right) +$$

$$+ \cot\theta\left(H_\theta - H\cot\theta + \frac{1}{\sin\theta}G_\phi\right) + \left(2\frac{\cos^2\theta}{\sin^2\theta} - 2\frac{1}{\sin^2\theta} + 2^*\right)H -$$

$$- 2H^* - \frac{2}{\sin\theta}G_{\theta\phi} + 2\lambda H\Big]\sin\theta\,\delta H\Big]\Big]\,d\theta d\phi \qquad (A.2)$$

The terms multiplied by $\sin\theta\,\delta G$ are arranged to form:

$$\{Q(\lambda F_\theta + 2F_{\theta\theta} + G_{\theta\theta} + G_\theta\cot\theta - \frac{1}{\sin^2\theta}G + \frac{1}{\sin\theta}H_{\theta\phi} - \frac{\cos\theta}{\sin\theta}H_\phi) +$$

$$+ 2(G_{\theta\theta} + F_\theta) + \cot\theta[Q(\lambda F + 2F + G_\theta + \frac{1}{\sin\theta}H_\phi + G\cot\theta) +$$

$$+ 2(G_\theta + F')] + \frac{1}{\sin\theta}(H_{\theta\phi} - H_\phi\cot\theta + \frac{1}{\sin\theta}G_{\phi\phi}) - 2\cot\theta(\frac{1}{\sin\theta}H_\phi +$$

$$+ G\cot\theta + F) + \lambda(\lambda + 1)G + 2F_\theta - Q\cot\theta(\lambda F + 2F + G_\theta +$$

$$+ \frac{1}{\sin\theta}H_\phi + G\cot\theta) + \lambda F_\theta - 2(\frac{1}{\sin^2\theta} - \frac{\cos^2\theta}{\sin^2\theta} - 1^*)G - 2G^*]\sin\theta\,\delta G$$

(A.3)

Placing Eq. (A.3) back into Eq. (A.2) and rearranging terms:

$$\int\int\Big[\{[Q(\lambda - 1) - 2](\lambda F + 2F + G_\theta + G\cot\theta + \frac{1}{\sin\theta}H_\phi) + 2\lambda(\lambda + 2)F$$

$$+ (\lambda G_\theta - G_\theta + F_{\theta\theta}) + \cot\theta(\lambda G - G + F_\theta)$$

$$+ \frac{1}{\sin\theta}\left(\frac{1}{\sin\theta} F_{\phi\phi} + \lambda H_{\phi} - H_{\phi}\right)\Big]\sin\theta\,\delta F$$

$$+ \{-Q\cot\theta(\lambda F + 2F + G_{\theta} + G\cot\theta + \frac{1}{\sin\theta} H_{\phi}) + \lambda F_{\theta}$$

$$- 2\cot\theta(\frac{1}{\sin\theta} H_{\phi} + F\cot\theta + F) + 2(\lambda G - G + F_{\theta}) + \lambda(\phi - 1)G$$

$$+ Q(\lambda F_{\theta} + 2F_{\theta} + G_{\theta\theta} + G_{\theta}\cot\theta - \frac{1}{\sin^2\theta} G + \frac{1}{\sin\theta} H_{\theta\phi} - \frac{\cos\theta}{\sin^2\theta} H_{\phi}) +$$

$$+ 2(G_{\theta\theta} + F_{\theta}) + \cot\theta[Q(\lambda F + 2F + G_{\theta} + G\cot\theta + \frac{1}{\sin\theta} H_{\phi}) +$$

$$+ 2(G_{\theta} + F)] + \frac{1}{\sin\theta}(H_{\theta\phi} - H_{\phi}\cot\theta + \frac{1}{\sin\theta} G_{\phi\phi})\Big]\sin\theta\,\delta G$$

$$+ \{\cot\theta(H_{\theta} - H\cot\theta + \frac{1}{\sin\theta} G_{\phi}) + 2(\frac{1}{\sin\theta} F_{\phi} + \lambda H - H)$$

$$+ \frac{\lambda}{\sin\theta} F_{\phi} + \lambda(\lambda - 1)H + (H_{\theta\theta} - H_{\theta}\cot\theta + \frac{1}{\sin^2\theta} H + \frac{1}{\sin\theta} G_{\theta\phi} - \frac{\cos\theta}{\sin^2\theta} G_{\phi})$$

$$+ \cot\theta(H_{\theta} - H\cot\theta + \frac{1}{\sin\theta} G_{\phi})$$

$$+ \frac{Q}{\sin\theta}(\lambda F_{\phi} + 2F_{\phi} + G_{\theta\phi} + G_{\phi}\cot\theta + \frac{1}{\sin\theta} H_{\phi\phi})$$

$$+ \frac{2}{\sin\theta}(\frac{1}{\sin\theta} H_{\phi\phi} + G_{\phi}\cot\theta + F_{\phi})\Big]\sin\theta\,\delta H \iint d\theta d\phi \qquad (A.4)$$

which can be written as

$$\iint\Big[\{\sin\theta(\lambda-1)-2](\lambda F+2F+G_\theta+G\cot\theta+\frac{1}{\sin\theta}H_\phi)+2\lambda\sin\theta(\lambda+2)F$$

$$+\frac{\partial}{\partial\theta}[\sin\theta(\lambda G-G+F_\theta]+\frac{\partial}{\partial\phi}[\frac{1}{\sin\theta}F_\phi+\lambda H-H]]\delta F$$

$$+\{(-[(Q+2)(2F+G_\theta+\beta\cot\theta+\frac{1}{\sin\theta}H_\phi)-2(G_\theta+F)+\lambda QF]\cot\theta$$

$$+2(F_\theta-G)+\lambda(\lambda+1)G+\lambda F_\theta)\sin\theta$$

$$+\frac{\partial}{\partial\theta}[\sin\theta((Q(\lambda F+2F+G_\theta+G\cot\theta+\frac{1}{\sin\theta}H_\phi)+2(G_\theta+F)))]$$

$$+\frac{\partial}{\partial\phi}[H_\theta-H\cot\theta+\frac{1}{\sin\theta}G_\phi]\}\,\partial G$$

$$\{\sin\theta[\cot\theta(H_\theta-H\cot\theta+\frac{1}{\sin\theta}G_\phi)+2(\frac{1}{\sin\theta}F_\phi-H)+$$

$$+\lambda(\lambda+1)H+\frac{\lambda}{\sin\theta}F_\phi]+\frac{\partial}{\partial\theta}[\sin\theta(H_\theta-H\cot\theta+\frac{1}{\sin\theta}G_\phi)]$$

$$+\frac{\partial}{\partial\phi}[Q(\hat{\lambda}F+2F+G_\theta+G\cot\theta+\frac{1}{\sin\theta}H_\phi)+2(\frac{1}{\sin\theta}H_\phi+G\cot\theta+$$

$$+F)]\delta H\Big]\Big]d\theta d\phi \qquad (A.5)$$

Integrating by parts with respect to θ and ϕ the respective terms whose partial derivatives are broughtout, and using the negative of Eq. (A.5):

$$\iint\!\!\!\int \sin\theta\{[Q(1-\lambda)+2](\lambda F+2F+G_\theta+G\cot\theta+\frac{1}{\sin\theta}H_\phi)-2\lambda(\lambda+2)F\}\delta H$$

$$+\sin\theta(\lambda G-G+F_\theta)\delta F_\theta+(\frac{1}{\sin\theta}F_\phi+\lambda H-H)\delta F_\phi$$

$$+\sin\theta\{[(Q+2)(2F+G_\theta+G\cot\theta+\frac{1}{\sin\theta}H_\phi)-2(G_\theta+F)+\lambda QF)\cot\theta$$

$$-2(F_\theta-G)-\lambda(\lambda+1)-\lambda F_\theta\}\delta G$$

$$\sin\theta[Q(\lambda F+2F+G_\theta+G\cot\theta+\frac{1}{\sin\theta}H_\phi)+2(G_\theta+F)]\delta G_\theta$$

$$+(H_\theta-H\cot\theta+\frac{1}{\sin\theta}G_\phi)\delta G_\phi$$

$$-\sin\theta[\cot\theta(H_\theta-H\cot\theta+\frac{1}{\sin\theta}G_\phi)+2(\frac{1}{\sin\theta}F_\phi-H)+\lambda(\lambda+1)H+$$

$$+\frac{\lambda}{\sin\theta}F_\phi]\delta H+\sin\theta[H_\theta-H\cot\theta+\frac{1}{\sin\theta}G_\phi)\delta H_\theta$$

$$+[Q(\lambda F+2F+G_\theta+G\cot\theta+\frac{1}{\sin\theta}H_\phi)+2(\frac{1}{\sin\theta}H_\phi+G\cot\theta+F)]$$

$$\delta H_\phi]]d\theta d\phi$$

$$+\int_r\{\{\sin\theta\{(\lambda G-G+F_\theta)\delta G+[Q(\lambda F+2F+G_\theta+G\cot\theta+\frac{1}{\sin\theta}H_\phi)+$$

$$+ 2(G_\theta + F)]\delta G + (H_\theta - H \cot\theta + \frac{1}{\sin\theta} G_\phi)\delta H\}n_\theta$$

$$+ \sin\theta\{\frac{1}{\sin\theta}(\frac{1}{\sin\theta} F_\phi + \lambda H - H)\delta F + \frac{1}{\sin\theta}(H_\theta - H \cot\theta +$$

$$+ \frac{1}{\sin\theta} G_\phi)\delta G + \frac{1}{\sin\theta}[Q(\lambda F + 2F + G_\theta + G \cot\theta + \frac{1}{\sin\theta} H_\phi) +$$

$$+ 2(\frac{1}{\sin\theta} H_\phi + G \cot\theta + F)]\delta H\}n_\phi]\}ds \qquad (A.6)$$

Substituting the boundary conditions, Eqs. (1.11a-c), and Eq. (A.6) into Eq) (1.12) one can see that the line integral of Eq. (A.6) cancels the line integral of Eq. (1.12). Thus, the boundary conditions are automatically included, and the following variational equation results:

$$\iint\{\{\{[[Q(1-\lambda)+2](\lambda F + 2F + C_\theta + G \cot\theta + \frac{1}{\sin\theta} H_\phi) - 2\lambda(\lambda+2)F]\delta F$$

$$+ (\lambda G - G + F_\theta)\delta F_\theta + \frac{1}{\sin\theta}(\frac{1}{\sin\theta} F_\phi + \lambda H - H)\delta F_\phi$$

$$+ \{[(Q+2)(G_\theta + 2F + G \cot\theta + \frac{1}{\sin\theta} H_\phi) - 2(G_\theta + F) + \lambda QF]\cot\theta$$

$$- 2(F_\theta - G) - \lambda(\lambda+1)G - \lambda F_\theta\}\delta G$$

$$+ [Q(\lambda F + 2F + G_\theta + G \cot\theta + \frac{1}{\sin\theta} H_\phi) + 2(G_\theta + F)]\delta G_\theta$$

$$+ \frac{1}{\sin\theta}\left(H_\theta - H\cot\theta + \frac{1}{\sin\theta}G_\phi\right)\delta G_\phi$$

$$- \left[\cot\theta\left(H_\theta - H\cot\theta + \frac{1}{\sin\theta}G_\phi\right) + 2\left(\frac{1}{\sin\theta}F_\phi - H\right) + \lambda(\lambda+1)H + \right.$$

$$\left. + \frac{\lambda}{\sin\theta}F_\phi\right]\delta H + \left(H_\theta - H\cot\theta + \frac{1}{\sin\theta}G_\phi\right)\delta H_\theta$$

$$+ \frac{1}{\sin\theta}\left[Q\left(\lambda F + 2F + G_\theta + G\cot\theta + \frac{1}{\sin\theta}H_\phi\right) + 2\left(\frac{1}{\sin\theta}H_\phi + \right.\right.$$

$$\left.\left. + G\cot\theta + F\right)\right]\delta H_\phi\Big\}\Big\}\sin\theta\, d\theta d\phi \qquad \text{(A.7)}$$

Note that Eq. (A.7) does not have any second order derivatives and that the notations in Eq. (1.14) are those shown in Eq. (A.7).

APPENDIX B

FINITE ELEMENT PROGRAM WHEN EIGNEVALUE, λ, IS REAL
(See Chapter II).

```
      PROGRAM SING(TAPE 99,INPUT,OUTPUT)
      DIMENSION A(459,65),B(459),AAA(65),NGLO(12),QQ(20),PPOIS(8),AL(20)
     1,POINT(3),WEI(3)
      DIMENSION CORETA(6)
      DIMENSION ALR(20), QQR(20),ALI(20)
      COMMON/C1/ NINTE,P,KSKEW(128),WEIGHT(9),S(4,9),STH(4,9),SPH(4,9),
     1 THEPO(9),PHIPO(9),Q,QA,QAA,QA2,QA21,QALL,Q2,ALL,ALI,AAL,AAL2,
     2NELHF,RATIO
      COMMON/C2/ STIFEL(12,12),NOP(128,4),PH(153),THE(153)
      COMMON/C3/ NSKEW,MSKEW,TANB

C  DATA FOR POISSON  RATIO
      DATA PPOIS/ 0.3 /
C  INCLINATION ANGLE OF CRACK FRONT EDGE
      CORETA(1) = 0.8557

      PI = 3.14159265358979323846
C  DIMENSIONS OF BODY
      THE1 = PI / 2.
      PHI1 = PI
C PHI BOUNDARY FOR A NOTCH
      PHI11=0.0
C  THE BOUNDARY FOR A NOTCH
      THE11=0.0
C MAX. NUMBER OF ITERATIONS, AND MAX. ERROR ON LAMDA= AL
      NITER = 10
C NUMBER OF STUDY CASES
      MGRID = 5
      NGRID = 5
      MPOIS = 1
      NPOIS = 1
      MBETA = 1
      NBETA = 1
      KBETA = 1

C NUMERICAL INTEGRATION DATA
C NINE ELEMENT SCHEME
      NINT = 3
      NINTE = NINT * NINT
      POINT(3) =  0.77459666924148
      POINT(2) = 0.
      POINT(1) = - POINT(3)
      WEI(1) = 0.555555555555555555
      WEI(2) = 0.888888888888888888
      WEI(3) = WEI(1)


C  GENERATE SHAPE FUCTIONS FOR NUM. INTEG. POINTS IN THE ELEMENT
      DO 10  IS = 1, NINT
      PH2 = POINT(IS) * .5
      PHI = PH2 + .5
      PHI1 = PH2 - .5
      DO 10  JS = 1, NINT
      NS = IS + (JS-1)*NINT
      WEIGHT(NS) = WEI(IS) * WEI(JS)
      TH2 = POINT(JS) * .5
      THI = TH2 + .5
      THI1 = TH2 - .5
      THEPO(NS) = TH2*2.0
      PHIPO(NS) = PH2*2.0
C VALUE OF F,G,OR H
      S(1,NS) =   PHI1 * THI1
      S(2,NS) = - PHI * THI1
      S(3,NS) =  - PHI1 * THI
      S(4,NS) = PHI * THI
C PARTIAL DERIVATIVE W.R.T. PHI OF (F,G,OR H)
      SPH(1,NS) = THI1*0.5
      SPH(2,NS) = - THI1*0.5
      SPH(3,NS) = - THI*0.5
      SPH(4,NS) = THI*0.5
C PARTIAL DERIVATIVE W.R.T. THETA OF (F,G,OR H)
      STH(1,NS) = PHI1*0.5
      STH(2,NS) = - PHI1*0.5
      STH(3,NS) = - PHI1*0.5
   30 STH(4,NS) = PHI*0.5

C VALUE OF P, WHERE DISPL. COMP. ASSUME A FORM
C      R**AL*(SIN(THETA)**P)*(F,G,OR H)
      P = 0.0

C NUMBER OF DIVIDING LINES IN THE THETA AND PHI DIRECTIONS
      DO 9999 KGRID = MGRID,NGRID
      IF( KGRID .EQ. 1) GO TO 1
      IF( KGRID .EQ. 2) GO TO 2
      IF( KGRID .EQ. 3) GO TO 3
      IF( KGRID .EQ. 4) GO TO 4
      IF(KGRID .EQ. 5) GO TO 5
    1 NT = 4
      NF = 7
      GO TO 6
    2 NT = 5
      NF = 9
      GO TO 6
    3 NT = 7
      NF = 13
      GO TO 6
    4 NT = 9
      NF = 17
      GO TO 6
    5 NT = 11
      NF = 21
    6 CONTINUE

C NUMBER OF ELEMENTS IN THETA AND PHI DIRECTIONS
      NT1 = NT - 1
      NF1 = NF - 1
C  NUMBER OF ELEMENTS
      NUMEL = NT1 * NF1
      NELHF = NUMEL/2 + 1
C NO. OF POINTS
      NP = NT * NF
C NO. OF EQUATIONS
      NEQ = 3 * NP
C DIMENSIONS OF MATRIX A
      NHALF = 3*(NT+2)
      NBAND = 2*NHALF - 1
      NDIM = NEQ
      NDIMB = NBAND
      NHALF1 = NHALF - 1

C  MODE I OPENING APPLIED AT PHI = PI/2
      NFIX = (NF1/2 + 1)*3*NT - 2

      PRINT 47, NT,NF,NP,NUMEL,NEQ,NBAND,NINT,NDIM,NDIMB
```

```
    47 FORMAT(4X*NT  NF   NP  NUMEL NEQ NBAND NINT*/ 1X 1015 )
       IF(NDIM.LT.NEQ .OR. NDIMB.LT.NBAND) GO TO 5000

 C GENERATE ELEMENT NUMBERING
 C NOP(NEL,I)= NODAL POINTS OF ELEMENT NEL, I=1,2,3,4
       DO 50  JF = 1, NF1
       JF1 = JF - 1
       NO = JF1 * NT
       NE = NO - JF1
       DO 50  JT = 1, NT1
       NEL = NE + JT
 C REGISTER ELEMENTS WITH SKEW BOUNDARIES
       KSKEW(NEL) = 0
       IF( JT .EQ. NT1 ) KSKEW(NEL) = 1
       NOP(NEL,1) = NO + JT
       NOP(NEL,2) = NOP(NEL,1) + NT
       NOP(NEL,3) = NOP(NEL,1) + 1
    50 NOP(NEL,4) = NOP(NEL,2) + 1


 C  GENERATE COORDINATES, BETA NOT PI/2
       BETA = CORLTA(KBETA)*PI
       TANB = TAN(BETA)
       DF = (PHI1 - PHI11)/FLOAT(NF1)
       FNT1 = NT1
       PHI = PHI11 - DF
       DO 60 JF = 1,NF
       PHI = PHI + DF
       CO = COS(PHI)
       IF( ABS(CO) .LT. 1.E-8 ) GO TO 65
       BOUNDA = ATAN(TANB/CO)
       IF( BOUNDA .LT. 0.0 ) BOUNDA = BOUNDA + PI
       GO TO 66
    65 BOUNDA = PI*0.5
    66 DT = BOUNDA/FNT1
       NO = NT*(JF - 1)
       THET = THET1 - DT
       DO 60 JT = 1,NT
       THET = THET + DT
       N = NO + JT
 C COORDINATES OF POINT N
       PH(N) = PHI
    60 THE(N) = THET


       PRINT 69
    69 FORMAT(* ELEMENT NUMBERING*/*     NEL        NODES*13X*PH*8X*THE*)
       DO 70  NEL = 1, NUMEL
       NOD = NOP(NEL,1)
       NODD = NOP(NEL,4)
    70 PRINT 71, NEL, (NOP(NEL,J),J=1,4), PH(NOD), THE(NOD),PH(NODD),
      1 THE(NODD)
    71 FORMAT(1X 5I5, 4F10.5 )
```

```
 C CASE STUDIES FOR DIFFERENT VALUES OF POISON RATIO
       DO 2001 IPOIS = MPOIS,NPOIS
       POIS = PPOIS(IPOIS)
       Q = POIS/(0.5-POIS)

       PRINT 292, P,POIS
   292 FORMAT(20X,*P = *F4.2,*   POIS = *F7.4)


 C REGULAR ITERATION SCHEME IN SEARCH OF EIGENVALUE LAMDA= AL

 C  ITERATE REAL PART OF LAMDA
       ICONVR = 0
       DO 2003 ITERR = 1,NITER
       IF(ITERR .LE. 2) GO TO 600
       CALL FITTER(ITERR,ICONVR,ALR,COR)
   600 IF(ITERR .GT. 1) GO TO 620
 C  INITIAL VALUES OF LAMDA
       CALL ALLINI(KGRID,ALR,ALI)
       GO TO 630
   620 CONTINUE
       IF(ICONVR .EQ. 0) GO TO 911
       PRINT 12, ALR(ITERR),ITERR
    12 FORMAT(/60X*...CONVERGED.     ALL = * F9.6,          *ITER = *I2)
       GO TO 2003
   911 CONTINUE
       ALL = ALR(ITERR)
       AAL2 =ALL*(ALL+1.0)-2.0
       AAL1=ALL-1.0
       AL1=ALL+2.0
       Q2=Q*2.0
       QA2=Q2-Q*ALL
       QA21=Q*(ALL+2.0)+2.0
       QALL=Q*ALL
       QA=2.0*Q2+QALL-2.0
       QAA=-Q2*AL1*AAL1

 C ASSEMBLE STIFFNESS MATRIX
       DO 300  I = 1, NEQ
       DO 300 J=1, NBAND
   300 A(I,J) = 0.

       NSKEW = 4
       DO 400  NEL = 1, NUMEL

       NSKEW = 3
       IF( NEL .EQ. NT1 ) NSKEW = 4
       IF( NEL .EQ. NUMEL ) NSKEW = 3
       CALL LLSTIF(NEL)

 C CONMPUTE N-GLOBAL CORRESP.TO LOCAL  I
       DO 340  IN = 1, 4
       IPRE = 3*IN - 3
       NPRE = 3 * NOP(NEL,IN) - 3
       DO 340  IX = 1, 3
       I = IPRE + IX
   340 NGLO(I) = NPRE + IX

 C COMPUTE ROW AND COLUMN WHERE STIFF. SHOULD BE ADDED
       DO 350  I = 1, 12
```

```
      NGLI = NGLO(I)
      K = NHALF - NGLI
      DO 350  J = 1, 12
      N = NGLO(J) + K
      IF(N.LT.1 .OR. N.GT.NBAND)  GO TO 5000
      A(NGLI,N) = A(NGLI,N) + STIFFL(I,J)
  350 CONTINUE
  400 CONTINUE


C MODE I OPENEING
C       SYMMETRY ON TOP SHOULD BE AUTOMATIC.  ON RIGHT...H=0.
      N1 = NEQ - 3*NT1
      DO 500  N = N1, NEQ, 3
  500 A(N,NHALF) = 1.E50
C NO PERPENDICULAR DISPLACEMENT ON BOUNDA
      N2 = 3*NT
      N1 = N2 - 1
      DO 510 N = N1,NEQ,N2
  510 A(N,NHALF) = 1.E50


C SOLUTION OF EIGENVECTOR BY ITERATION
      DO 410  N = 1, NEQ
  410 B(N) = 0.
C FIX ONE DISPLACEMENT
      DO 420  J = 1, NBAND
      AAA(J) = A(NFIX,J)
  420 A(NFIX,J) = 0.
      A(NFIX,NHALF) = 1.
      B(NFIX) = 1000.


C  INVERT STIFFNESS MATRIX TO SOLVE FOR DJAPL.
      CALL BANDSL(A, 459 , NEQ, NBAND, 1, B, 1.E-8, IERR )
C     NOTE THAT  NDIM.GE.NEQ, NDIMB.GE.NBAND  ARE ADMISSIBLE
      RHS = 0.
C  RIGHT HAND SIDES
      DO 430  J = 1, NBAND
      N =  J - NHALF + NFIX
  430 IF(N.GT.0 .AND. N.LE.NEQ)  RHS = RHS + AAA(J)*B(N)
      PRINT 432, IERR, ITERI,ALL, RHS
  432 FORMAT(*  IERR = *I2,*  ITER = *I3,*     ALL = *,2F9.6,2H*I,
     1*   RHS = *2E16.5,2H*I)
C  STORE RHS FOR ITERATION
      QQR(ITERR) = REAL(RHS)


 2000 CONTINUE
      PRINT 2006
 2006 FORMAT(60X,*   NO CONVERGANCE ON LAMDA*)
      STOP
 2003 IF(ICONVR .EQ. 1) GO TO 9999
 2010 CONTINUE
 2001 CONTINUE
 2002 CONTINUE
 9998 CONTINUE
 9999 CONTINUE
C IF LAST CASE CONVERGED FIND BEST M
      STOP
 5000 PRINT 5001
 5001 FORMAT(*0 DIMENSIONS TOO SMALL. EXECUTION TERMINATED* )
      STOP
      END


      SUBROUTINE ELSTIF(NEL)
C COMPUTES STIFFNESS MATRIX FOR ELEMENT NEL BY NUMERICAL
C INTEGRATION  UTILIZING SHAPE FUNCTIONS
      COMPLEX ALL,AAL2,AAL1,QA2,QA21,QALL,QA,QAA,STIFEL,AL1
      COMMON/C1/ NINTE,P,KSKEW(128),WEIGHT(9),S(4,9),STH(4,9),SPH(4,9),
     1 THEPO(9),PHIPO(9),Q,QA,QAA,QA2,QA21,QALL,Q2,ALL,AL1,AAL1,AAL2,
     2NELHF,RATIO
      COMMON/C2/ STIFEL(12,12),NOP(120,4),PH(153),THE(153)
      DIMENSION F(12,9),FT(12,9),FPH(12,9),G(12,9),GT(12,9),GPH(12,9),
     1 H(12,9),HT(12,9),HPH(12,9),COF(12,9),COFT(12,9),COFPH(12,9),
     2 COG(12,9),COGT(12,9),COGPH(12,9),COH(12,9),COHT(12,9),
     3 COHPH(12,9),WE(9)
      K = NOP(NEL,1)
      L = NOP(NEL,2)
      M = NOP(NEL,3)
      N = NOP(NEL,4)

C TRANSFORMATION CONSTANTS
      PHK = PH(K)
      PHL = PH(L)
      THK = THE(K)
      THL = THE(L)
      THM = THE(M)
      THN = THE(N)
      AA2 = (PHL - PHK)*0.5
      BB1 = (THK+THL+THM+THN)*0.25
      BB2 =(-THK+THL-THM+THN)*0.25
      BB3 = (-THK-THL+THM+THN)*0.25
      BB4 = (THK-THL-THM+THN)*0.25

C COMPUTE DISPL.AND STRAIN INTERPOLATION FUNCTIONS IN ALL POINTS OF NUMER.INTEG.
      DO 200 NS = 1,NINTE
      PHIP = PHIPO(NS)
      THEP = THEPO(NS)
      BT24 = BB2 + BB4*THEP
      BP34 = BB3 + BB4*PHIP
      THETA = BB1 + BB3*THEP + BT24*PHIP
      SI = SIN(THETA)
      CO = COS(THETA)
      SII=1.0/SI
      COTG=SII*CO
      DETJ = AA2*BP34
      DETI = 1.0/DETJ
      AADET = AA2*DETI
      APDET = BP34*DETI
      BTDET = BT24*DETI
      WE(NS) = WEIGHT(NS)*SI*DETJ
C X= VALUE FOR (F,G,OR H)*SIN(THETA)**P
C XTH= PARTIAL DERIV. W.R.T. THETA OF X
```

```
C XPH= PARTIAL DERIV. W.R.T. PHI OF X
      DO 190 IN = 1,4
      X = SIN(IN,NS)
      ST = STH(IN,NS)
      XTH = AADET*ST
      XPH = BPDET*SPH(IN,NS) - BTDET*ST
      XPHSI = SII*XPH
      XCOTG = X*COTG

C RESPECTIVE VALUES OF F,G,H AND ITS DERIVATIVES
      DO 190 II = 1, 3
      I = II + (IN-1)*3
      IF(II.NE.1) GO TO 160
      F(I,NS) = X
      FT(I,NS)=XTH
      FPH(I,NS)=XPH
      G(I,NS) = 0.
      GT(I,NS) = 0.
      GPH(I,NS) = 0.
      H(I,NS) = 0.
      HT(I,NS) = 0.
      HPH(I,NS) = 0.
      COF(I,NS)=QAA*X
      COFT(I,NS)=XTH
      COFPH(I,NS)=SII*XPHSI
      COG(I,NS)=QA*XCOTG-AL1*XTH
      COGT(I,NS)=QA21*X
      COGPH(I,NS) = 0.
      COH(I,NS)=-AL1*XPHSI
      COHT(I,NS) = 0.
      COHPH(I,NS)=QA21*SII*X
      GO TO 190
  160 IF(II.NE.2)  GO TO 170
      F(I,NS) = 0.
      FT(I,NS) = 0.
      FPH(I,NS) = 0.
      G(I,NS) = X
      GT(I,NS)=XTH
      GPH(I,NS)=XPH
      H(I,NS) = 0.
      HT(I,NS) = 0.
      HPH(I,NS) = 0.
      EV=XTH+XCOTG
      COF(I,NS)=QA2*EV
      COFT(I,NS)=AAL1*X
      COFPH(I,NS) = 0.
      COG(I,NS)=(Q2*EV-2.0*XTH)*COTG-AAL2*X
      COGT(I,NS)=Q2*XTH-Q*XCOTG
      COGPH(I,NS)=SII*XPHSI
      COH(I,NS)=-XPHSI*COTG
      COHT(I,NS)=XPHSI
      COHPH(I,NS)=SII*(Q2*XCOTG-Q*XTH)
      GO TO 190
  170 F(I,NS) = 0.
      FT(I,NS) = 0.
      FPH(I,NS) = 0.
      G(I,NS) = 0.
      GT(I,NS) = 0.
      GPH(I,NS) = 0.
      H(I,NS) = X
      HT(I,NS)=XTH
      HPH(I,NS)=XPH
      ETF=XTH-XCOTG
      COF(I,NS)=QA2*XPHSI
      COFT(I,NS) = 0.
      COFPH(I,NS)=SII*AAL1*X
      COG(I,NS)=Q2*XPHSI*COTG
      COGT(I,NS)=Q*XPHSI
      COGPH(I,NS)=ETF*SII
      COH(I,NS)=-ETF*COTG-AAL2*X
      COHT(I,NS)=ETF
      COHPH(I,NS)=SII*Q2*XPHSI
  190 CONTINUE
  200 CONTINUE

C ELEMENT STIFFNESS MATRIX (12 BY 12)  -  LOOP OVER ALL ITS COEFFICIENTS
      DO 300  I = 1, 12
      DO 300  J = 1, 12
C NUMERICAL INTEGRATION
      SUM = 0.
      DO 280 NS=1,NINTE

C EVALUATE INTEGRAND FOR EACH POINT OF NUMER.INTEGRATION
      SUM = SUM +        WE(NS)*(COF(I,NS)*F(J,NS)*COFT(I,NS)*FT(J,NS)*
     1COFPH(I,NS)*FPH(J,NS)*COG(I,NS)*G(J,NS)*COGT(I,NS)*GT(J,NS)*
     2COGPH(I,NS)*GPH(J,NS)*COH(I,NS)*H(J,NS)*COHT(I,NS)*HT(J,NS)*
     3COHPH(I,NS)*HPH(J,NS))

  280 CONTINUE
      IF(NEL.GE.NELHF)SUM=SUM/RATIO
      STIFEL(J,I)=SUM
  300 CONTINUE

      IF( KSKEW(NEL) .EQ. 1) CALL SKEWRD(NEL)

      RETURN
      END



      SUBROUTINE SKEWRD(NEL)
C  SUBROUTINE SKEWRD OPERATES ON THE STIFFNESS MATRIX OF A
C  BOUNDARY ELEMENT WHERE SKEWED BOUNDARY CONDITIONS ARE
C  PRESCRIBED WITH RESPECT TO THE (THETA-PHI)-PLANE. FIRST,
C  IT FINDS THE ANGLE OF SUCH NODAL POINTS AND FORMS THE
C  TRANSFORMATION MATRIX D ACCORDING TO THE PRESCRIBED
C  BOUNDARY CONDITIONS. THEN, IT MULTIPLIES D(TRANSPOSE)*STIFFL*D.
      COMMON/C2/ STIFEL(12,12),NOP(128,4),PH(153),THE(153)
      COMMON/C3/ NSKEW,MSKEW,TAND
      DIMENSION D(2,2),VECT(2),ALPHA(4)

      M = NOP(NEL,3)
      N = NOP(NEL,4)
      PHM = PH(M)
      PHN = PH(N)
      TAND2 = TAND*TAND
C SLOPE AT NODE
      ALPHA(3) = TAND*SIN(PHM)/(COS(PHM)*COS(PHM) + TAND2)
      ALPHA(4) = TAND*SIN(PHN)/(COS(PHN)*COS(PHN) + TAND2)
C ANGLE AT NODE
      ALPHA(3) = ATAN( ALPHA(3) )
      ALPHA(4) = ATAN( ALPHA(4) )
```

```
      DO 500 ISKEW = NSKEW,MSKEW
C TRANSFORMATION MATRIX D
      D(1,1) = COS( ALPHA(ISKEW) )
      D(2,2) = D(1,1)
      D(1,2) = SIN( ALPHA(ISKEW) )
      D(2,1) = -D(1,2)
      KM = 3*ISKEW - 2
C MULTIPLY STIFEL * D
      SUM = 0.
      DO 490 II = 1,12
      DO 480 JJ = 1,2
      DO 470 KK = 1,2
      KN = KM + KK
  470 SUM = SUM + STIFEL(II,KN) * D(KK,JJ)
  480 VECT(JJ) = SUM
      DO 460 KK = 1,2
      KN = KM + KK
  460 STIFEL(II,KN) = VECT(KK)
  490 CONTINUE

C MULTIPLY D(TRANSPOSE) * (STIFEL*D)
      DO 450 II = 1,12
      DO 440 JJ = 1,2
      SUM = 0.
      DO 430 KK = 1,2
      KN = KM + KK
  430 SUM = SUM + D(KK,JJ) * STIFEL(KN,II)
  440 VECT(JJ) = SUM
      DO 420 KK = 1,2
      KN = KM + KK
  420 STIFEL(KN,II) = VECT(KK)
  450 CONTINUE
  500 CONTINUE
      RETURN
      END


      SUBROUTINE FITTER(ITER,ICONV,AL,QQ)
C  SUBROUTINE FITTER USES THE REGULA-FALSI NEWTON ITERATION
C  METHOD. FIRST, IT SEARCHES FOR THE SMALLEST QQ AND THEN
C  ITERATES. IT ALSO AVOIDS DUPLICATION OF VALUES. ITERATION
C  IS STOPPED WHEN THE DIFFERENCE OF THE LAST TWO LAMBDA VALUES
C  IS LESS THAN 0.00003
      DIMENSION AL(20),QQ(20)
      DAM = 0.0005
      N = ITER - 1
C       FIND SMALLEST PREVIOUS QW OF OPPOSITE SIGN
      JT2 = ITER - 2
      QW= 1.E00
      DO 800  JT = 1, JT2
      X1 = ABS(QQ(JT))
      IF(QQ(JT)*QQ(N) .GT. 0.)  X1 = X1 + X1
      IF(X1 .GT. QW) GO TO 800
      QW = X1
      N = JT
  800 CONTINUE
      IF( ABS(AL(N)-AL(N)) .LT. .0000) )  N = JT2
C ITERATION FORMULA
      AL(ITER)=(AL(N)*QQ(N)-AL(N)*QC(N))/(QQ(N)-QQ(N))
      X1 = AL(ITER) - AL(N)
      X2 = AL(ITER) - AL(N)
      IF(ABS(X1).LT.DAM .OR. ABS(X2).LT.DAM)  GO TO 909
C     ...DIRECTION TO CHANGE
      QW= DAM
      IF( X1 .LT. 0. ) QW = - DAM
C     ...CLOSEST VALUE
      X3 = AL(N)
      IF(ABS(X2) .LT. ABS(X1))  X3  = AL(N)
      AL(ITER) = X3 + QW
C     AVOID DUPLICATION OF CALCULATIONS
  804 DO 805  JT = 1, JT2
      IF( AL(ITER).EQ. AL(JT) )  GO TO 806
  805 CONTINUE
      GO TO 909
  806 AL(ITER) = AL(ITER) +QW*.25
      GO TO 804
  909 IF( ABS(X1) .GT. .00003 )  GO TO 911

C  AL CONVERGED TO WITHIN 0.00003
      ICONV = 1
  911 CONTINUE
      RETURN
      END
      SUBROUTINE ALLINI(KGRID,ALR,ALI)
C  SUBROUTINE ALLINI INITIATES THE FIRST TWO VALUES OF LAMBDA,
C  WHOSE REAL AND IMAGINARY PARTS ARE ALR AND ALI, RESPECTIVELY.
      DIMENSION ALR(20),ALI(20)
      IF(KGRID .EQ. 2) GO TO 20
      IF(KGRID .EQ. 3) GO TO 30
      IF(KGRID .EQ. 4) GO TO 40
      IF(KGRID .EQ. 5) GO TO 50
   20 ALR(1) = 0.37
      ALR(2) = 0.3705
      GO TO 100
   30 ALR(1) = 0.3127
      ALR(2) = 0.3130
      GO TO 100
   40 ALR(1) = 0.288
      ALR(2) = 0.2881
      GO TO 100
   50 ALR(1) = 0.375
      ALR(2) = 0.3755

  100 CONTINUE
      RETURN
      END

R  END OF RECORD
0  END OF INFORMATION


      PROGRAM BESTM(INPUT,OUTPUT)
C  EXTRAPOLATION PROGRAM USING BEST FIT STRAIGHT LINE
   WITH RESPECT TO LEAST ABSOLUTE SUM OF DEVIETIONS
      DIMENSION AGRID(4),Y(4),X(4),WORK(6,6)
      DOUBLE PRECISION A(2)
C NO. OF FINITE ELEMENTS
      AGRID(1) = 200.0
      AGRID(2) = 200.0
      AGRID(3) = 120.0
```

```
      AGRID(4) = 72.0
C  NUMBER OF CASES
      NC = 1
      NC = 4
C  NUMBER OF POINTS
      NP = 3
      NP = 4
      DO 310 KK = 1,NC
C  DATA - LAMBDA VALUES
      READ 500, (Y(L),L=1,NP)
500 FORMAT(F10.7)

      PRINT 10
 10   FORMAT(//*   M/2   *18X,13H1000/(N**M/2),18X*COEFFICIENTS*8X,*IER*)

      SUM1 = 100.
      K = 1400
      M = 2600
      N = 20
      KCOUNT = 1
800   DO 100 I = K,M,N
      L = I
      A1 = I
C  CONVERGENCE RATE = A1
      A1 = A1/2000.
      DO 200 J = 1,NP
200   X(J) = 1000./(AGRID(J)**A1)
C  CALL BEST FIT LINE
      CALL POLFIT(NP,1,X,Y,A,WORK,IERR)
      A1 = A(1)
      A2 = A(2)
      SUM = 0.0
C  SUM OF DIFFERENCES
      DO 300 J = 1,NP
      DIFF = Y(J) - A1 - A2*X(J)
      DIFF2 = ABS(DIFF)
300   SUM = SUM + DIFF2
C  FIND LEAST SUM
      IF(SUM .GE. SUM1) GO TO 220
      SUM1 = SUM
100   CONTINUE
220   K = L-N-1
      M = L+1
      N = 1
      SUM1 = 100.
      IF(KCOUNT .EQ. 2) GO TO 320
      KCOUNT = KCOUNT + 1
      GO TO 800
320   CONTINUE
      PRINT 1,A1
1     FORMAT(/F6.3)
      PRINT 5, (X(J),J=1,NP),A1,A2,IER
5     FORMAT(10X,6F10.5,I9)
      PRINT 20, SUM
20    FORMAT(90X,*ABS(DIFF) = *F12.5)
310   CONTINUE
      END
$ENTRY
0.584890
0.550036
0.532969
```

APPENDIX C

FINITE ELEMENT PROGRAM WHEN EIGENVALUE, λ, IS COMPLETE (See Chapter II).

```
      PROGRAM SING(TAPE 99,INPUT,OUTPUT)
      COMPLEX A,B,AAA,ALL,AAL2,AAL1,AL1,QA2,QA21,QALL,QA,QAA,STIFEL,RHS
      DIMENSION A(459,65),B(459),AAA(65),NGLO(12),QQ(20),PPOIS(8),AL(20)
     1,POINT(3),WEI(3)
      DIMENSION COBETA(6)
      DIMENSION ALR(20), QQR(20),AL1(20)
      COMMON/C1/ NINTE,P,KSKEW(128),WEIGHT(9),S(4,9),STH(4,9),SPH(4,9),
     1 THEPO(9),PHIPO(9),Q,QA,QAA,QA2,QA21,QALL,Q2,ALL,AL1,AAL1,AAL2,
     2NELHF,RATIO
      COMMON/C2/ STIFEL(12,12),NOP(128,4),PH(153),THE(153)
      COMMON/C3/ NSKEW,MSKEW,TAND

C     DATA FOR POISSON  RATIO
      DATA PPOIS/ 0.3 /
C  DATA FOR RATIO OF MATERIAL PROPERTIES
C  RATIO = 0 ) KEER AND PARIHAR - S PROBLEM
      RATIO = 1.0
C  INCLINATION ANGLE OF CRACK FRONT EDGE
      COBETA(1) = 0.85571

      PI = 3.14159265358979323846
C  DIMENSIONS OF BODY
      THE1 = PI / 2.
      PHI1 = PI
C PHI BOUNDARY FOR A NOTCH
      PHI11=0.0
C  THE BOUNDARY FOR A NOTCH
      THE11=0.0
C MAX. NUMBER OF ITERATIONS, AND MAX. ERROR ON LAMDA= AL
      NITER = 10
C NUMBER OF STUDY CASES
      MGRID = 5
      NGRID = 5
      MPOIS = 1
      NPOIS = 1
      MBETA = 1
      NBETA = 1
      KBETA = 1

C NUMERICAL INTEGRATION DATA
C NINE ELEMENT SCHEME
      NINT = 3
      NINTE = NINT * NINT
      POINT(3) =  0.7745966924148
      POINT(2) = 0.
      POINT(1) = - POINT(3)
      WEI(1) = 0.555555555555555555
      WEI(2) = 0.888888888888888888
      WEI(3) = WEI(1)


C  GENERATE SHAPE FUCTIONS FOR NUM. INTEG. POINTS IN THE ELEMENT
      DO 30  IS = 1, NINT
      PH2 = POINT(IS) * .5
      PH1 = PH2 + .5
      PH11 = PH2 - .5
      DO 30  JS = 1, NINT
      NS = IS + (JS-1)*NINT
      WEIGHT(NS) = WEI(IS) * WEI(JS)
      TH2 = POINT(JS) * .5
      TH1 = TH2 + .5
      TH11 = TH2 - .5
      THEPO(NS) = TH2*2.0
      PHIPO(NS) = PH2*2.0
C VALUE OF F,G,OR H
      S(1,NS) =   PH11 * TH11
      S(2,NS) = - PH11 * TH1
      S(3,NS) =  - PH1 * TH11
      S(4,NS) = PH1 * TH1
C PARTIAL DERIVATIVE W.R.T. PHI OF (F,G,OR H)
      SPH(1,NS) = TH11*0.5
      SPH(2,NS) = - TH11*0.5
      SPH(3,NS) = - TH1*0.5
      SPH(4,NS) = TH1*0.5
C PARTIAL DERIVATIVE W.R.T. THETA OF (F,G,OR H)
      STH(1,NS) = PH11*0.5
      STH(2,NS) = - PH1*0.5
      STH(3,NS) = - PH11*0.5
   30 STH(4,NS) = PH1*0.5

C VALUE OF P, WHERE DISPL. COMP. ASSUME A FORM
C     R**AL*(SIN(THETA)**P)*(F,G,OR H)
      P = 0.0

C NUMBER OF DIVIDING LINES IN THE THETA AND PHI DIRECTIONS
      DO 9999 KGRID = MGRID,NGRID
      IF( KGRID .EQ. 1) GO TO 1
      IF( KGRID .EQ. 2) GO TO 2
      IF( KGRID .EQ. 3) GO TO 3
      IF( KGRID .EQ. 4) GO TO 4
      IF(KGRID .EQ. 5) GO TO 5
    1 NT = 4
      NF = 7
      GO TO 6
    2 NT = 5
      NF = 9
      GO TO 6
    3 NT = 7
      NF = 13
      GO TO 6
    4 NT = 9
      NF = 17
      GO TO 6
    5 NT = 11
      NF = 21
    6 CONTINUE

C NUMBER OF ELEMENTS IN THETA AND PHI DIRECTIONS
      NT1 = NT - 1
      NF1 = NF - 1
C  NUMBER OF ELEMENTS
      NUMEL = NT1 * NF1
      NELHF = NUMEL/2 + 1
C NO. OF POINTS
      NP = NT * NF
C NO. OF EQUATIONS
      NEQ = 3 * NP
C DIMENSIONS OF MATRIX A
      NHALF = 3*(NT+2)
      NBAND = 2*NHALF - 1
      NDIM = NEQ
      NDIM0 = NBAND
      NHALF1 = NHALF - 1
```

```
C  MODE I OPENING APPLIED AT PHI = PI/2
      NF1X = (NF1/2 + 1)*3*NT - 2

      PRINT 67, NT,NF,NP,NUMEL,NEQ,NBAND,NINT,NDIM,NDIMB
67    FORMAT(4X*NT   NF   NP  NUMEL NEQ NBAND NINT*/ 1X 10I5 )
      IF(NDIM.LT.NEQ .OR. NDIMB.LT.NBAND) GO TO 5000

C GENERATE ELEMENT NUMBERING
C NOP(NEL,I)= NODAL POINTS OF ELEMENT NEL, I=1,2,3,4
      DO 50  JF = 1, NF1
      JE1 = JF - 1
      NO = JF1 * NT
      NE = NO - JF1
      DO 50  JT = 1, NT1
      NEL = NE + JT
C REGISTER ELEMENTS WITH SKEW BOUNDARIES
      KSKEW(NEL) = 0
      IF( JT .EQ. NT1 ) KSKEW(NEL) = 1
      NOP(NEL,1) = NO + JT
      NOP(NEL,2) = NOP(NEL,1) + NT
      NOP(NEL,3) = NOP(NEL,1) + 1
   50 NOP(NEL,4) = NOP(NEL,2) + 1

C  GENERATE COORDINATES, BETA NOT PI/2
      BETA = CONETA(KBETA)*PI
      TANB = TAN(BETA)
      DF = (PHI1 - PHI11)/FLOAT(NF1)
      ENT1 = NT1
      PHI = PHI11 - DF
      DO 60 JF = 1,NF
      PHI = PHI + DF
      CO = COS(PHI)
      IF( ABS(CO) .LT. 1.E-8 ) GO TO 65
      BOUNDA = ATAN(TANB/CO)
      IF( BOUNDA .LT. 0.0 ) BOUNDA = BOUNDA + PI
      GO TO 66
   65 BOUNDA = PI*0.5
   66 DT = BOUNDA/ENT1
      NO = NT*(JF - 1)
      THET = THE11 - DT
      DO 60 JT = 1,NT
      THET = THET + DT
      N = NO + JT
C COORDINATES OF POINT N
      PH(N) = PHI
   60 THE(N) = THET

      PRINT 69
   69 FORMAT(* ELEMENT NUMBERING*/*     NEL       NODES*13X*PH*8X*THE*)
      DO 70  NEL = 1, NUMEL
      NOD = NOP(NEL,1)
      NODD = NOP(NEL,4)
   70 PRINT 71, NEL, (NOP(NEL,J),J=1,4), PH(NOD), THE(NOD),PH(NODD),
     1 THE(NODD)
   71 FORMAT(1X 5I5, 4F10.5 )
```

```
C CASE STUDIES FOR DIFFERENT VALUES OF POISON RATIO
      DO 2001 IPOIS = MPOIS,NPOIS
      POIS = PPOIS(IPOIS)
      Q = POIS/(0.5-POIS)

      PRINT 292, P,POIS
292   FORMAT(20X,*P = *F4.2,*   POIS = *F7.4)

C REGULAR ITERATION SCHEME IN SEARCH OF EIGENVALUE LAMDA= AL

C  ITERATE REAL PART OF LAMBDA
      ICONVR = 0
      DO 2003 ITERR = 1,NITER
      IF(ITERR .LE. 2) GO TO 600
      CALL FITTER(ITERR,ICONVR,ALR,COR)
600   IF(ITERR .GT. 1) GO TO 620
C  INITIAL VALUES OF LAMBDA
      CALL ALLINI(KGRID,ALR,ALI)
      GO TO 630
620   ALI(1) = ALI(ITERI) + 0.0005
      ALI(2) = ALI(ITERI) - 0.0005
630   CONTINUE
C  ITERATE IMAGINARY PART OF LAMBDA
      ICONV = 0
      DO 2000 ITERI = 1,NITER
      IF(ITERI .LE. 2) GO TO 911
      CALL FITTER(ITERI,ICONV,ALI,QC)
      IF(ICONV .EQ. 0) GO TO 911
      PRINT 12, ALR(ITERR),ALI(ITERI),ITERI
12    FORMAT(/60X*...CONVERGED.    ALL = *2F9.6,2H*I,*   ITER = *I2)
      GO TO 2001
911   CONTINUE
      ALL = CMPLX(ALR(ITERR),ALI(ITERI))
      AAL2 =ALL*(ALL+1.0)-2.0
      AAL1=ALL-1.0
      AL1=ALL+2.0
      Q2=Q+2.0
      QA2=Q2-Q*ALL
      QA21=Q*(ALL+2.0)+2.0
      QALL=Q*ALL
      QA=2.0*Q2+QALL-2.0
      QAA=-Q2*AL1*AAL1

C ASSEMBLE STIFFNESS MATRIX
      DO 300  I = 1, NEQ
      DO 300 J=1, NBAND
300   A(I,J) = (0.0,0.0)

      NSKEW = 4
      DO 400  NEL = 1, NUMEL

      NSKEW = 3
      IF( NEL .EQ. NT1 ) NSKEW = 4
      IF( NEL .EQ. NUMEL ) NSKEW = 2
      CALL ELSTIF(NEL)
```

```
C COMPUTE N-GLOBAL CORRESP.TO LOCAL  I
      DO 340  IN = 1, 4
      IPRE = 3*IN - 3
      NPRE = 3 * NOP(NEL,IN) - 3
      DO 340  IX = 1, 3
      I = IPRE + IX
  340 NGLO(I) = NPRE + IX

C COMPUTE ROW AND COLUMN WHERE STIFF. SHOULD BE ADDED
      DO 350  I = 1, 12
      NGLI = NGLO(I)
      K = NHALF - NGLI
      DO 350  J = 1, 12
      N = NGLO(J) + K
      IF(N.LT.1 .OR. N.GT.NBAND)  GO TO 5000
      A(NGLI,N) = A(NGLI,N) + STIFEL(I,J)
  350 CONTINUE
  400 CONTINUE



C  INSERT BOUNDARY CONDITIONS FOR WELD
C  ZERO DISPLACEMENTS AT PHI = PI, F=G=H=0.
      N1 = NEQ -3*NT + 1
      DO 500 N = N1,NEQ
  500 A(N,NHALF) = (1.E50,1.E50)
C NO PERPENDICULAR DISPLACEMENT ON BOUNDA
      N2 = 3*NT
      N1 = N2 - 1
      DO 510 N = N1,NEQ,N2
  510 A(N,NHALF) = (1.E50,1.E50)



C SOLUTION OF EIGENVECTOR BY ITERATION
      DO 410  N = 1, NEQ
  410 B(N) = (0.0,0.0)
C FIX ONE DISPLACEMENT
      DO 420  J = 1, NBAND
      AAA(J) = A(NFIX,J)
  420 A(NFIX,J) = (0.0,0.0)
      A(NFIX,NHALF) = (1.,0.)
      B(NFIX) = (1000.0,1000.0)


C  INVERT STIFFNESS MATRIX TO SOLVE FOR DIAPL.
      CALL BANDSL(A, 459 , NEQ, NBAND, 1, B, 1.E-8, IERR )
C       NOTE THAT  NDIM.GE.NEQ, NDIMB.GE.NBAND  ARE ADMISSIBLE
      RHS = (0.0,0.0)
C  RIGHT HAND SIDES
      DO 430  J = 1, NBAND
      N =  J - NHALF + NFIX
  430 IF(N.GT.0 .AND. N.LE.NEQ)  RHS = RHS + AAA(J)*B(N)
      PRINT 432, IERR, ITER1,ALL, RHS
  432 FORMAT(*  IERR = *I2,*  ITER = *I3,*     ALL = *,2F9.6,2H*I,
     1*   RHS = *2E16.5,2H*I)
C  STORE RHS FOR ITERATION
      DDR(ITERR) = REAL(RHS)
      QQ(ITER1) = AIMAG(RHS)



 2000 CONTINUE
      PRINT 2006
 2006 FORMAT(60X,*   NO CONVERGANCE ON LAMDA*)
      STOP
 2003 IF(ICONVR .EQ. 1) GO TO 9999
 2010 CONTINUE
 2001 CONTINUE
 2002 CONTINUE
 9998 CONTINUE
 9999 CONTINUE
C IF LAST CASE CONVERGED FIND REST
      STOP
 5000 PRINT 5001
 5001 FORMAT(*0 DIMENSIONS TOO SMALL, EXECUTION TERMINATED* )
      STOP
      END



      SUBROUTINE ELSTIF(NEL)
C COMPUTES STIFFNESS MATRIX FOR ELEMENT NEL BY NUMERICAL
C INTEGRATION  UTILIZING SHAPE FUNCTIONS
      COMPLEX ALL,AAL2,AAL1,QA2,QA21,QALL,QA,QAA,STIFEL,AL1
      COMPLEX COF,COFT,COFPH,COG,COGT,COH,COHPH,SUM
      COMMON/C1/ NINTE,P,KSKEW(128),WEIGHT(9),S(4,9),STH(4,9),SPH(4,9),
     1 THEPO(9),PHIPO(9),Q,QA,QAA,QA2,QA21,QALL,Q2,ALL,AL1,AAL1,AAL2,
     2NELHF,RATIO
      COMMON/C2/ STIFEL(12,12),NOP(128,4),PH(153),THE(153)
      DIMENSION F(12,9),FT(12,9),FPH(12,9),G(12,9),GT(12,9),GPH(12,9),
     1 H(12,9),HT(12,9),HPH(12,9),COF(12,9),COFT(12,9),COFPH(12,9),
     2 COG(12,9),COGT(12,9),COGPH(12,9),COH(12,9),COHT(12,9),
     3 COHPH(12,9),WE(9)
      K = NOP(NEL,1)
      L = NOP(NEL,2)
      M = NOP(NEL,3)
      N = NOP(NEL,4)

C TRANSFORMATION CONSTANTS
      PHK = PH(K)
      PHL = PH(L)
      THK = THE(K)
      THL = THE(L)
      THM = THE(M)
      THN = THE(N)
      AA2 = (PHL - PHK)*0.5
      AA1 = (THK+THL+THM+THN)*0.25
      AA2 =(-THK+THL-THM+THN)*0.25
      AA3 = (-THK-THL+THM+THN)*0.25
      AA4 = (THK-THL-THM+THN)*0.25

C COMPUTE DISPL.AND STRAIN INTERPOLATION FUNCTIONS IN ALL POINTS OF NUMER.INTEG.
      DO 200 NS = 1,NINTE
      PHIP = PHIPO(NS)
      THEP = THEPO(NS)
      AT24 = AA2 + AA4*THEP
      AT34 = AA3 + AA4*PHIP
```

```
      THETA = AB1 + BB3*THEP + BT24*PHIP
      SI = SIN(THETA)
      CO = COS(THETA)
      SII=1.0/SI
      COTG=SII*CO
      DETJ = AA2*BP34
      DETI = 1.0/DETJ
      AADET = AA2*DETI
      BPDET = BP34*DETI
      BTDET = BT24*DETI
      WE(NS) = WEIGHT(NS)*SI*DETJ
C X= VALUE FOR (F,G,OR H)*SIN(THETA)**P
C XTH= PARTIAL DERIV. W.R.T. THETA OF X
C XPH= PARTIAL DERIV. W.R.T. PHI OF X
      DO 190 IN = 1,4
      X = S(IN,NS)
      ST = STH(IN,NS)
      XTH = AADET*ST
      XPH = BPDET*SPH(IN,NS) - BTDET*ST
      XPHSI = SII*XPH
      XCOTG = X*COTG

C RESPECTIVE VALUES OF F,G,H AND ITS DERIVATIVES
      DO 190  II = 1, 3
      I = II + (IN-1)*3
      IF(II.NE.1)  GO TO 160
      F(I,NS) = X
      FT(I,NS)=XTH
      FPH(I,NS)=XPH
      G(I,NS) = 0.
      GT(I,NS) = 0.
      GPH(I,NS) = 0.
      H(I,NS) = 0.
      HT(I,NS) = 0.
      HPH(I,NS) = 0.
      COF(I,NS)=QAA*X
      COFT(I,NS)=XTH
      COFPH(I,NS)=SII*XPHSI
      COG(I,NS)=QA*XCOTG-AL1*XTH
      COGT(I,NS)=QA21*X
      COGPH(I,NS) = 0.
      COH(I,NS)=-AL1*XPHSI
      COHT(I,NS) = 0.
      COHPH(I,NS)=QA21*SII*X
      GO TO 190
  160 IF(II.NE.2)  GO TO 170
      F(I,NS) = 0.
      FT(I,NS) = 0.
      FPH(I,NS) = 0.
      G(I,NS) = X
      GT(I,NS)=XTH
      GPH(I,NS)=XPH
      H(I,NS) = 0.
      HT(I,NS) = 0.
      HPH(I,NS) = 0.
      EV=XTH+XCOTG
      COF(I,NS)=QA2*EV
      COFT(I,NS)=AAL1*X
      COFPH(I,NS) = (0.0,0.0)
      COG(I,NS)=(Q2*EV-2.0*XTH)*COTG-AAL2*X
      COGT(I,NS)=Q2*XTH+Q*XCOTG
      COGPH(I,NS)=SII*XPHSI
      COH(I,NS)=-XPHSI*COTG
      COHT(I,NS)=XPHSI
      COHPH(I,NS)=SII*(Q2*XCOTG+Q*XTH)
      GO TO 190
  170 F(I,NS) = 0.
      FT(I,NS) = 0.
      FPH(I,NS) = 0.
      G(I,NS) = 0.
      GT(I,NS) = 0.
      GPH(I,NS) = 0.
      H(I,NS) = X
      HT(I,NS)=XTH
      HPH(I,NS)=XPH
      ETF=XTH-XCOTG
      COF(I,NS)=QA2*XPHSI
      COFT(I,NS) = (0.0,0.0)
      COFPH(I,NS)=SII*AAL1*X
      COG(I,NS)=Q2*XPHSI*COTG
      COGT(I,NS)=Q*XPHSI
      COGPH(I,NS)=ETF*SII
      COH(I,NS)=-ETF*COTG-AAL2*X
      COHT(I,NS)=ETF
      COHPH(I,NS)=SII*Q2*XPHSI
  190 CONTINUE
  200 CONTINUE

C ELEMENT STIFFNESS MATRIX (12 BY 12)  -  LOOP OVER ALL ITS COEFFICIENTS
      DO 300  I = 1, 12
      DO 300  J = 1, 12
C NUMERICAL INTEGRATION
      SUM = (0.0,0.0)
      DO 280 NS=1,NINTE

C EVALUATE INTEGRAND FOR EACH POINT OF NUMER.INTEGRATION
      SUM = SUM + WE(NS)*(COF(I,NS)*F(J,NS)+COFT(I,NS)*FT(J,NS)+
     1COFPH(I,NS)*FPH(J,NS)+COG(I,NS)*G(J,NS)+COGT(I,NS)*GT(J,NS)+
     2COGPH(I,NS)*GPH(J,NS)+COH(I,NS)*H(J,NS)+COHT(I,NS)*HT(J,NS)+
     3COHPH(I,NS)*HPH(J,NS))

  280 CONTINUE
      IF(NLL.GE.NELHF)SUM=SUM/RATIO
      STIFEL(J,I)=SUM
  300 CONTINUE

      IF( KSKEW(NEL) .EQ. 1) CALL SKEWRD(NEL)

      RETURN
      END
```

```
      SUBROUTINE BANDSL (A,KA,N1I,NII,NVI,V,EPSI,IERR)
C  SUBROUTINE BANDSL SOLVES THE MATRIX EQUATION AX = B,WHERE
C  A IS THE OVERALL BANDED STIFFNESS MATRIX, B IS THE COLUMN MATRIX
C  OF THE PRESCRIBED NODAL FORCES, AND X IS THE COLUMN MATRIX
C  OF THE NODAL DISPLACEMENTS.  N IS THE COLUMN ORDER OF A, AND M
C  IS THE BAND WIDTH AND THE NUMBER OF COLUMNS IN A. M MUST BE AN
CC ODD NUMBER.
C  GAUSS ELIMINATION IS USED. THE TRIANGULATION IS PERFORMED IN
C  N - 1 STEPS, AT EACH STEP K, COLUMN K OF A IS SEARCHED FOR
```

```
C  MAXIMUM ELLMLNT A(I,K), AND ROWS I AND K ARE INTERCHANGED. AFTER
C  TRIANGULATION THE SOLUTION IS COMPLETED BY BACK SUBSTITUTION.
C  CONTENTS OF A AHL DESTROYED DURING COMPUTATION. ON RETURN
C  B CONTAINS THE SOLUTION X.
      COMPLEX A,V,T
      DIMENSION A(KA,1),V(KA)
      EPS = ABS(EPSI)
      IERR = 0
      N = NI1
      M = MI1
      NV = NV1
C BAND WIDTH TOO SMALL
      IF(M .LT. 3) GO TO 130
C BAND WIDTH GREATER THAN THE ORDER OF C
      IF(N .LT. M) GO TO 135
      LR = (M - 1)/2
C  BAND WITH AN EVEN NUMBER
      IF(2*LR .NE. M-1) GO TO 130
      LR1 = LR - 1
      M1 = M + 1
      N1 = N + 1
C ROW SHIFTING AND 0 PLACEMENT
      DO 20 K = 1,LR1
      LR2 = LR - K
      II = N1 - K
      DO 20 I = 1,LR2
      DO 10 J = 2,M
   10 A(K,J-1) = A(K,J)
      JJ = M1 - I
      A(I,JJ) = (0.,0.)
   20 A(K,M) = (0.,0.)
      N1 = N - 1
      DO 90 I = 1,N1
      IV = I
      II = I + 1
C FIND MAXIMUM ELEMENT OF COLUMN I
      DO 30 K = II,LR
      IF( CABS(A(K,1)) .LE. CABS(A(IV,1)) ) GO TO 30
      IV = K
   30 CONTINUE
      IF( IV .EQ. I ) GO TO 50
C  INTERCHANGE ROWS
      T = V(I)
      V(I) = V(IV)
      V(IV) = T
      DO 40 J = 1,M
      T = A(I,J)
      A(I,J) = A(IV,J)
   40 A(IV,J) = T
   50 IF( CABS(A(I,1)) .LE. EPS) GO TO 140
C  TRIANGULARIZATION
      V(I) = V(I)/A(I,1)
      DO 60 J = 2,M
   60 A(I,J) = A(I,J)/A(I,1)
      DO 80 K = II,LR
      T = A(K,1)
      V(K) = V(K) - T*V(I)
      DO 70 J = 2,M
   70 A(K,J-1) = A(K,J) - T*A(I,J)
   80 A(K,M) = (0.,0.)
      IF(LR .EQ. N) GO TO 90
      LR = LR + 1
   90 CONTINUE
      IF( CABS(A(N,1)) .LE. EPS ) GO TO 150
C  BACK SUBSTITUTION
      V(N) = V(N)/A(N,1)
      JM = 2
      KK = N1
      KK1 = KK - 1
      DO 110 K = 1,N1
      DO 100 J = 2,JM
      KJ = KK1 + J
  100 V(KK1) = V(KK1) - A(KK,J)*V(KJ)
      IF(JM .NE. M) JM = JM + 1
      KK = KK1
  110 KK1 = KK1 - 1
      RETURN
  130 PRINT 900,M
      IERR = 1
      RETURN
  135 PRINT 902,N,M
      IERR = 1
      RETURN
  140 IERR = I
      GO TO 160
  150 IERR = N
  160 PRINT 901,IERR,EPS
      RETURN
  900 FORMAT(6(/)20X*ARGUMENT LIST ERROR. BAND WITH =* I5)
  901 FORMAT(6(/)20X*ERROR. MAXIMUM ELEMENT AT STEP*I5,*IS L.SS THAN OR
     1 EQUAL TO *E12.3)
  902 FORMAT(6(/)20X*ARGUMENT LIST ERROR. ORDER OF MATRIX =*I5,10X
     1 *BAND WITH =*I5)
      END

      SUBROUTINE SKEWBD(NEL)
C  SUBROUTINE SKEWBD OPERATES ON THE STIFFNESS MATIX OF A
C  BOUNDARY ELEMENT WHERE SKEWED BOUNDARY CONDITIONS ARE
C  PRESCRIBED WITH RESPECT TO THE (THETA-PHI)-PLANE. FIRST,
C  IT FINDS THE ANGLE OF SUCH NODAL POINTS AND FORMS THE
C  TRANSFORMATION MATRIX D ACCORDING TO THE PRESCRIBED
C  BOUNDARY CONDITIONS. THEN, IT MULTIPLIES D(TRANSPOSE)*STIFEL*D.
      COMPLEX STIFEL,SUM,VECT
      COMMON/C2/ STIFEL(12,12),NOP(120,4),PH(153),THE(153)
      COMMON/C3/ NSKEW,MSKEW,TANB
      DIMENSION D(2,2),VECT(2),ALPHA(4)

      M = NOP(NEL,3)
      N = NOP(NEL,4)
      PHM = PH(M)
      PHN = PH(N)
      TANB2 = TANB*TANB
C SLOPE AT NODE
      ALPHA(3) = TANB*SIN(PHM)/(COS(PHM)*COS(PHM) + TANB2)
      ALPHA(4) = TANB*SIN(PHN)/(COS(PHN)*COS(PHN) + TANB2)
C ANGLE AT NODE
      ALPHA(3) = ATAN( ALPHA(3) )
      ALPHA(4) = ATAN( ALPHA(4) )



      DO 500 ISKEW = NSKEW,MSKEW
C TRANSFORMATION MATRIX D
      D(1,1) = COS( ALPHA(ISKEW) )
```

```
      D(2,2) = D(1,1)
      D(1,2) = SIN( ALPHA(ISKEW) )
      D(2,1) = -D(1,2)
      KM = 3*ISKEW - 2
C MULTIPLY STIFEL * D
      DO 490 II = 1,12
      DO 480 JJ = 1,2
      SUM = (0.0,0.0)
      DO 470 KK = 1,2
      KN = KM + KK
  470 SUM = SUM + STIFEL(II,KN) *D(KK,JJ)
  480 VECT(JJ) = SUM
      DO 460 KK = 1,2
      KN = KM + KK
  460 STIFEL(II,KN) = VECT(KK)
  490 CONTINUE
C MULTIPLY D(TRANSPOSE) * (STIFEL*D)
      DO 450 II = 1,12
      DO 440 JJ = 1,2
      SUM = (0.0,0.0)
      DO 430 KK = 1,2
      KN = KM + KK
  430 SUM = SUM + D(KK,JJ) * STIFEL(KN,II)
  440 VECT(JJ) = SUM
      DO 420 KK = 1,2
      KN = KM + KK
  420 STIFEL(KN,II) = VECT(KK)
  450 CONTINUE
  500 CONTINUE
      RETURN
      END


      SUBROUTINE FITTER(ITER,ICONV,AL,QQ)
C  SUBROUTINE FITTER USES THE REGULA-FALSI NEWTON ITERATION
C  METHOD. FIRST, IT SEARCHES TO THE SMALLEST QQ AND THEN
C  ITERATES. IT ALSO AVOIDS DUPLICATION OF VALUES. ITERATION
C  IS STOPPED WHEN THE DIFFERENCE OF THE LAST TWO LAMBDA VALUES
C  IS LESS THAN 0.00003
      DIMENSION AL(20),QQ(20)
      DAM = 0.0005
      M = ITER - 1
C       FIND SMALLEST PREVIOUS QW OF OPPOSITE SIGN
      JJ2 = ITER - 2
      QW= 1.E00
      DO 800  JJ = 1, JJ2
      X1 = ABS(QQ(JJ))
      IF(QQ(JJ)*QQ(M) .GT. 0.)  X1 = X1 + X1
      IF(X1 .GT. QW) GO TO 800
      QW = X1
      N = JJ
  800 CONTINUE
      IF( ABS(AL(N)-AL(M)) .LT. .00003 )  N = JJ2
C ITERATION FORMULA
      AL(ITER)=(AL(N)*QQ(M)-AL(M)*QQ(N))/(QQ(M)-QQ(N))
      X1 = AL(ITER) - AL(M)
      X2 = AL(ITER) - AL(N)
      IF(ABS(X1).LT.DAM .OR. ABS(X2).LT.DAM)  GO TO 909
C     ...DIRECTION TO CHANGE
      QW= DAM
      IF( X1 .LT. 0. ) QW = - DAM
C     ...CLOSEST VALUE
      X3 = AL(M)
      IF(ABS(X2) .LT. ABS(X1))  X3  = AL(N)
      AL(ITER) = X3 + QW
C     AVOID DUPLICATION OF CALCULATIONS
  804 DO 805  JJ = 1, JJ2
      IF( AL(ITER).EQ. AL(JJ) )  GO TO 806
  805 CONTINUE
      GO TO 909
  806 AL(ITER) = AL(ITER) +QW*.25
      GO TO 804
  909 IF( ABS(X1) .GT. .00003 )  GO TO 911

C  AL CONVERGED TO WITHIN 0.00003
      ICONV = 1
  911 CONTINUE
      RETURN
      END
      SUBROUTINE ALLINI(KGRID,ALR,ALI)
C  SUBROUTINE ALLINI INITIATES THE FIRST TWO VALUES OF LAMBDA,
C  WHOSE REAL AND IMAGINARY PARTS ARE ALR AND ALI, RESPECTIVELY.
      DIMENSION ALR(20),ALI(20)
      IF(KGRID .EQ. 2) GO TO 20
      IF(KGRID .EQ. 3) GO TO 30
      IF(KGRID .EQ. 4) GO TO 40
      IF(KGRID .EQ. 5) GO TO 50
   20 ALR(1) = 0.37
      ALR(2) = 0.3705
      ALI(1) = 0.046
      ALI(2) = 0.0466
      GO TO 100
   30 ALR(1) = 0.3127
      ALR(2) = 0.3130
      ALI(1) = 0.045
      ALI(2) = 0.046
      GO TO 100
   40 ALR(1) = 0.288
      ALR(2) = 0.2881
      ALI(1) = 0.0451
      ALI(2) = 0.04516
      GO TO 100
   50 ALR(1) = 0.375
      ALR(2) = 0.3755
      ALI(1) = 0.045
      ALI(2) = 0.0445

  100 CONTINUE
      RETURN
      END

R  END OF RECORD
Q  END OF INFORMATION
```


DA
FILM